Addis Ababa University
Addis Ababa Institute of Technology
Center of Biomedical Engineering
School of Graduate Studies

Investigation of photo-induced actuation achieved through electro-spun PLA/MWCNT nanocomposite fibers for artificial skeletal muscle fabrication

By

Rakeb Debalkew

In partial fulfillment of the requirements for the degree of master science in Biomedical Engineering

Advisor: **Professor Gyeong-Man Kim**

June, 2022

Declaration

I, the undersigned, declare that this thesis and the work presented in it are my own and have been generated by me as the result of my own original research.

I confirm that:

- This work was done wholly or mainly while in candidature for a research degree at this University;
- Where any part of this thesis has previously been submitted for a degree or any other qualification at this University or any other institution, this has been clearly stated;
- Where I have quoted from the work of others, the source is always given. With the exception of such quotations, this thesis is entirely my own work;
- I have acknowledged all main sources of help;
- This work or any part of this work has not been published before submission;

Name: _____

Signature: _____

Date: _____

This MSc. thesis has been submitted for examination with my approval as an advisor,

_____

Professor Gyeong-Man Kim

Addis Ababa University
School of Graduate Studies

Certificate of examination

This is to certify that the thesis prepared by **Rakeb Debalkew** entitled by **Investigation of photo-induced actuation achieved through electro-spun PLA/MWCNT nanocomposite fibers for artificial skeletal muscle fabrication;** Submitted in partial fulfillment of the requirements for the degree of Master of Science in Biomedical Engineering (Biomedical Rehabilitation) complies with the regulations of the University and meets the accepted standards with respect to originality and quality.

Signed by the examining committee

Examiner: _____ Signature: _____ Date: _____

Examiner: _____ Signature:_____ Date: _____

_____

Chief of department or Graduate program coordinator

Acknowledgement

Above all, my deepest gratitude goes to the almighty God for giving me the courage, patience and health to get to the final part of my master thesis. I thank God for giving me a wonderful family and spectacular friends that supported me day in and day out through the process of working on this master thesis. My parents and, in general, my family deserve my intense and heartfelt gratitude for their support. University of Martine Luther Halley, Germany deserves an ample amount of credit for the work that is done on this master thesis. Had it not been for the data provided by this university, none of the conclusions and recommendations drawn from this master thesis would have been determined.

I am also extremely grateful to all the people and institutes that helped me finalize and write this master thesis. My advisors, Professor Gyeong-Man Kim and Mrs. Leelavathy Rajesh deserves my extreme thanks for all the support and assistance they have provided for me. Addis Ababa Institute of Technology undergraduate coordinator Mr. Biruk Abraham and postgraduate coordinator Dr. Dawit Haile has also assisted me enormously with their advice and opinions. They have provided me with bright advice and gave me the strength to go forward. It was truly an honor to work with such highly educated and experienced professionals.

Jimma University, Institute of technology, lecturer Mohammed Aliy has also given me incredible support throughout this research. I owe an ample amount of gratitude to him. And my friends from both Addis Ababa Institute of technology and Jimma Institute of technology post graduate class have been an amazing support system for me and I can't thank them enough for their feedback, motivation and team spirit, even though we were working on different areas. My dearest friends, Bethlehem Tamrat and Habtamu have also supported me decidedly to finalize this master thesis.

Abstract

Introduction: One of the major challenges in the medical industry is the area of technical orthopedics. Technical orthopedics is a branch of rehabilitation engineering that deals with the design of artificial limbs for people with physical disabilities. Plenty of materials and methods have been presented to the scientific community so far, but there still is a considerable gap in replacing the function of human skeletal muscle. This research project deals with the morphological and thermo-mechanical analysis of a PLA/MWCNTs nanocomposite fiber that can be applied as an actuator in the area of technical orthopedics, particularly for the fabrication of artificial muscles.

Methodology: The characterization techniques output of the PLA/MWCNT nanocomposite fiber has been provided by Martine Luther University, Halle-Wittenberg, Germany. The morphological characterization outputs from SEM technique making use of image analysis software Image J and the mechanical characterization outputs from the Dynamic Mechanical Analysis (DMA) technique by theoretical approach and mathematical approach through MATLAB are analyzed to compare the behavior of actual human skeletal muscles with the proposed nanocomposite fiber.

Results and Discussion: The output of the SEM characterization analysis clearly showed that there is Gaussian distribution of fiber diameter. Both manual and automated measurements were performed and both presented a normal distribution function with equivalent measurements of 6.7 µm and 7.7 µm mean respectively. The Gaussian distribution shows that the fabricated nano-composite fiber has high reactivity with an external stimulus, in this case infrared radiation (IR). As for the DMA, the storage modulus showed a significant change from 327MPa to 371 MPa & the loss modulus increased from 62.5 MPa to 76.1 MPa up on the addition of MWCNT in the pure PLA. This shows improved mechanical (Elastic and Viscous) behavior of the nanocomposite fibers. The viscoelasticity of the fiber was also modeled by making use of the three element (Standard Linear Solid) Model and the temperature dependent modulus change is presented in this master thesis.

Conclusion and recommendation: From the results acquired, the fabricated nanocomposite fibers showed properties that proved applicability for the fabrication of artificial human skeletal muscle. The fibers can also further be used for the detailed study and analysis of several forms of muscular malfunctions, such as, paralysis, cerebral palsy etc.

Key words: Technical Orthopedics, Nanocomposite, Viscoelasticity

Table of content

List of figures

List of tables

List of Abbreviations/ Symbols

CNTs: Carbon Nanotubes

DMA: Dynamic Mechanical Analysis

EAP: Electro Active Polymer

ESF: Electro Spun Fiber

FSE: Fast Secondary Electrons

IR: Infrared Radiation

MWCNT: Multi-Walled Carbon Nanotube

SWCNT: Single-Walled Carbon Nanotube

PLA: Poly lactic acid

ROM: Range of Motion

SMA: Shape memory alloy

SEM: Scanning Electron Microscope

SD: Standard Deviation

SSA: Specific Surface Area

XRD: X-Ray Diffraction (or X-ray Powder Diffraction)

TTN: Titin protein

PAM: Pneumatic artificial muscle

$\boldsymbol{\sigma}$ **:** Applied stress

$\boldsymbol{\varepsilon_d}$ **:** Strain of viscous element

$\boldsymbol{\varepsilon_{s1}}$**:** Strain of spring element

$\boldsymbol{\varepsilon_{s2}}$: Strain of spring element

$\dot{\boldsymbol{\varepsilon}}$: Strain rate

$\dot{\boldsymbol{\sigma}}$**:** Stress rate

$\boldsymbol{\mu}$: The viscosity of the dashpot and

$\boldsymbol{\epsilon}$: The stiffness of the spring

$\boldsymbol{\sigma_0}$: Initial stress

$\boldsymbol{\varepsilon_0}$: Initial strain

ω: Is the angular frequency

t: Time

$\boldsymbol{\delta}$: Is the loss angle

Chapter One

Introduction

1.1.Background

According to the last WHO disability report, about 15% of the world's population lives with some form of disability, of which 2-4% experience significant difficulties in functioning. The given comprehensive estimate for disability is up surging due to population ageing and the rapid spread of chronic diseases, accidents/traumas, as well as improvements in the methodologies used to measure disability [1]. The number of lower limb and upper limb amputees is increasing in an alarming rate over the past few years but the exact number of people around the world who have a major amputation is difficult to ascertain because many developing countries do not keep records of the number of people with limb amputation. The World Report on Disability jointly issued by the World Bank and World Health Organization estimated that 17.6% of the Ethiopian populations have disability [2].

Amputation is the loss of a certain body part, most commonly a limb. The word amputation is derived from the Latin amputare, "to cut away", from ambi- ("about", "around") and putare ("to prune"). Amputation can be caused by peripheral and vascular disease, infection, tumors, congenial anomalies/deformities, thermal burns/cold injuries and Trauma [3]. People that undergo amputation will be physically disabled. Technical orthopedics is a category of rehabilitation engineering concerned with prosthetic and orthotic appliance for peoples with physical disability. Orthopedics is the branch of medicine dealing with the correction of deformities of bones or muscles. Orthopedics is a medical specialty concerned with the prevention and treatment of disorders of the musculoskeletal system by use of surgical and non-surgical methods. [4]It deals with the design, production and fitting of these devices. These designs should be well suited for the musculoskeletal system of the body. Before going deeper in to these artificial designs, it is necessary to understand the natural structure, property and function of these parts of the body

Any damage or loss on the human musculoskeletal system can be rehabilitated by making use of orthotics or prosthesis. An artificial rehabilitation device used to replace the missing part of the limb is called prosthesis. Prosthesis has many different types and forms depending on the amputation [5]. Nevertheless, the technology behind the application of all these types of rehabilitation devices has improved quite nicely within the past couple of decades. The initial objective of prosthesis was to give an aesthetic replacement of the missing part of the body. Eventually, the function of the missing limb started to be considered in the designs made for replacing these limbs. The first attempts in the prosthesis were incorporating the joint systems [6].

Multiple attempts were made and are still being made but the most common and advanced ones are Targeted Muscle Re-innervation (TMR) and robotic limbs [7]. These technologies both have their own benefits and drawbacks but they are likely the most advanced and handy technologies on the area of technical orthopedics at this time.

Robotics, considered to be one of the drivers of the so-called fourth industrial revolution, are starting to find no limitations in regarding to variety of applications in a vast field of areas. [8] Actuators are key elements of a robotic system in conjunction with sensors and controllers to allow the intended type and extent of motion. This robotic system can tactically be applied on the areas of technical orthopedics particularly in the areas of replacing the missing part of the limb. As it is true for any automated robotic system, the robotic limbs that are intended to replace the structure and function of the natural limb have major system parts called sensors, actuators and controller [8]. The figure below shows the basic workflow of any automated system including the robotic system. This research is mainly focused on the technology behind the actuators of such robotic systems.

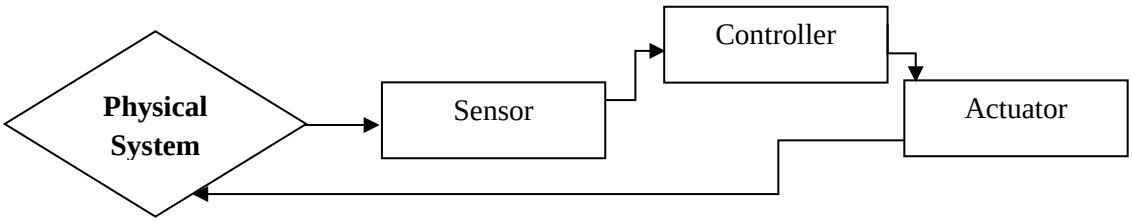

Figure 1: Automated system flow diagram [9]

1.2.Actuators

The literal definition of an actuator is a servomechanism that supplies and transmits a measured amount of energy for the operation of another mechanism or system. Actuators are energy conversion devices [9]. It turns a control signal in to mechanical action such as an electric motor. The widely applied definition of actuators is that they are components of a machine that is responsible for moving or acting upon a certain mechanism or system as ordered by the control unit driven by the input from a sensor [10]. They are on the path through which a control system influences an environment. Actuators are based on pneumatic, mechanical, piezoelectric, electromechanical and electrical means but are increasingly being driven by a controller.

In the broader view, as the science of actuators got more popular and advanced, material composites such as shape memory alloys and polymer composites started being manipulated. These actuator materials are able to change their shape in response to change to an environmental condition and perform mechanical work on nano-, micro- and macro-scales. Among these actuators, polymer-based actuators are the highly attractive ones because of the number of properties they possess, such as sensitivity to broad range of stimuli: such as electric, thermal and

photo stimuli [11]. They also have remarkable mechanical properties that are used today in many applications including the areas of biomedical engineering.

Taking a deeper look at the polymer actuators, the first polymer actuators ever presented to the scientific society were the electroactive polymers (EAPs). These EAPs exhibit size and shape change when stimulated by an external stimulus, particularly an electrical field. EAPs have two principal classes: the dielectric and ionic EAPs [11]. These EAPs are widely manipulated in the actuator and sensor application. A majority of historic actuators are made of ceramic piezoelectric materials. As great a discovery were these polymer actuators, they had their own disadvantage concerning their operational temperature, voltage, work density per cycle, complicated electrical connections and specific actuating medium requirements.

To overcome the gaps witnessed in the EAPs, polymers that are induced by other kinds of stimulus were introduced. More recently, photo-induced polymer actuators are the center of attention due to their unique characteristics and simple nature. These photo-induced polymer actuators have the ability to unlock the internal work in a solid-state structure [12] .This is of key importance for many potential applications. The photon energy from the external source initiates change in the internal structure. This will result in the mechanical action. Most of these polymer actuators act to result in a one-way response but some provide reversible response.

In order to alter the internal structure of these polymers under an external stimulus, complex behavior nanoparticles such as the carbon nanotubes (CNTs) are used. As mentioned above, shape memory alloys and polymer-based actuators are the most widely used actuators recently. The shape memory alloys usually end up resulting in a one directional actuation. This isn't a quiet desirable situation due to the fact that additional process is required to reset after the process of actuation. To overcome this additional requirement of a process, reversible or equilibrium response polymer actuators were discovered. Until now, liquid crystalline elastomers are the only proven polymer actuators that exhibit reversible actuation.

1.3.PLA/CNT nanocomposite

The handbook of polymer nanocomposite, processing, performance and application volume B has published quite an interesting literature on PLA/CNT composites in 2015. In this literature, the various recent developments in preparation and characterization of PLA/CNT have been highlighted. The two different types of CNTs have been detail discussed along with their benefit and drawback. And the most important input found from this literature was the detailed mechanical property of PLA alone as well as in comparison with other four polymers. These other polymers are polypropylene (PP), high density polyethylene (HDPE) [13].

Poly lactic Acid (PLA)

PLA is a biodegradable thermoplastic aliphatic polyester derived from renewable biomass, typically from fermented plant starch such as from corn, cassava, sugarcane or sugar beet pulp.

Due to its chiral nature, lactic acid has several forms such as PLA and PLLA. Chirality is a geometric property of some molecules and ions. A chiral molecule is non-superposable on its mirror image. PLA polymers range from amorphous glassy to semi crystalline polymer. It has a glass transition temperature of 60-65^{o}C, melting point of 130-180^{o}C [14].Several technologies such as annealing, adding nucleating agents, forming composites with fibers or nanoparticles, chain extending and introducing crosslink structure have been used to enhance their mechanical properties. PLA can be processed as a thermoplastic fiber or film by making use of melt spinning process or other conventional methods.

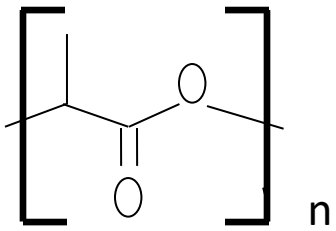

Figure 2: (a) Plastic sheet form of PLA (b) PLA chemical formula [15]

Table 1: Chemical properties of PLA [15]

Chemical properties of PLA	
Chemical formula	$(C_3H_4O_2)_n$
Melting Temperature	(130-180^{o}C)
Glass Transition temperature	(60-65^{o}C)
Heat Deflection temperature	(49-52^{o}C) at 0.46 MPa

Table 2: Physical properties of PLA [15]

Physical properties of PLA	
Tensile strength	61-66 MPa
Flexural strength	48-110 MPa
Specific gravity	1.24
Shrink rate	0.37-0.41%

Carbon Nanotubes (CNTs)

Publications about CNTs give credit to Sumio Lijimia, who in 1991 published a ground breaking paper in Nature Reporting the discovery of multiwall CNTs. CNTs are class of nanomaterials that consist of a two-dimensional hexagonal lattice of carbon atoms bent and joined in one direction so as to form a hollow cylinder. CNTs are allotropes of carbon with a cylindrical nanostructure. These cylindrical nanostructured carbon molecules have unique properties that account for their

application in many significant areas such as nanotechnology, electronics, optics and other areas of the material science [16]. There are two types of CNTs. These are single-walled (SWCNTs) with a diameter of less than one nanometer and multi-wall (MWCNTs) with a diameter reaching 1nm – 50nm. CNTs are well-suited for virtually any application requiring high strength, durability, electrical conductivity and light weight properties compared to conventional materials [17].

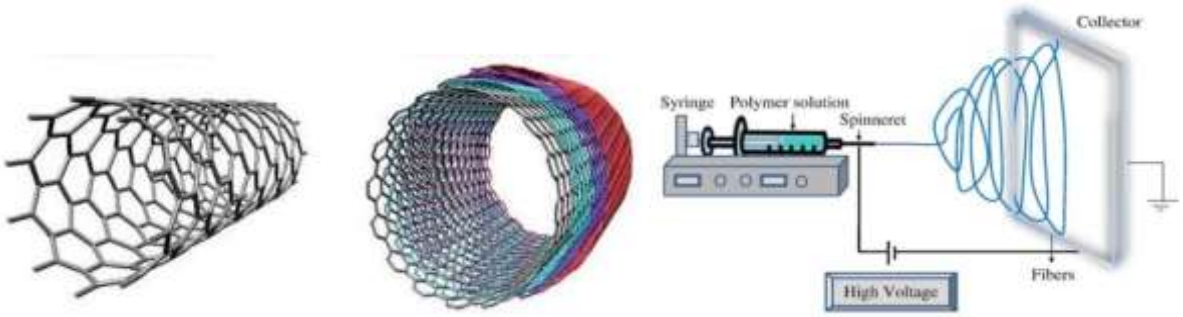

Figure 3: (a) Single walled CNT (b) Multi walled CNT [18] (c) Electrospinning Process [19]

1.4.Problem Statement

With the ever-increasing number of physical disabilities in the world, the need to replace limb aesthetics and functionality accurately has increased considerably. In order to replace the functionality of human artificial limbs, technology has gone to several remarkable stages, from wooden prosthesis to electroactive polymers and several other solutions. Even though there is a considerable amount of work done on the automation of human limbs, there is still a gap in the simplicity of designs proposed and applied to the area of technical orthopedics. Several of the existing models have complicated designs and uneasy application. This research project aims to solve this issue by analyzing a nanocomposite fiber fabricated to contribute a simple actuator that can achieve automation close to human skeletal muscle functionality.

1.5.Objective

1.5.1. General Objective

- Investigate the photo-induced actuation of a nanocomposite polymer fibers prepared for the application of fabricating artificial human skeletal muscles.

1.5.2. Specific objectives

- To analyze the fiber diameter distribution to understand morphological character of material.
- To verify the results of the morphological characterization related with actuation.
- To analyze the change of thermomechanical behavior of material up on MWCNT addition.
- To model the viscoelasticity of the material to understand the viscoelastic behavior.
- To compare the behavior of the nanocomposite fibers with human skeletal muscle fibers.

1.6.Significance of the thesis

This research project will contribute as an input to the global scientific society working in the area of nanotechnology as well as biomedical engineering. The fibers under study were fabricated at Martin Luther University, Halle-Wittenberg, Germany and the raw data collected from two characterization methods were analyzed in detail in this master thesis. From the analysis that was done, a certain conclusion was reached and based on that conclusion other researchers can develop other conclusions or make use of the analyzed fiber and work on a variety of application areas. In short, this research project is highly useful for confirming the scientific validity of the fibers that were thoroughly analyzed for further work in the future. It will also give ground for other correlative or comparative research in the area of artificial muscle fabrication.

1.7.Scope and delimitation of the thesis

The concept to be presented in this research project is the reversible response actuation achieved by the PLA nanocomposite containing MWCNTs that shows actuation under the illumination of infrared (IR). In this study, the main objective is to analyze a state-of-the-art optically driven actuation by uniform dispersion and alignment of MWCNTs by means of an ES process for future micro- and nanomachines. All the required data for this study will be presented by Martin Luther University, Halle-Wittenberg, Germany. The nature of regular human skeletal muscles will be studied as compared to that of the fabricated nanocomposite fibers justifying the application of Targeted Muscle Renervation (TMR) or robotic solutions proposed in technical orthopedics. In order to do this, two major characterization techniques outputs are analyzed. These are scanning electron microscopy (SEM) and Dynamic mechanical analysis (DMA). Morphological study of the fibers as compared to human skeletal muscle and thermomechanical study of the fiber and modeling the viscoelastic nature of the fiber will be the scope of the methodology used on this research project.

Chapter Two

Muscular System

2.1.Organ systems

The human body is composed of small structural units called cells. Plenty of these cells group themselves to form tissues. These tissues in turn group themselves to form organs, which make up the organ systems of a certain living organism. The organ system is what makes life possible by manipulating air, food and other useful resources from the environment [19]. The human body is generally composed of twelve basic systems as listed on Table 4 given below [20].

Table 3: Organ systems and their function and definition [20]

Organ System	Function and Definition
Circulatory system	Deals with blood circulation to organs from the heart.
Digestive system	Deals with food intake, processing and excretion.
Hematopoietic system	Deals with the formation of blood cells.
Endocrine system	Deals with hormonal actions and glands.
Integumentary system	Consists of skin, hair, nails and exocrine glands.
Immune system	Deals with the body's defense system from harm.
Nervous system	Facilitates the brain controlling mechanism of the body.
Muscular system	Responsible for voluntary and involuntary movement in the body.
Renal system	Consists of kidney, ureter, bladder and urethra.
Reproductive system	Deals with the system of sex organs for reproduction.
Respiratory system	Deals with O_2 inhalation, process and CO_2 exhalation.
Skeletal system	Deals with the frame of the body keeping proper structure and balance.

From the twelve organ systems listed above, the most important ones for technical orthopedics are the muscular system and skeletal system. These two systems are responsible for the movement of the human body with the assistance of all the other remaining systems. Unless energy isn't supplied form the digestive, circulatory and respiratory system and unless the nervous system controls it, the muscular and skeletal systems, collectively known as musculoskeletal system, will not be able to function alone [21]. This research project aims to study the detailed property of PLA/MWCNT nanocomposite for the application of artificial muscle fabrication. Before moving on to the detailed study of the nanocomposite fiber property, this chapter will provide all the information needed to know about the natural muscular system; mainly focusing on the skeletal muscle proteins whose function is assumed to be replaced on this research project by CNTs.

2.2.Muscular system

Muscles are parts of all animals made of smooth tissues functioning to maintain posture and locomotion of the body. There are two types of muscles in the body. These are voluntary and involuntary muscles [22].

2.2.1. Involuntary muscles

Involuntary muscles, smooth muscles and cardiac muscles, are not under the control of the brain. The systems such as the circulatory, respiratory, and digestive systems along with a few other systems drive their actions. In the cases of any malfunction of these types of muscles, replacement by an artificial material and system is an enormously difficult task that requires plenty of experiments with in vivo tests and extremely high technologies to assist the process [22].

2.2.2. Voluntary muscles

On the other hand, voluntary muscles, skeletal muscle, are muscles that are under the control of the brain. The movements of these muscles are in a controlled manner by the intention of the person. Therefore, in case of any malfunction with these kinds of muscles, it is a relatively easier approach to replace them. Even though there are many parts of the body that contain skeletal muscles, the arms and the legs are the most common and important ones for basic movement of a human being [22]. To make it even more vivid and easier to relate the need of artificial muscles in the area of technical orthopedics, let us see the anatomy and physiology of human muscles.

2.2.3. Skeletal Muscles Anatomy

All skeletal muscles are voluntary, striated, not branched and multinucleated. Skeletal muscles are contractile type of tissues that are found in animals. It is found between bones and it functions by creating movement of the bone. Skeletal muscles are adapted and shaped in many different ways; this gives rise to complex movements of the human skeletal system. Figure 4 shows the major skeletal muscles of the human skeletal system from the frontal and posterior location.

Muscle is an important part of the human body's physiology and anatomy. Even though it is difficult to tell the exact number, there are about 650 skeletal muscles in human body. These skeletal muscles are attached to bones by tendons. This, while the bone is used to bare high loads and maintain structure, the muscles are there to facilitate the movement by contracting and relaxing their structure [22]. This relaxation and contraction doesn't happen by only one whole part of the muscular system. It occurs as a result of a combined effort of a bundle of smaller structural units of the skeletal muscle called muscle fibers [19]. These muscle fibers possess multiple types of proteins that take in the signal that is sent from the brain and interpret it in to contraction and relaxation of the bundle of muscle fibers.

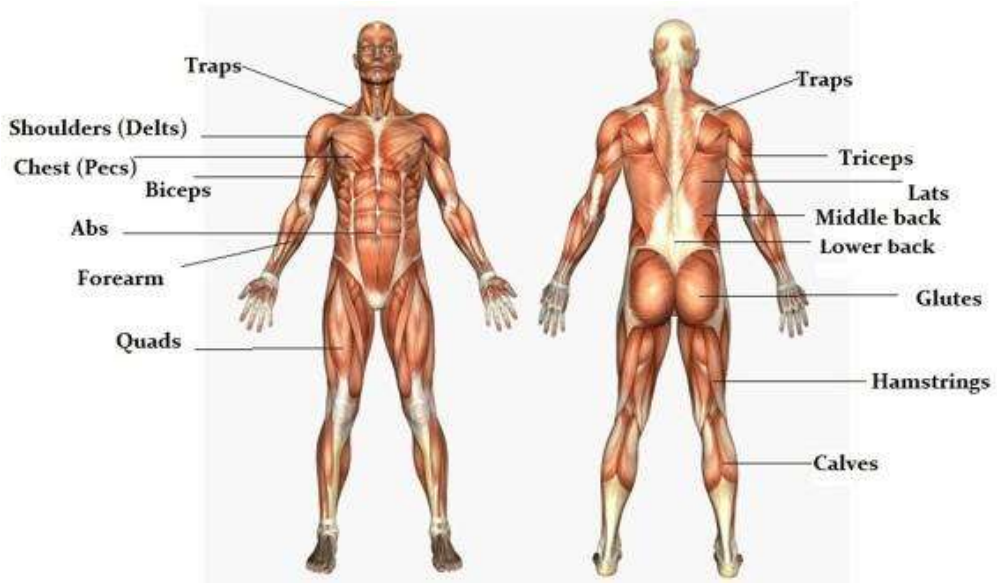

Figure 4: Human skeletal muscles [23]

Skeletal muscle tissues have complex geometries. The mechanism through which they work is by a complex biochemical reaction triggered by signals coming from the brain. Unlike cardiac and smooth muscles, the only way through which the skeletal muscle acts is through signaling from the nervous system. These muscles are ordered by the intention of the person intended to be moved or not moved based on the person. The way it operates is by causing contraction and relaxation through the action of complex proteins acting together. These proteins are the basic functional units of the skeletal muscle system of the human body.

As it is clearly shown on Figure 5, skeletal muscles are made of many muscle fascicles wrapped in an epimysium. And these fascicles are made of even smaller muscle fibers that are wrapped in a sarcolemma. Signals from the brain for either contraction or relaxation reach each muscle fiber and the action of all these bundled fibers is what creates a strong and efficient facilitation of the muscular system. This research project is aiming to replace these smaller muscle fibers by artificial nanocomposite fibers that are made of PLA/MWCNT. The addition of the MWCNTs to pure PLA

fibers is based on the intention of replacing the natural actuator skeletal muscle by an artificial photoinduced actuator.

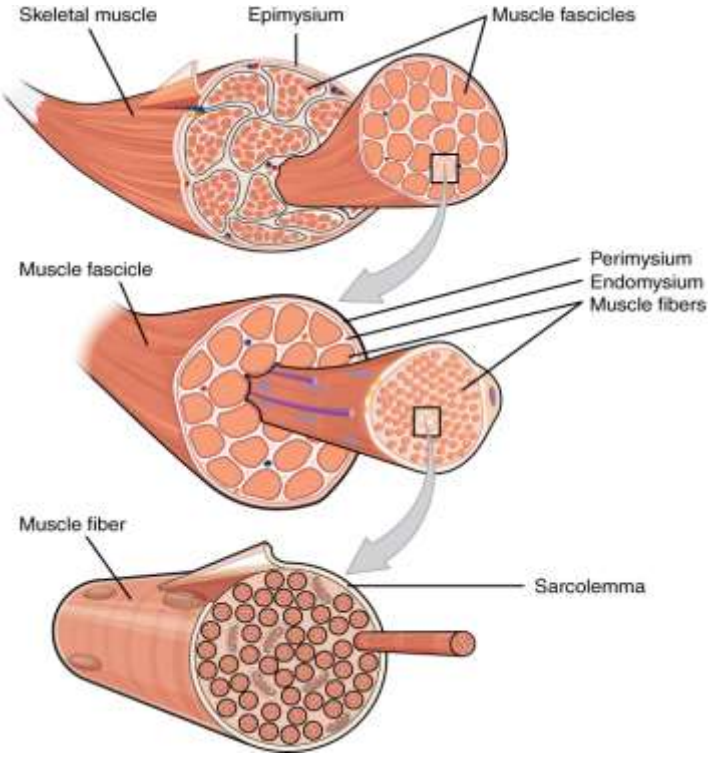

Figure 5: Muscular system gross anatomy [24]

2.2.4. Skeletal muscle proteins

The percentages of several proteins that are present in human muscle are higher than any other proteins found in other parts of the body. The energy needed for the contraction of these muscles is supplied by the oxidation process of carbohydrates and lipids. The mechanism of changing the chemical reaction into a mechanical energy is called a mechanochemical reaction [25]. These muscles go under a major conformational change in their peptide chains as a result of the mechanochemical reaction taking place to cause contraction.

One of the most important proteins in this mechanochemical reaction is Myosin. Myosin consists of an elongated and double stranded peptide chain that is coiled at both ends to form a terminal globule. Trypsin splits myosin into larger fragments called meromyosins. Myosin has a lot of positively and negatively charged side chains. There are smaller proteins called tropomyosin possessing a somewhat similar property with that of myosin. Myosin can easily combine with actin, which is another important skeletal muscle protein. Actomyosin is a combination of actin and myosin. It is composed of one molecule of myosin and one or two molecules of actin. The actins of the muscle are attached to one another by S filaments [26]. These connected actins are then oriented parallel with the myosin molecule. While contraction of the muscle is intended by

the brain, the S filaments are pulled shrinking the actin molecules past the myosin molecule. This causes shortening of the muscle fibers which as a bundle causes the whole skeletal muscle to shorten. When the intended contraction is not needed anymore, the S filaments will release the actin molecules enabling them to relax and thus the whole skeletal muscle fiber and their bundle skeletal muscle will relax.

Also titinis (TTN) an important protein, which is one of the most abundant proteins next to myosin and actin proteins found in human skeletal muscles. It is a large sized protein that is more than $1\mu m$ in length and it is used as a molecular spring by being encoded by TTN gene. It is the largest known protein and it has 244 individually folded protein domains connected by unstructured peptide sequence. These domains unfold when the protein is stretched as a result of a certain load and refold when the load applied is removed; thus controlling the elasticity of human muscle [27].

Skeletal muscles are voluntary muscles that are under the complete control of the brain. Signals transmitted from the brain order individual skeletal muscle fibers, which act together as a bundle [24]. The folding and unfolding of the muscle proteins ordered or controlled by the brain is responsible for the contraction and relaxation of skeletal muscles respectively.

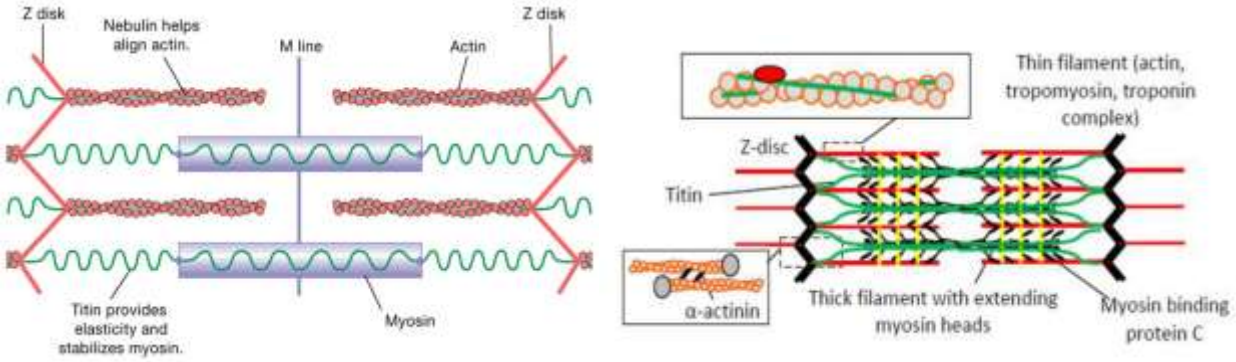

Figure 6: Schematic diagram of proteins of the skeletal muscles [28]

Chapter Three

Literature review

3.1.The History of Actuators

In the ancient times, if anything needed to be moved, the only option around was to actually move it physically. As time went by, the human brain evolved in to thinking of making use of wheels to make the process of moving materials easier. Eventually, the invention of a battering ram took place. A battering ram is a siege engine that was designed to break open a wall or a gate. The battering ram could be considered the first actuator in history since it created a motion in straight line. But it still was not automated. It did make the effort for the motion easier but it still needed the power of people to move it [29].

As the human brain started to advance its ingenuity to many systems around it, the pneumatic and hydraulic actuators emerged marking the beginning of the modern actuator technology we have today. In the 1800's, the air compressor was developed and that led to the use of using compressed air in cylinders. This paved the way for the use of pneumatic actuators which were developed in the 1900's. The first history of pneumatic actuation system dates back to the time around the World War II happened when Xhiter Anckeleman came up with the use of pneumatic and hydraulic actuation systems [30]. After this marking point of actuator, many different types of actuators with multiple types of mechanisms started to emerge.

There are many different types of actuators in the automated systems of the world. Plenty types of actuators have been presented to the scientific community over the past few decades. The major and common types are pneumatic, Hydraulic, mechanical, electrical, piezoelectric, electro-mechanical and photo induced actuators. The most common and recent types of actuating materials are shape memory alloys and polymer composites.

3.2.Shape memory alloy-based actuators

A shape memory alloy (SMA) is an alloy that can be deformed by temperature change and in normal getting back to its original shape when it is heated [31]. The basic phenomenon of shape memory effect is led by the thermoplastic behavior of the martensite phase of Cu-Zn alloy. Around 1962, Nickel Titanium alloy was developed by the American State Naval Ordance Laboratory and was commercialized under the name Nitinol. Both Cu-Zn alloy and Nickel Titanium alloy displayed the actuation only when exposed to temperature variation [31]. The heating and cooling process were behind the actuation. Later on, ferromagnetic SMAs were discovered. These materials were found to be interesting due to the fact that they used magnetic stimulus to actuate. Magnetic reaction of alloys is much faster and accurate that of thermal stimulus.

SMAs are also known as smart metals, smart alloys or muscle wire. Parts of shape memory alloys can be lightweight, solid state alternatives to conventional actuators such as hydraulic, pneumatic and motor based systems [32]. Shape memory alloys are applied in variety of areas in the world at this time. Some of the major application areas are; automotive, robotics (bioengineered robotic arm), civil structure (intelligent reinforced concrete (IRC)), piping, telecommunication (smart phones), medicine (stents), optometry (eyeglass frames) and many more application areas can be listed [33]. Recently, a prosthetic hand was introduced by Loh et al. that can almost replicate the motion of a human hand. Other biomimetic applications are also being explored. Weak points of SMAs are energy inefficiency, slow response time and large hysteresis [34].

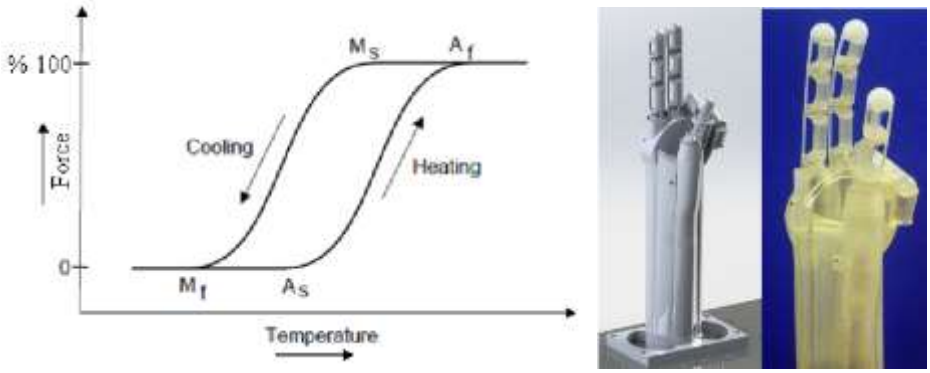

Figure7: (a) Hysteresis curve of SMA [35] (b) SMA powered robotic arm [36]

3.3.Polymer composite based actuators

The earliest recorded polymer actuator discovery was in 1880, when Wilhelm Rontgen experimented towards actuating a stripe of rubber material by using many kinds of stimulus. His series of attempts led to the emergence of EAPs about twenty-five years later. Wilhelm Rontgen designed an experiment to test the effect of electrostatic field on the mechanical property of a rubber material and discovered that the sprayed electric charges affected the length of the rubber by elongating it by several centimeters. Following Rontgen's lead, M. P. Sacerdote continued experimenting on the area and ended up formulating a theory on strain response to an applied electric field about two decades later, in 1899 [37].

These discoveries were like basements to all the other studies and discoveries done on the area of polymer actuators. But they were back warded techniques with many limitations such as complicated connections and reserved medium of actuation. Later on, piezoelectric polymers called the Electrets were discovered. But before the discovery of these piezoelectric polymer actuators the experiments mentioned above laid the foundation of polymer actuation. It was around 1925 that the first piezoelectric polymer actuator was introduced. Electrets were made of bee wax, rosin and carnauba wax [38]. The cooled mixture of these ingredients was then exposed to an applied electrical source. This resulted in a solidified polymeric material that exhibited a

piezoelectric effect. Still, the actuation achieved was not satisfactory by the end of this discovery. One sided actuation with moderate sensitivity was simply not good enough for the ever-growing technology of the planet [39].

3.4.Light activated polymers (LAPs)

The simplified and to the point definition of an actuator is that it is a mover. It moves because of an external stimulus triggering it and it moves in order to make an impact on a certain system that will be applied to some sort of human related application. Since this is a research done in the biomedical engineering department of Addis Ababa University, the area of application that is of interest to the nanocomposite fibers studied on the thesis is a biomedical rehabilitation area such as artificial muscles and robotic arms actuator.

It was in 2005 that Samit V. Ahir and Eugene M. Terentjev reported a magnificent phenomenon that initiated this mater thesis research. They were the first to reveal the photo-induced mechanical actuation observed in a polymer-nanotube composite when under the illumination of IR radiation. In the experiment that they held, they showed that at small strains, the polymer nanotubes composite tended to expand and while exposed to large strain, the polymer nanotubes composite contracts under identical IR excitation. Their work introduced a remarkable property of certain rubber-nanotube composites, a continuously reversible response under the exposure of IR radiation [40]. Despite the fact that this was one of the greatest discoveries in the area, it still couldn't provide uniform spread of nanotubes to maximize actuation.

A master thesis paper done by Zahid S. Mahmwalla in September 2012, at McGill University, Montreal, Canada by the title "Characterization of photo-induced mechanical responses in Azobenzene polymers" has revealed the photomechanical effect that was defined as a reversible molecular shape change up on absorption of light, resulting in a significant mechanical macroscopic deformation of the host material. This exhibits the ability of this thin polymer layers to act as strong light driven artificial muscles for larger mechanical systems as a result of the quantitative characterization of the photomechanical effect of Azobenzene based polymers [41]. Azobenzene based systems are excellent candidates for photomechanical actuation for many niche applications involving small size localized actuation, remoteness of the power source, and freedom from the encumbrance of batteries, electrons, and internal moving parts.

In 2014, a research published in the nature communications site has caught attention. Through this research, the authors Xiaobo, Zhibin and fourteen others demonstrated a highly versatile photo actuators, oscillators and motors based on polymer nanotube composites. These nanotubes used were SWCNTs. By utilizing these SWCNTs with different chirality distributions, chromatic actuators that are responsive to selected wavelength ranges were achieved [42]. However, light controlled actuators that are able to exhibit continuous motions with adjustable moving speed and movement direction control is still a challenging issue in the field.

In 2017, Yan Li from a research group at Sichuan University under the title "Light driven polymer actuators with pre-stored strain energy", demonstrated a strategy of using a photo responsive malleable actuator with mechanical strain energy stored in the benign polymer. The fact that the stored strain is required is because of its use to amplify the magnitude of photo-induced mechanical force and that was the main achievement of this research [43]. As noble as this idea is, it is too complicated to fabricate and use it to certain applications. Instead, uniform distribution achieved by electrospun MWCNTs is suggested in this research so as to improve the magnitude and reversibility of the actuation achieved by a polymer nanotubes composite.

3.5. Literatures on artificial muscles

Artificial muscles are divided in to three major groups based on their actuation mechanism. These are,

- Pneumatic actuation
- Electrical actuation and,
- Thermal actuation

Pneumatic artificial muscles (PAMs) are the very first artificial muscles invented in the 1950s. They were invented to be applied in the design of a certain artificial limb. These artificial muscles are devices that work by making use of a pressurized air filling pneumatic mechanism. These artificial muscles have very light weight. This feature makes them extremely convenient for the application of replacing defective human muscles. Their loose-weave nature of the outer fiber shell allows PAMs to be flexible and to imitate biological systems. Based on these pneumatic actuators based artificial muscles, hydraulic artificial muscles were invented in Tokyo institute of technology, in 2017. Somewhere along the way and in latest years, electrical and thermal actuator based artificial muscles were also introduced to the area of technical orthopedics.

Just as the case of natural muscles, any artificial muscle is evaluated by its ability to relax and contract in response to any kind of stimulus. There indeed are many mechanisms through which devices and systems might respond to a certain stimulus. But it can be generalized that any material that can change shape as a result of any stimulus can be engaged on a technological area of replacing an artificial muscle [44].

So far, there is no such thing as a general theory of actuators. All the actuators that exist to this day are defined and categorized based on their energy conversion or by the criteria on which they are selected. But, there isn't a concrete comparison approach towards all actuators. As a result of this, artificial muscle technologies choose to consider criteria that can specify actuation as compared to a natural actuator, skeletal muscle actuators.

Human muscular system involves a mechanism that incorporates both active and passive properties. The passive mechanism is induced as a result of the resistance of elastin and collagen

fibers in soft tissue while stretching takes place. Passive tissues of human muscular system possess viscoelastic effects like stress relaxation and creep. While active muscle tissues are induced by the action of sarcomeres in response to neural stimulus. Properties worth being studied in active muscles are contraction velocity and the activation level or amount of neural stimulation provided to the muscle [45].

A research published on 2020 on advances in Mechanical Engineering Journal revealed the actuation performance difference among ten biological muscle applied materials and material composites. These are pneumatic artificial muscles (PAM), shape memory alloys (SMA), dielectric actuators (DEA), relaxer ferroelectric polymers (RFP), conducting polymers (CP), carbon nanotubes (CNT), ionic polymer metal composites (IPMC), twisted fiber actuator (TFA), hydrogel actuator (HGA), and hydraulically amplified self-healing electrostatic actuators (HASEL). The parameters used as pillar of comparison are strain, stress, strain rate, work density, specific power & efficiency. PAM was found to be similar with that of biological muscles. The actuation parameters are actually superior to those of biological muscles but there is a little decrease on strain. But PAM need heavy gas tank included in the process and the hysteresis is not compatible with the target property. SMAs have great suit on stress, work density and specific power due to their high elastic moduli. But they have low strain and strain rate under thermal actuation process. EAPs have great strain, strain rate, work density and specific power. However, the electric field needed for actuation is large. HGA are biocompatible, but the valves of actuation parameters are lower than other materials. HASEL actuators have the thick elastomer shells need large electrical supply to get sufficient power for actuation and large space is required for electrodes [46].

A review of an article on the advances in stimuli-responsive soft robots with integrated hybrid material stated that carbon nanotubes have been intensively utilized in soft robotics because of their top notch optical, thermal, electrical and Mechanical properties. SWCNT and Polycarbonate (PC) has been investigated by Zhang et al. of their photo actuation behavior. The nanocomposite demonstrated that the SWCNT/PC can curl and flatten reversibly [47]. MDPI Molecules in September 16, 2020 published another article review that described the mechanism, application and challenges of shape-memory polymeric artificial muscles. SMPs can be classified based on their reaction to stimulus as one way, two way and multiple way shape memory effect. The first one irreversible, the second one is reversible and the third one returns to the initial shape step by step [48].

Chapter Four

Morphological Characterization

The detailed definition of polymer and polymer composites has been discussed on chapter one. On this chapter, one of the most important polymer composites morphology characterization techniques, Scanning Electron Microscopy (SEM) techniques, will be thoroughly discussed.

4.1.Polymer Morphology

Polymer morphology is a strong function of the level of magnification at which a material is observed. Morphology of material is a thorough consideration of its phase or phases, which is distinguished physical feature of the material. Morphology involves the relative arrangement of phases in space. Polymer morphology is the form of polymer structure including crystallinity, branching, molecular weight, cross linking and many more. Polymer morphology is different from metals or ceramics due to the fact that it is a description of the statistical average of morphological features [49]. Morphology is observed using structural characterization techniques such as AFM (atomic force microscopy), STM (scanning tunneling microscopy), TEM (transition electron microscopy), SEM (scanning electron microscopy), and OM (optical microscopy).

4.1.1. Internal polymer morphology

The internal structure of a polymer tells a lot about the property. TEM is the commonly used characterization technique used to study the internal morphology of polymeric materials. [50] Additives and nanofiller type of particles within the matrix of a polymer are visualized and studied under the internal morphology of polymers.

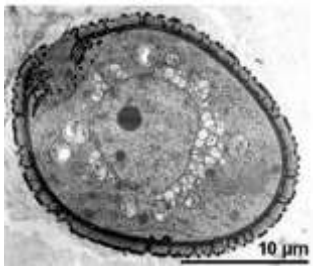

Figure 8: Pollen grain under TEM [51]

4.2. Scanning Electron Microscopy (SEM)

4.2.1. Definition

SEM is an electron microscopy type that generates images of a certain sample material by scanning the material's surface area with electrons beam in a focused manner.

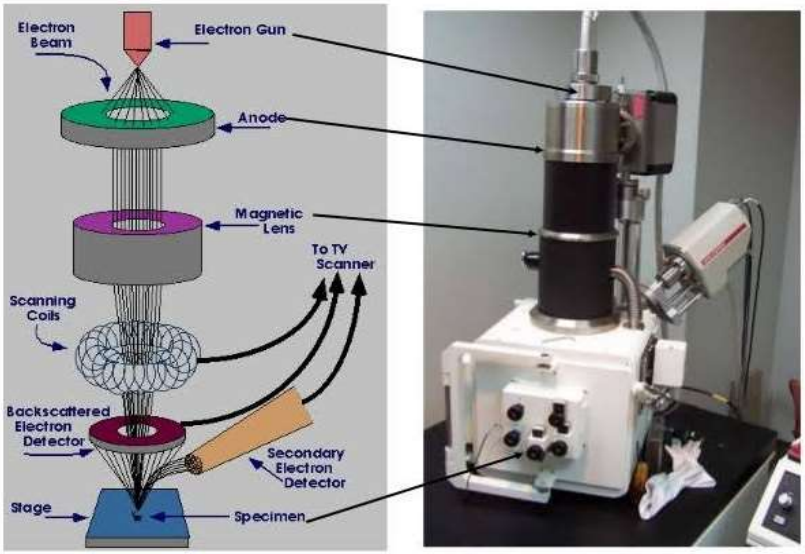

Figure 9: SEM Instrumentation [52]

4.2.2. Operating Principle

The SEM is used for observing the surface topography, morphology or composition of a sample under study. This information is observed by two-dimensional scanning of the electron probe over the surface and acquisition of an image from the detected electrons. The electron beams ejected or reflected back from the sample material are scanned in a roaster scan pattern and combined it with the position of the beam and the intensity of the detected signal then an image is produced.

The schematic diagram of a typical SEM presented on Figure 9 shows the detailed bioinstrumentation of SEM .As it is clearly shown on the figure, the electron beam that hits the surface of the material sample originated from an electron gun. The electron beam is then condensed by making use of two condenser lenses. These condensers define the size of the electron beam which in turn defines the resolution of image that is formed. There are also objective lenses in the device to focus the electron beam to the sample. Scanning coils are used to roaster the beam onto the sample [53]. The condensers have deflectors between them and they are oriented to collimate the electron beam ejected from the surface of the sample material generating three major outputs that are used to various application areas. These outputs are:

- Secondary electrons (Slow, Fast and Auger electrons)
- X-Rays
- Back scattered electrons

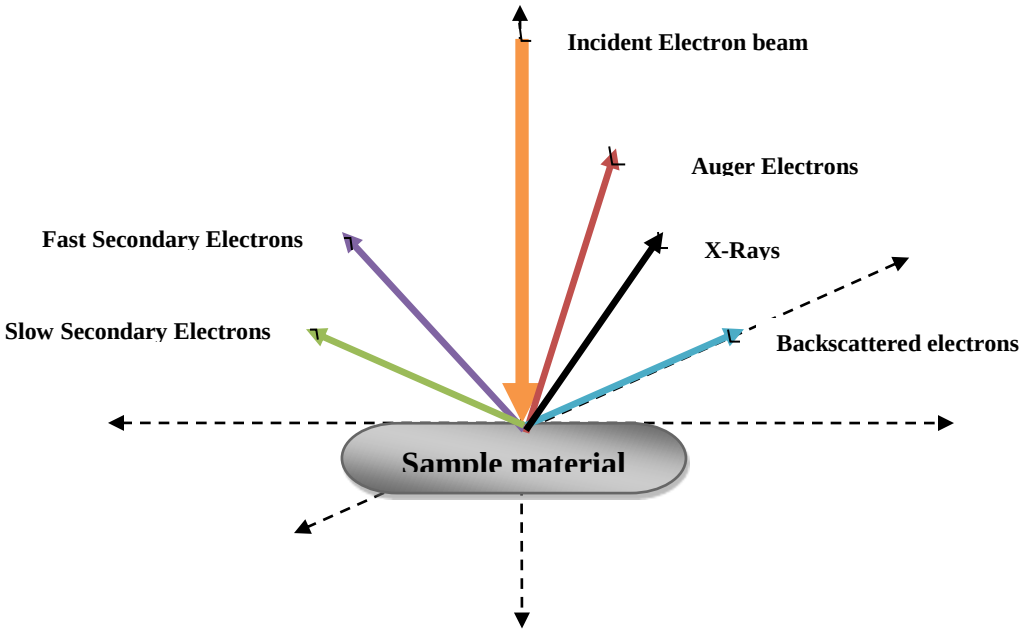

Figure 10: Outputs of incident electron beam on SEM [54]

I. Secondary Electrons (SEs)

SEs are electrons that are ejected by the incident beam of electrons. If the secondary electrons emitted are in the valence band or conduction band or the outer most shell of the material's surface atom, not much energy is required to eject them. These types of secondary electrons are called **slow secondary electrons (SSEs).**

If the secondary electrons to be ejected from the surface of the sample material as a result of the incident electron beam are firmly attached to the atom on the surface of the sample material; due to the fact that they are found in the inner shells, an enormous amount of energy is required to eject or remove them. And these are called **fast secondary electrons (FSEs)**.

When the electrons of the sample material surface are ejected from an inner shell by the energy released when ionized atoms return to the ground state, then these secondary electrons are called **Auger electrons**. The table below is a short summery of secondary electrons along with their applications [53].

Table 4: Secondary electron characteristics and their application [54]

Slow secondary electrons	Fast secondary electrons	Auger Electrons
Ejected from valence or conduction band	Ejected from inner shell	Ejected from inner shell
Has energy < 5eV	Has energy ~ 50- 200 eV	Has energy from few hundred eV to few thousands eV
Used to form images of the sample material surface (Used for SEM)	Do not form SEM images and create low quality spectroscopic data. But it is useful for TEM.	It is given by the difference between the original excitation energy and binding energy of the outer most shell from which the electron is ejected.
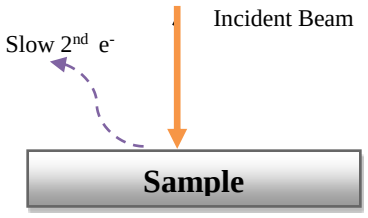	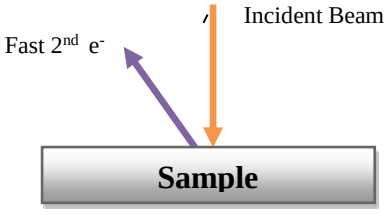	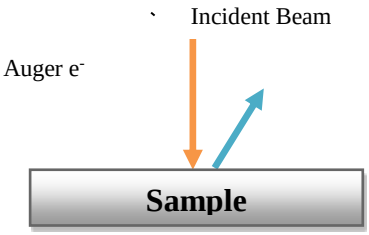

4.2.3. Applications of SEM

Plenty of cutting edge industrial, commercial and research areas have made use of SEM for multiple characterizations and studies. Some of these areas are materials science, particularly in nanotubes and nanofibers, mesoporous architecture and alloy strength, all manipulate the SEM for research, characterization and advancements.

Chapter Five

Thermo-mechanical Characterization

This chapter gives an elaborate explanation on the concept of DMA characterization technique. It involves the viscoelasticity models of polymers as well as polymer composites. The brief yet critical explanation given on this chapter gives the base that will help understand the methods used in the methodology section as well as the results found along with their interpretations.

5.1.Dynamic Mechanical Analysis (DMA)

5.1.1. Definitions

DMA is a material characterization technique that gives information on bulk properties and thermal transitions. Bulk properties of a material are defined by its grain size and grain size distribution, as well as by its bulk density. DMA is a measurement by which sinusoidal stress or strain is given as the input, and the strain or stress, respectively is measured as out puts that give information about the property of the polymer [55]. It is used to analyze the viscoelasticity of polymers or polymer composites. This is because of the fact that the properties measured on this technique are:

- **The dynamic modulus:** Which is a ratio of stress to strain under vibratory conditions and
- **Damping Coefficient:** Which is a materials property that indicates whether a material will bounce back or return energy to a system.

Both the properties mentioned above change significantly when crystalline structures transition to amorphous phase.

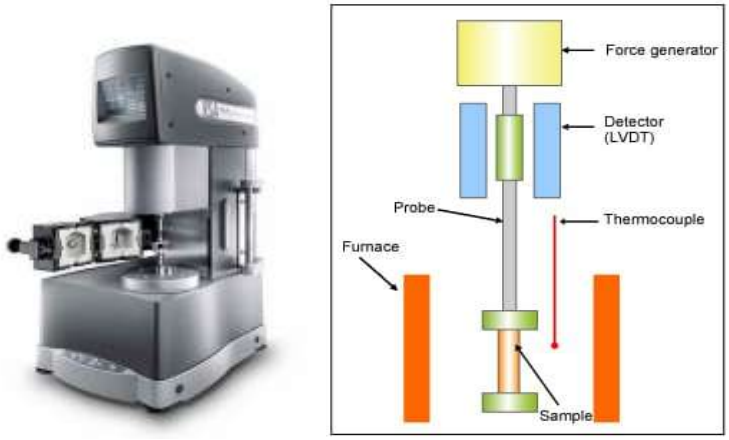

Figure11: Schematic diagram of DMA [56]

5.1.2. Operational Principles

On DMA characterization technique, a sinusoidal stress is applied on a certain sample material and the strain in the material is measured allowing one to determine the complex modulus. Modulus is a mechanical property that measures the stiffness of a material. It defines the relationship between stress and strain in a material in the linear elasticity regime of a uniaxial deformation.

DMA is carried out in torsion with a rotational rheometer when the temperature is continuously changing. When temperature is continuously changing, the material is exposed to oscillatory shear. DMA is a thermo-mechanical characterization technique that enables to identify three major properties which will help to get to a conclusion about the behavior of the sample under study. Temperature of the sample or the frequencies of the stress are often varied leading to variations in the complex modulus [57]. This is useful to locate two major concepts. These are:

- The glass transition temperature of material and
- Identifying transitions corresponding to molecular motions

The three major types of output data being dealt with while working on DMA characterization are given below [58].

I. Loss Modulus (E'')

The loss modulus is a representation of the viscous properties of a certain sample material under study. The viscous stress is used to calculate the viscous modulus thus calculating the loss modulus. Viscous Modulus is a measure of the energy dissipated (lost) as heat.

II. Storage Modulus (E')

The storage modulus is a representation of the elastic properties of a certain sample material under study. The elastic stress is used to calculate the elastic modulus thus calculating the storage modulus. Elastic modulus is a measure of the recoverable stored strain energy.

III. Loss (Damping factor) ($tan\ \delta$)

The loss or damping factor is the ratio of the loss modulus and storage modulus. Damping modulus is a very good measure of the leather like midpoint between the glassy and rubbery states of a certain material under investigation.

5.1.3. Application of DMA

DMA can be used to test the mechanical properties of a polymer nanocomposite. Polymer deformation is highly dependent on time. Moreover, their response to a load or deformation in some cases depends on previous load, deformation or temperature history [59]. This time dependence is seen in two forms. These are:

- **Creep**: which is a progressive increase in deformation under a constant stress
- **Stress relaxation**: This is a gradual decrease in stress under a constant deformation.

5.2.Models of viscoelasticity

Materials in any area of application exhibit certain type of properties based on many factors. This master thesis mainly revolves around the idea of actuation and the actuation achieved by electrospun PLA/MWCNTs nanocomposite fibers. As it was described earlier in previous chapters, actuation is a movement resulting from an input stimulus from the sensor section of a certain system. This can give us the ground to conclude that actuation and deformation refer to the same thing while dealing with material property.

Based on their deformation or actuating property, materials can be classified in to three [59]. These are:

- Elastic materials
- Viscous materials
- Viscoelastic materials

Elastic materials are type of materials that deform instantaneously when stretched and then instantaneously get back to its original configuration when the load (stress) is removed.

Viscous materials are type of materials that possess time dependent behavior when load (stress) is applied on them. They deform constantly under constant stress and when the stress is removed it stays as it is and forgets its original configuration.

Viscoelasticity is the property of materials that exhibit both viscous and elastic characteristics when undergoing deformation. It is a property that represents both viscous and elastic behavior; which also means that the material possesses both fluid like and solid like behavior.

Viscoelastic materials have elements of both viscous and elastic properties exhibiting time dependent strain showing a ‘fading memory’. There are two major categories of Viscoelasticity models of which plenty of other detailed models are included under. These are:

- Linear Viscoelastic models
- Non-linear Viscoelastic models

Linear Viscoelasticity

Linear Viscoelasticity is a property of a material which possesses a linear relationship between stress and strain at any given time.

Stress α Strain

The strains are required to be small so that the engineering strain measures can be manipulated. Linear Viscoelasticity is a reasonable approximation to the time dependent behavior of metals and ceramics under relatively low temperature and low stress. But, the most common application of linear viscoelasticity is in the modeling of polymers and polymer composites [59].

1. Spring (Elastic) Model
2. Dashpot (Viscous) Model
3. Maxwell Model
4. Kelvin/Voight Model
5. Three elements Model
6. Four element Model
7. Generalized Model
    a. Generalized Maxwell model
    b. Generalized Kelvin Chain

5.3.Standard Linear Solid Model

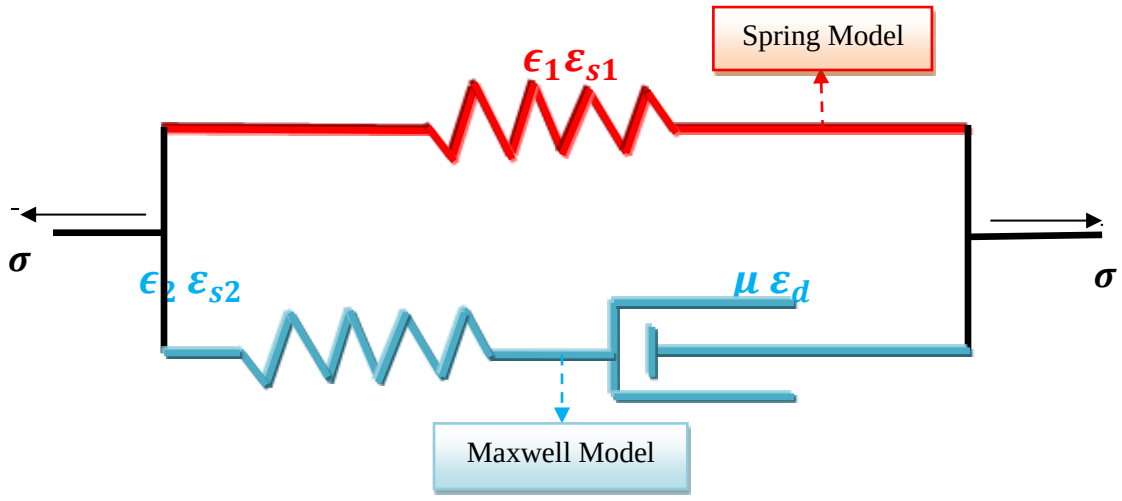

Figure 12: Standard Linear Solid model

Where, σ is applied stress

$\varepsilon_d$is strain of viscous element

$\varepsilon_{s1}$is strain of spring element

$\varepsilon_{s2}$is strain of spring element

$\dot{\varepsilon}$is strain rate

$\dot{\sigma}$is stress rate

μ is the viscosity of the dashpot and

$\epsilon$is the stiffness of the spring

As shown on the diagram above, the Standard Linear Solid model (SLS) is a parallel combination of the elastic spring model and the Maxwell model.

5.3.1. Static Loading

The first crucial step towards deriving the general equation of the three-element model is to mathematically represent the stress and strain relationship between the different elements that are connected in parallel connection and in series connection in the model shown on the figure above.

In elements that are connected in series, the applied stress is equal in all the elements.
In elements that are connected in series, the applied strain is the summation of the strain in all the elements.
In elements that are connected in parallel, the applied stress is summation of the stress in all the elements.
In elements that are connected in parallel, the applied strain is equal in all the elements.

To better understand the chosen viscoelasticity model, it would be smart to look at the two simple models connected in parallel individually. These models are clearly discussed in chapter four of this paper; the spring model and Maxwell model.

The spring model

$$\sigma_{s1} = \varepsilon_{s1}\epsilon_1$$

The Maxwell Model

$$\dot{\varepsilon_{max}} = \frac{\sigma_d}{\mu} + \frac{\dot{\sigma_{s2}}}{\epsilon_1}$$

As it was mentioned before, for series connection, stress applied is equal all the elements connected. Therefore, $\sigma_d = \sigma_{s2}$ so, let us rename both as σ_{max} to represent the overall stress applied on the Maxwell model generally.

The three-element model

Based on the fact mentioned on the methodology section, the stress of elements connected in parallel is the summation of the element's individual applied stress.

$$\sigma_T = \sigma_{s1} + \sigma_{max}$$

It is known that for elements connected in parallel connection, strain is equal in all elements. Therefore, we can use $\varepsilon_{s1} = \varepsilon_{max} = \varepsilon_T$

$$\sigma_T + \frac{\mu}{\epsilon_2}\dot{\sigma_T} = \varepsilon_T\epsilon_1 + \mu\left(\frac{\epsilon_1 + \epsilon_2}{\epsilon_2}\right)\dot{\varepsilon_T}$$

Three element model equation is the general constitutive equation of the SLS three element model. It is written on the standard form which requires the stress to be on the left and the strain on the right. A lot can be understood from this general function once the raw data of the stiffness, coefficient of viscosity and stress values are inserted and the required relations are computed and plotted.

Creep Test

One of the two most important tests performed to make a thorough study of the viscoelastic behavior of a material is the creep test. The test makes use of a constant stress and studies the deformation that takes place on the material. Going back to some of the basic contents discussed in chapter four, particularly the Maxwell and Kelvin-Voight model, a conclusion about the two different springs that are included in the model selected for this research project.

- If $\epsilon_1 > \epsilon_2$, ϵ_2 will deform after the dashpot
- If $\epsilon_2 > \epsilon_1$, ϵ_1 will deform after the dashpot
- Dashpot element deforms first and remains in its deformed state when load is removed but the springs try to restore to their initial stress.

$$\sigma_T + \cancel{\frac{\mu}{\epsilon_2}\dot{\sigma_T}} = \varepsilon_T\epsilon_1 + \mu\left(\frac{\epsilon_1+\epsilon_2}{\epsilon_2}\right)\dot{\varepsilon_T}$$

On creep test, stress has a constant value. Thus, stress rate or the first order derivative of stress is zero $\sigma_T = 0$ and initial strain $\varepsilon = \varepsilon_0$.

$$\varepsilon_T = \varepsilon_0 e^{-\frac{\epsilon_1}{\mu\left(\frac{\epsilon_1+\epsilon_2}{\epsilon_2}\right)}t} + \frac{\sigma_T}{\epsilon_1}\left(1 - e^{-\frac{\epsilon_1}{\mu\left(\frac{\epsilon_1+\epsilon_2}{\epsilon_2}\right)}t}\right)$$

This is the final equation that will later be used to in detail describe a material's property under constant stress. As it is seen above that the strain or deformation, even more suited to the objective of this research project, the actuation of the material is clearly represented along with the factors that affect the actuation or deformation. As it will be in detail presented on the methodology section of the paper, this equation is applied to plot the strain of the material versus time by making use of MATLAB.

Stress Relaxation Test

Stress relaxation is in contrast to creep test a measure of the stress under constant strain. It represents the gradual decay of stress while the deformity of the material is kept constant.

In order to derive the general equation of stress relaxation test, there are two pre-conditions. Since strain is constant $\dot{\varepsilon_T} = 0$ and initial stress, $\sigma = \sigma_0$.

$$\sigma_T = \sigma_0 e^{-\frac{t}{\frac{\mu}{\epsilon_2}}} + \varepsilon_T \epsilon_1 \left(1 - e^{-\frac{t}{\frac{\mu}{\epsilon_2}}}\right)$$

The stress relaxation general equation given on the equation is a mathematical representation of the gradual decrease of the stress under constant strain. This gradual decrease of the stress of a material is a manifestation of the mechanical property of the material and it is a clear presentation of the transition point of the material from glassy to rubbery state. The master curve is a plot of the stress relaxation represents the materials property at the glass transition temperature. As temperature goes above or below that, the stress relaxation plots will be presented above and below the master curve showing positive and negative shifts.

5.3.2. Dynamic Loading

Dynamic mechanical thermal analysis is a thermal analysis technique that measures the property of materials as they deform under periodic stress. The variable sinusoidal stress results on sinusoidal strain of the material. Creep and stress relaxation of a step excitation do not give adequate information about the sudden response of a material. Often creep and stress relaxation of step excitation provides test data ranging from 10 seconds to 10 years. But it is important to know the response of materials to stress in a very short duration.

Harmonic excitation is a sinusoidal external force of a certain frequency applied to a system. Using the concept of harmonic excitation helps to realize the response of material within a short period of time such as seconds and microseconds. This research project is mainly concerned with thermal characterization and morphological characterization of PLA/MWCNT nanocomposite. The thermal characterization is done by making use of DMA/DTMA and by the thorough analysis of the data acquired from the technique.

For harmonic excitation, the stress and strain functions become sinusoidal functions. They can be represented as either a cosine function or sine functions.

Harmonic stress

$$\sigma(t) = \sigma_0 \cos \omega t \quad \textbf{Or} \quad \sigma(t) = \sigma_0 \sin \omega t$$

Harmonic strain

$$\varepsilon(t) = \varepsilon_0 \cos(\omega t - \delta) \quad \textbf{Or} \quad \varepsilon(t) = \varepsilon_0 \sin(\omega t - \delta)$$

Where, σ_0 is initial stress

ε_0 is initial strain

ω is the angular frequency

t is time and

δ is the loss angle representing the lag or lead of the stress and strain

As it was mentioned several times in previous chapters, DMA has three major outputs. These are the storage modulus, loss modulus and tan δ. The third output, tangent delta, is a representation of the lagging or leading of the stress behind the strain or the vice versa. The degree of lagging or leading on its own is a manifestation of the viscose, elastic or Viscoelastic property of a material.

- If $\boldsymbol{\delta = 0}$……then stress and strain are in phase. This is an indication of elastic property of a material.
- If $0 < \delta < \frac{\pi}{2}$ ……then stress and strain are slightly out of phase. This is an indication of viscoelastic property of a material.
- If $\boldsymbol{\delta = \frac{\pi}{2}}$……...then stress and strain are completely out of phase. This is an indication of viscous property of a material.

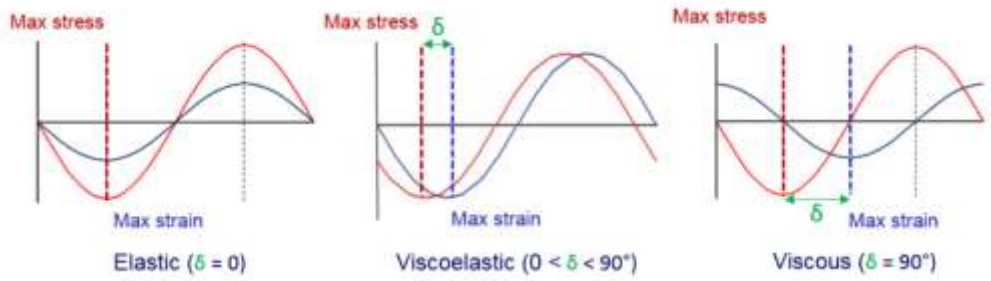

Figure 13: tan δ phase shift description [60]

Complex Compliance

J_1 and J_2 are measures of how in phase or out of phase stress and strain are.

$$J_1 = \frac{\varepsilon_0}{\sigma_0}\cos\delta \text{……..…. Storage Compliance}$$

$$J_2 = \frac{\varepsilon_0}{\sigma_0}\sin\delta \text{…….…….Loss Compliance}$$

$$J^* = J_1 + J_2 \text{…….....Complex Compliance}$$

Complex Modulus

E_1 and E_2 are measures of the response in or out of phase.

$$E_1 = \frac{\varepsilon_0}{\sigma_0}\cos\delta \ldots\ldots\ldots\ldots\ldots\ldots\text{Loss Modulus}$$

$$E_2 = \frac{\varepsilon_0}{\sigma_0}\sin\delta \ldots\ldots\ldots\ldots\ldots\ldots\text{Storage Modulus}$$

$$E^* = E_1 + E_2 \ldots\ldots\ldots\ldots\ldots\ldots\text{Complex Modulus}$$

The relationship between complex compliance and complex modulus is $\boldsymbol{J^*E^* = 1}$.

Creep Test

For constant stress,

$$\varepsilon(t) = \frac{1}{\omega}\left(\frac{\sigma\epsilon_2}{\mu(\epsilon_1+\epsilon_2)} - \frac{\epsilon_1\epsilon_2\varepsilon_0\cos\delta}{\mu(\epsilon_1+\epsilon_2)}\right)\sin\omega t + \frac{1}{\omega}\left(\frac{\epsilon_1\epsilon_2\varepsilon_0\sin\delta}{\mu(\epsilon_1+\epsilon_2)}\right)\cos\omega t$$

Loss Compliance J_1 is the coefficient of $\sin\omega t$.

Storage Compliance J_2 is the coefficient of $\cos\omega t$.

Complex Compliance is $J^* = J_1 + J_2$

Stress Relaxation

For constant strain,

$$\sigma_T = \left(\frac{-\epsilon_2\epsilon_1\varepsilon_0}{\omega\mu} + \frac{\epsilon_2\sigma_0\cos\delta}{\omega\mu}\right)\sin\omega t + \left(\frac{\epsilon_2\sigma_0\sin\delta}{\omega\mu}\right)\cos\omega t$$

Loss Modulus, E_1 is the coefficient of $\cos\omega t$.

Storage Modulus $E_2$is the coefficient of $\sin\omega t$.

Complex Modulus is $E^* = E_1 + E_2$.

The raw data are loss modulus, storage modulus and tan delta. Therefore, to find the stiffness of the two spring elements on the three-element model that was chosen for this research project, they have to be indirectly calculated in order to be exploited to interpret the property of the PLA/MWCNT nanocomposite fibers under investigation.

Chapter Six

Methodology

As it was mentioned plenty of times on the previous sections of this research project, the fibers whose characterization technique's output is being analyzed on this research project was generated in the University of Martin Luther, Halle, Germany. The raw data that is needed for this research along with the experimental details was provided by the main advisor of this master thesis professor Gyeong-Man Kim. This chapter will cover the methods of analysis used for the raw data analysis acquired by the various characterization outputs of PLA/MWCNTs nanocomposite fibers that are presented on previous chapters.

6.1. SEM data analysis

The details of the characterization technique SEM and the concept of surface polymer morphology have been presented on Chapter Three of this paper. On this section the surface morphology is analyzed. The SEM image analysis is mainly targeting to prove the fiber diameter distribution (Gaussian distribution) of the polymer composites fibers. Two methods were used to identify the normal distribution of the SEM images. These are:

- Manual Measurement
- Automated measurement

The reason why both techniques were used is to minimize the error that can be caused by just using one method. A literature published in 2017 on the characterization of fiber diameter proved that the manual measurement of an SEM image is the perfect proven technique for fiber diameter distribution measurement. But it takes an enormous amount of time and is subjected to human error. So, on this master thesis, in order to prove the normal (Gaussian) distribution of the fiber diameter, not only manual measurement but also automated fiber diameter measurement was used.

6.1.1. Manual Measurement

Manual measurement is basically the process of counting the pixels between the start and end of a certain fiber diameter perpendicular to the fiber axis [28]. Plenty of the literatures published these days concerning the measurement of fiber diameter distribution suggest that the manual measurement of fiber diameter is the best possible way to get a perfect result. The averages of multiple SEM images with variety of magnifications are to be measured on the manual measurement of this master thesis. Therefore, there is a chance of error occurrence due to user error or other factors.

Image J image analysis software, Microsoft excel and Origin pro Graphing and Analysis are the three computer tools. The image data were first investigated for the purpose of identifying the

necessary scaling that is to be used to adjust Image J in to the proper setting to make the manual measurements. Once the scale is set, the manual measurement can be done. As the magnification of the image gets larger the zooming intensity needed also goes high. The same zooming intensity cannot be used to manually measure a 100μm and a 30μm scaled images.

After all fibers in one SEM image are measured, the measured values are summarized on image J in order to identify important values such as standard deviation, mean, lowest and highest fiber diameter. The manual measurement that is done as carefully as possible on a certain image, is automatically saved to Microsoft Excel through the Image J image analysis software. This Microsoft file is used to make the necessary analysis on the measurements acquired. The mean diameter or average diameter and the standard deviation of the fiber diameters that are measured can also be found by using Microsoft Excel. After arranging the fiber diameters on a decreasing or increasing order, the major purpose of using Microsoft Excel is to identify the frequency of occurrence for every fiber diameter that was measured. Microsoft Excel makes use of a ceil type of rounding technique to simplify the process of finding the frequency of occurrence. The bins and frequency value represent the fiber diameters and number of occurrences of each fiber diameter respectively.

Once the frequency of occurrence is identified on Microsoft Excel, the measured diameters and the frequency of occurrence is taken to Origin Pro Graphing and Analysis, which in turn is used to plot the distribution graph of the fiber diameter of the fibers measured. The plot could have been easily made by making use of Microsoft excel but Origin Pro Graphing and Analysis was used to make use of the Gauss fit curve fitting settings. Making use of this gauss fit, the normal distribution of the manual measurement of the distribution of the fiber diameter is represented. This normal distribution is a proof of an improved actuation achieved by an electrospun PLA/MWCNTs nanocomposite fibers.

6.1.2. Automated Measurement

6.1.2.1.Image J (Diameter J)

Diameter J is a validated plug-in of Image J that is created for nanofiber diameter characterization purpose. It is capable of analyzing an image and finding the diameter of nano-and microfibers based on every single pixel value along the axis of a fiber. Based on these pixel values, a histogram plot is produced for diameter of fibers. Not only histogram but also summary and diameter analysis images of the analyzed SEM images are acquired as a result of diameter J plug-in. Mean, mode, maximum and minimum diameter are presented along with the histogram plot and the summary excel files.

Steps of Diameter J

1. Segmentation of image into binary image by making use of the Diameter J segment algorithm of Diameter J plug-in. This algorithm produces sixteen default segmentations. With other undesirable segmentation outputs, a total of twenty-four segmented images appear in the segmented images folder. The selection of the best segmentation image is the tricky part here. But since the fibers are represented by whites and the background by black, it is easy to visually inspect the best segmented image in the montage images by comparing it to the grayscale image prior to segmentation.
2. Segmented image analysis then follows. This is the last but extremely tedious task of this plug-in. Under this analysis, fiber diameter histogram, which represents the plot of fiber diameter distribution, is the major output desired to give the detailed values of counts per image, mean, mode, maximum and minimum diameter values and the standard deviations of diameters measured.

By making use of this automated image analysis software plug-in, the measurement of fiber diameters or more professionally the characterization of the surface morphology is achieved with in a very short period of time. The detailed steps of the Diameter J plug-in have been experimented and tested on MATLAB by using the segmentation, distance transform, Skeletonization and thinning, noise removals such as sliding neighborhood operation, measurement of the intersection points, deleting these intersection points and tracking the diameters of the fiber's algorithms. But it is an extremely tedious task which can easily be done by incorporating the Diameter J plug-in in Image J image processing tool. Even though it is tedious and exhausting to perform the manual measurement, it was worth it when thinking of the extremely accurate result acquired. But the detailed MATLAB steps can easily be done by making use of Diameter J plug-in. There is absolutely no need to go through the preprocessing and processing of the SEM image in MATLAB.

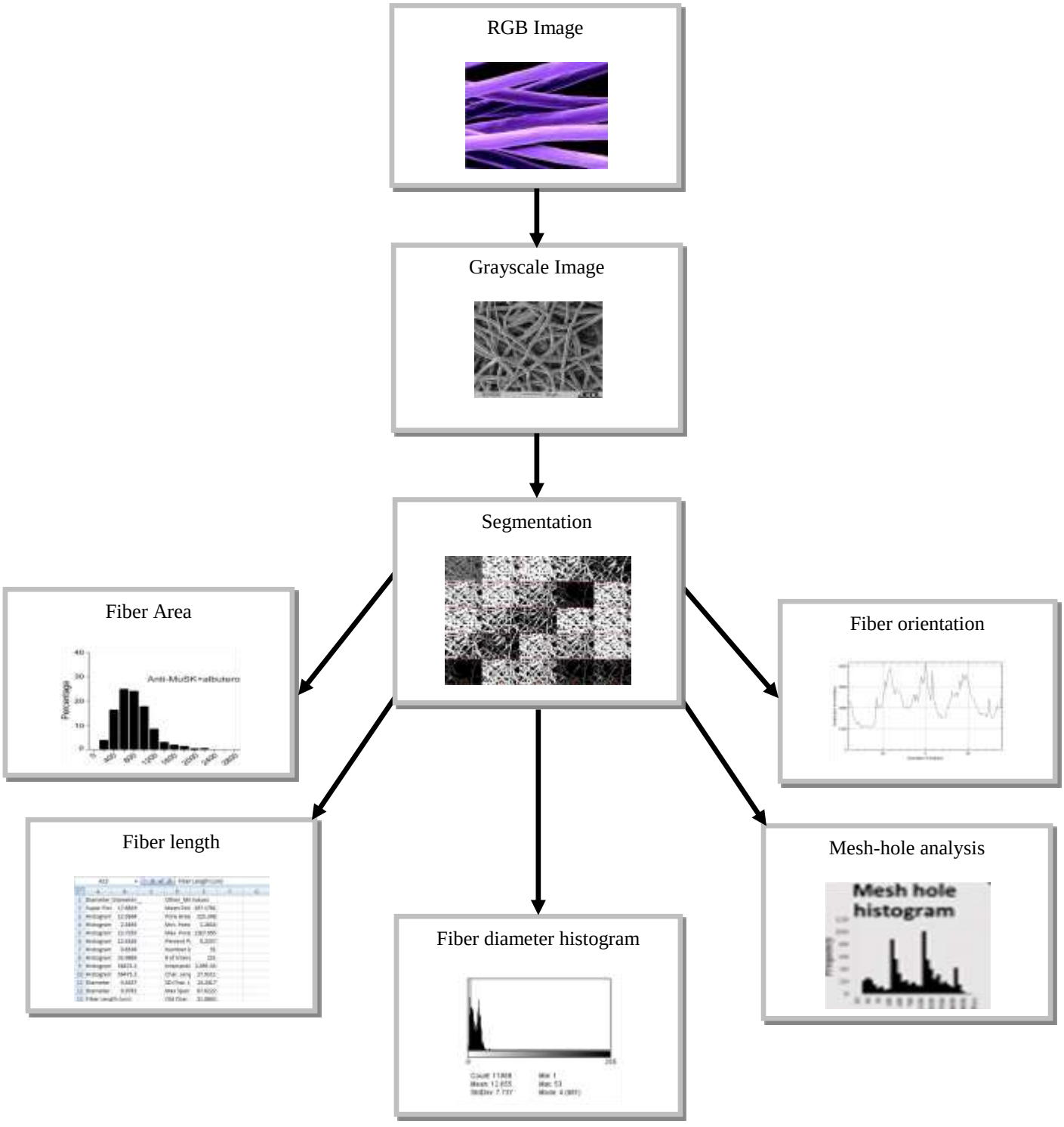

Figure 14: Block diagram of how Diameter J works

6.2.DMA data Analysis

The fiber under study is destined to replace the structure and function of human muscle fiber. In order to be able to compare it with human muscle, it is a necessity to thoroughly investigate its elastic and viscous property. The collective name given to the elastic and viscous property of a material is called Viscoelasticity. The concept of viscoelasticity has already been discussed in the previous Chapter. Therefore, in this section, we will cover the methodology through which the viscoelasticity of a material is studied.

This master thesis uses two widely popular approaches to analyze and discuss the viscoelasticity of the nanocomposite fiber under study. These are;

- Theoretical approach
- Mathematical approach

6.2.1. Theoretical approach

As it was clearly discussed in Chapter Four, the outputs of the DMA data are majorly three. These are the storage modulus (E'), loss modulus (E'') and $tan\ \delta$ (Damping factor). These three outputs are plotted on Origin Pro (data analysis software). The plots are temperature versus modulus plots since the stress applied is IR. From these plots, detailed theoretical explanations concerning the viscoelasticity of the material can be discussed. The viscoelastic property of PLA/MWCNTs composite that is under investigation is clearly discussed and further compared with native human muscles. The protein actions and the MWCNTs action are comparatively discussed.

6.2.2. Mathematical Approach

On this approach, the three data acquired from the DMA are mathematically manipulated to model the viscoelasticity of the PLA/MWCNT nanocomposite fiber. From the variety of Viscoelasticity models discussed on previous chapters, the three-element standard model is to be manipulated to draw conclusions about the viscoelasticity of the nanocomposite fiber.

The first thing needed to be done while mathematically modeling the viscoelasticity of the PLA/MWCNTs nanocomposite fibers under analysis is to thoroughly understand all of the viscoelasticity models discussed in Chapter Four. Once a certain model is selected, three-element model in our case, the data available and how to manipulate it is the second task. The data available on this master thesis is the range of thermal stresses applied on the nanocomposite fiber, the storage modulus (E') which is a representation of the elastic property of the fiber, the loss modulus (E") which is a representation of the viscous property of the fiber and tan δ which is a representation of how in or out of phase the stress and strain are with each other.

A rigorous mathematical computation is required to represent the experimental outputs of DMA. From the static and dynamic loading creep and stress relaxation equations of SLS model, it is

possible to plot the master curve along with the lower and higher thermal stress responses. The process is purely numeric and MATLAB was used for plots presented in the results and discussion chapter of this master thesis.

In order to perform a creep and stress relaxation test on the nanocomposite fibers, it is necessary to consider the general creep and stress relaxation functions of dynamic loading. Since the raw data are loss modulus (E''), storage modulus (E') and $tan\,\delta$ along with the thermal stresses applied, the dynamic loading functions are manipulated in order to find the values of the two spring elements $\epsilon_1$and ϵ_2. These stiffness values of the two spring elements are parts of the most essential inputs for creep and stress relaxation tests.

Creep test general function,

$$\varepsilon(t) = \underbrace{\frac{1}{\omega}\left(\frac{\sigma\epsilon_2}{\mu(\epsilon_1+\epsilon_2)} - \frac{\epsilon_1\epsilon_2\varepsilon_0\cos\delta}{\mu(\epsilon_1+\epsilon_2)}\right)}_{\text{Loss Compliance } (J')}\sin\omega t + \underbrace{\frac{1}{\omega}\left(\frac{\epsilon_1\epsilon_2\varepsilon_0\sin\delta}{\mu(\epsilon_1+\epsilon_2)}\right)}_{\text{Storage Compliance } (J'')}\cos\omega t$$

Stress relaxation function,

$$\sigma_T = \underbrace{\left(\frac{-\epsilon_2\epsilon_1\varepsilon_0}{\omega\mu} + \frac{\epsilon_2\sigma_0\cos\delta}{\omega\mu}\right)}_{\text{Loss Modulus } (E')}\sin\omega t + \underbrace{\left(\frac{\epsilon_2\sigma_0\sin\delta}{\omega\mu}\right)}_{\text{Storage modulus } (E'')}\cos\omega t$$

Therefore,

- $\frac{1}{\omega}\left(\frac{\sigma\epsilon_2}{\mu(\epsilon_1+\epsilon_2)} - \frac{\epsilon_1\epsilon_2\varepsilon_0\cos\delta}{\mu(\epsilon_1+\epsilon_2)}\right) = J''$
- $\frac{1}{\omega}\left(\frac{\epsilon_1\epsilon_2\varepsilon_0\sin\delta}{\mu(\epsilon_1+\epsilon_2)}\right) = J'$
- $\frac{1}{\omega}\left(\frac{-\epsilon_2\epsilon_1\varepsilon_0}{\mu} + \frac{\epsilon_2\sigma_0\cos\delta}{\mu}\right) = E'$
- $\frac{1}{\omega}\left(\frac{\epsilon_2\sigma_0\sin\delta}{\mu}\right) = E''$

The values of the two-spring element stiffness ϵ_1 and ϵ_2 are found by making use of E' and E''. The value of delta is determined from the $tan\,\delta$which is available from the raw output data of the DMA machine. Other unknown values of the function such as viscosity (μ), initial stress (σ_0), initial strain (ε_0) and angular frequency (ω) are taken from existing literatures and basic logical assumptions. By making use of the stiffness values and the other variables found in the general equations, the loss compliance and storage compliance J'' and $J'$are found. The ultimate purpose of finding all the essential variables values is in order to make use of the complex modulus and compliance functions. These functions are used for drawing conclusion about the stress relaxation and creep property of the nanocomposite fiber respectively.

Chapter Seven

Results and discussion

7.1.SEM Data Analysis

The effective physical and mechanical performance of polymer nanocomposite fibers highly depends on the structural characteristics of the nanocomposite. The major structural characteristics that are dealt with are fiber diameter, fiber orientation, pore size, uniformity, fiber crimp…etc. The fiber diameter is one of the most basic structural characteristics to decide the higher specific area.

In order to achieve this photo-induced actuation as best as possible, multiple characterizations have been performed on the resulting nanocomposite. Among these, the major characterization was SEM characterization.

7.1.1. Manual measurement results

Through the SEM characterization, three magnifications have been used for the images. These three magnifications have all been analyzed by making use of Image J, Microsoft Excel and Origin Pro.

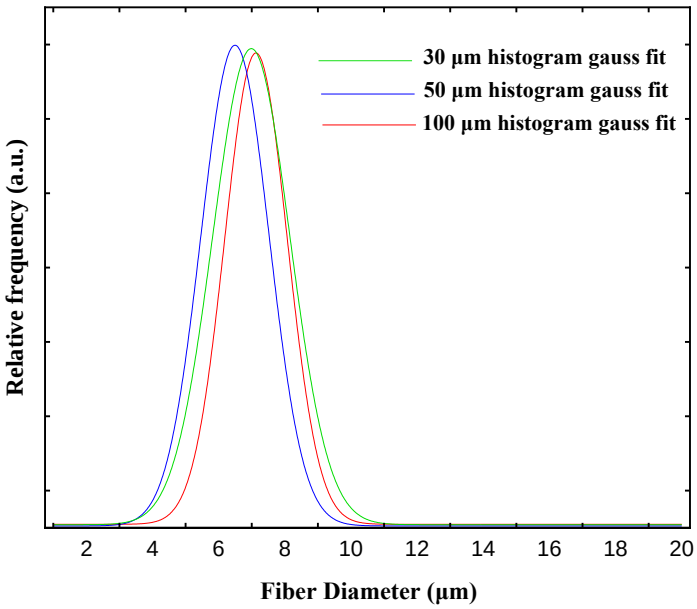

Figure 15: Total fiber Diameter distribution of SEM images

These are the analyzed image magnifications and their amount:

- 30 micrometer images(14 in number)
- 50 micrometer images (4 in number) and
- 100 micrometer images (3 in number)

For each 30-micrometer image, 196% zoom was used and 300 measurements were done for each image. And for each 50-micrometer image, 400 % zoom was used and 500 measurements were done for each image. And for 100 micrometer images, 600% zoom was used and 1000 measurements were done for each image. The plot achieved by the measurement of the images under three magnifications is as displayed below. All have achieved an almost perfect Gaussian distribution function.

Table 5: Measurement Value of SEM images

	30 micrometer (μm) scale Images	50 micrometer (μm) scale Images	100 micrometer (μm) scale Images
Average Value	6.85μm	6.39μm	6.93μm
Standard Deviation (SD)	1.34μm	1.16μm	1.19μm
Maximum value	19μm	12.5μm	15.5 μm
Minimum value	1μm	3.5μm	3.5 μm
Mode (most frequently occurring value)	7μm	6.5μm	7 μm
Number of counts	4200	2000	3000
	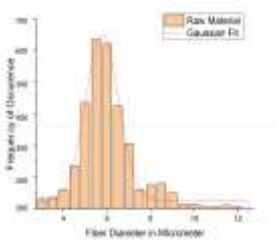	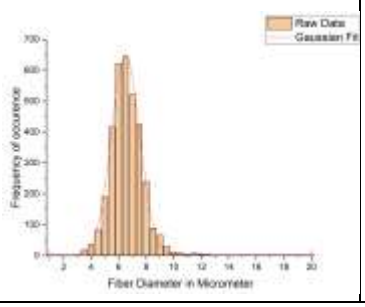	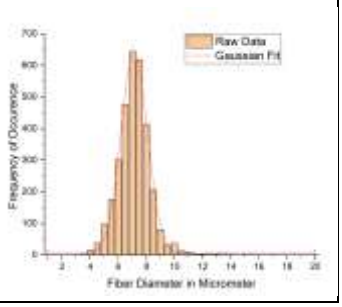

7.1.2. Automated measurement results

The Diameter J plug-in incorporated in the image J image processing tool was able to give the results given below. The hundred micrometer, fifty micrometer and thirty micrometer magnification SEM images were analyzed individually just as the case of the manual measurement. The default segmentation outputs along with the original grayscale image are montage together. After the best segmented image is identified, the diameter analyses steps, the Skeletonization and axial thinning, the Euclidean distance transform and pores area identification are displayed below along with the diameter distribution histogram.

Hundred Micrometer Magnification SEM image Automated measurement

The Diameter J plug-in took 35,177 numbers of measurements by default and did all the analysis incorporated in it. The intention of this particular section is the study of the surface morphology of the nanocomposite fiber under investigation. Thus, only the diameter histogram is presented of all the other plenty analyses done by making use of this plug-in.

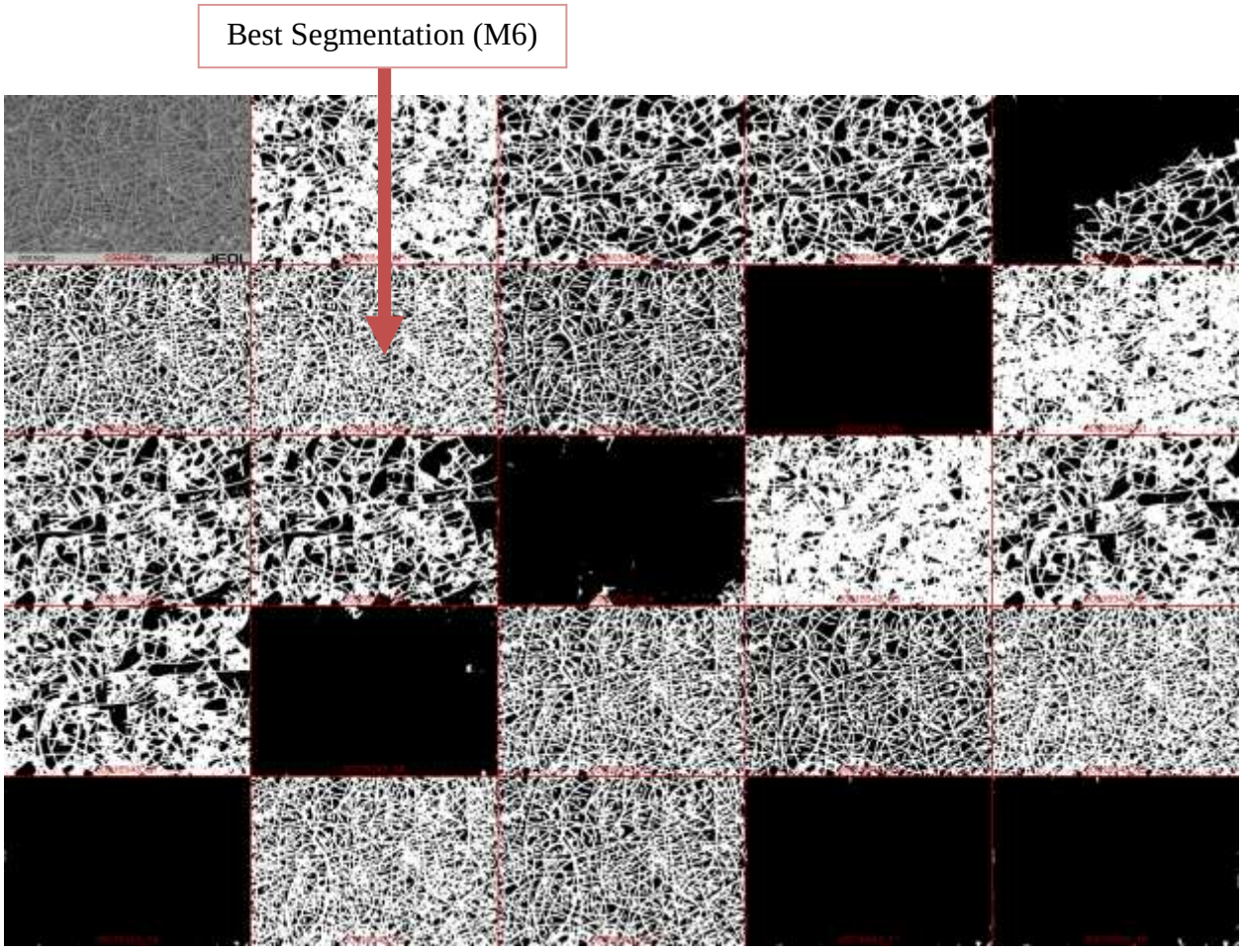

Figure16: Montage of segmented images of 100 micrometer magnification SEM images

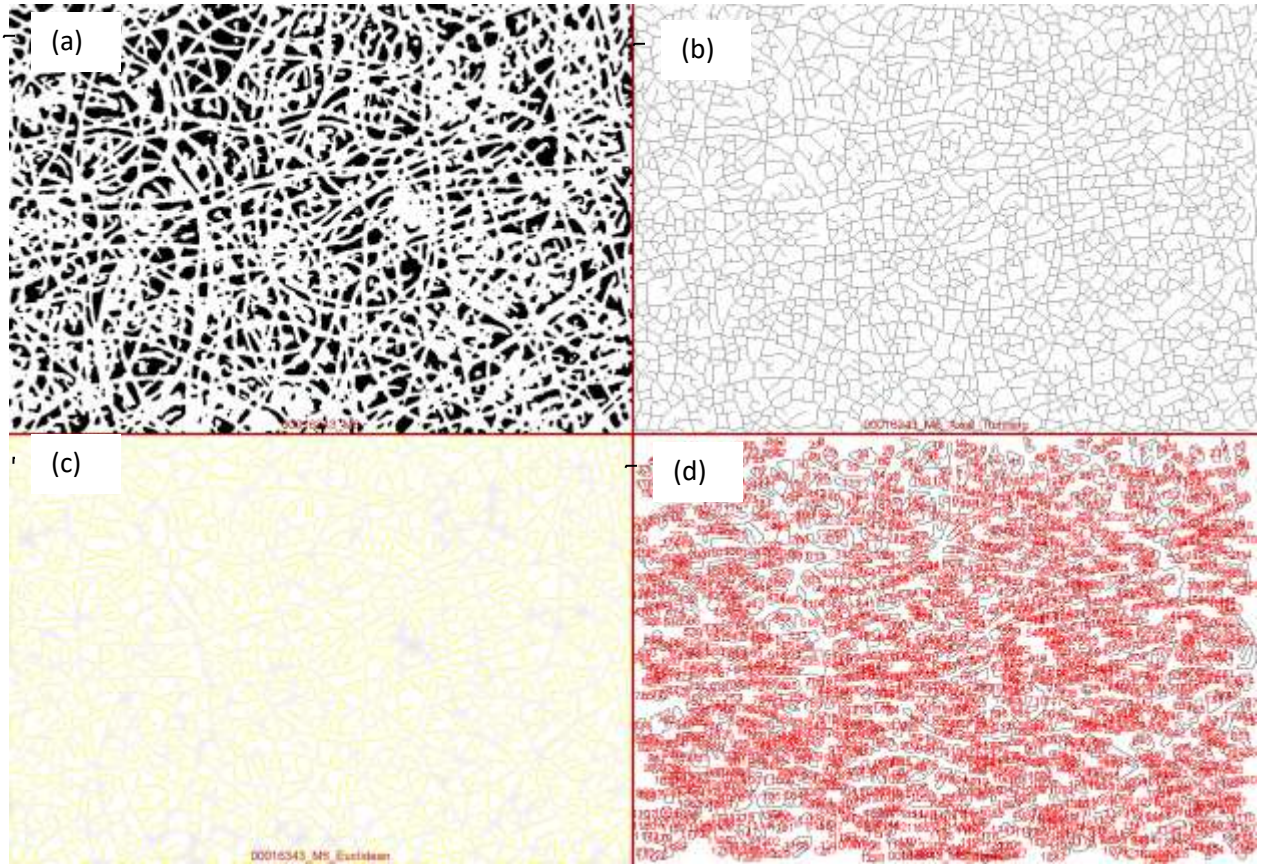

Figure 17 (a) Segmented image (b) Skeletonization/thinning (c) Euclidean distance transform (d) measurement of fiber diameter

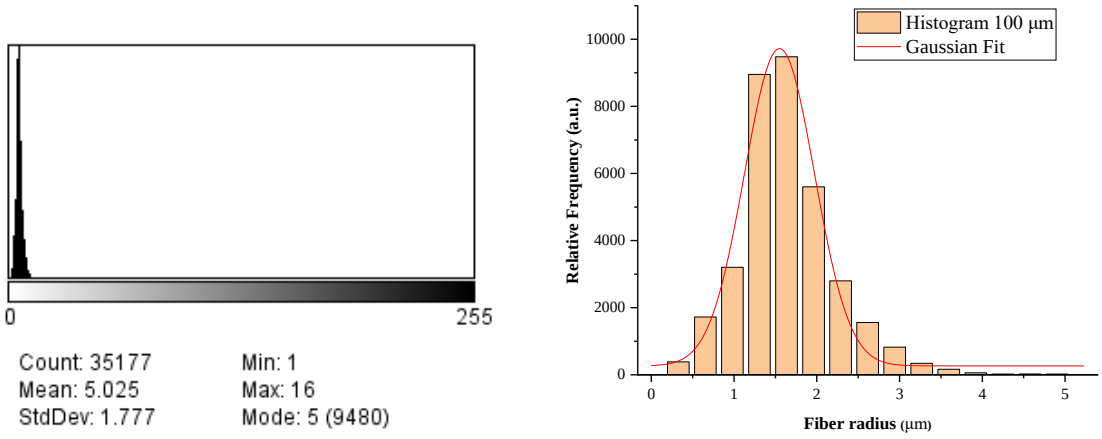

Figure18: (a) Histogram of fiber diameter (b) Gaussian fit of histogram

Fifty Micrometer Magnification SEM image Automated measurement

For the fifty micrometer measurement SEM images, 22,146 numbers of measurements were done. The numbers of measurements are lower than that of the hundred micrometer magnification SEM images. This is due to the fact that when the magnification is higher, the number of measurements should also go higher to make the result more accurate. Not only the numbers of measurements but also the mean fiber diameter, minimum fiber diameter, maximum fiber diameter, mode and standard deviation values have all shown significant raise in their value and it is all because of the higher value of magnification used in the SEM image.

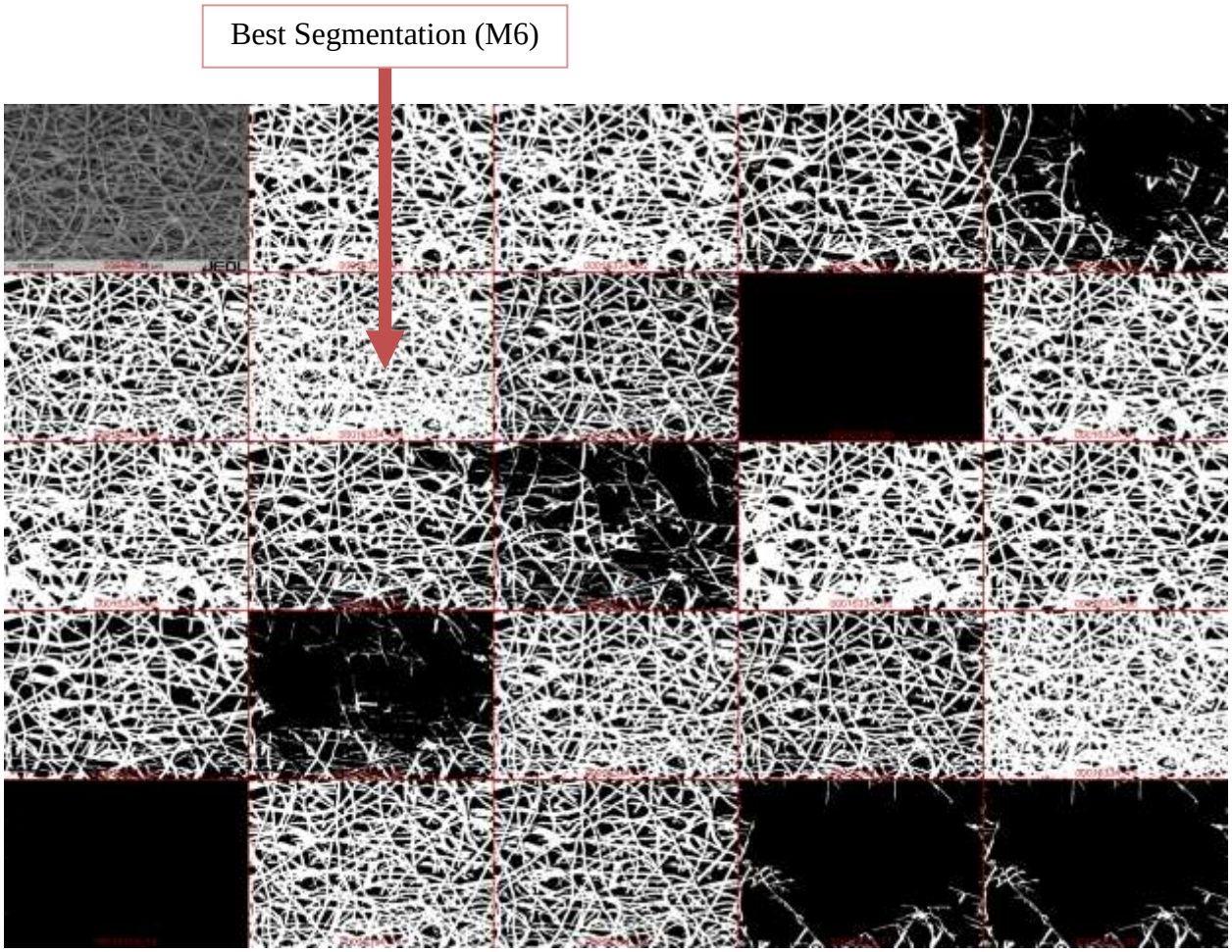

Figure 19: Montage of segmented images of 50 micrometer magnification SEM images

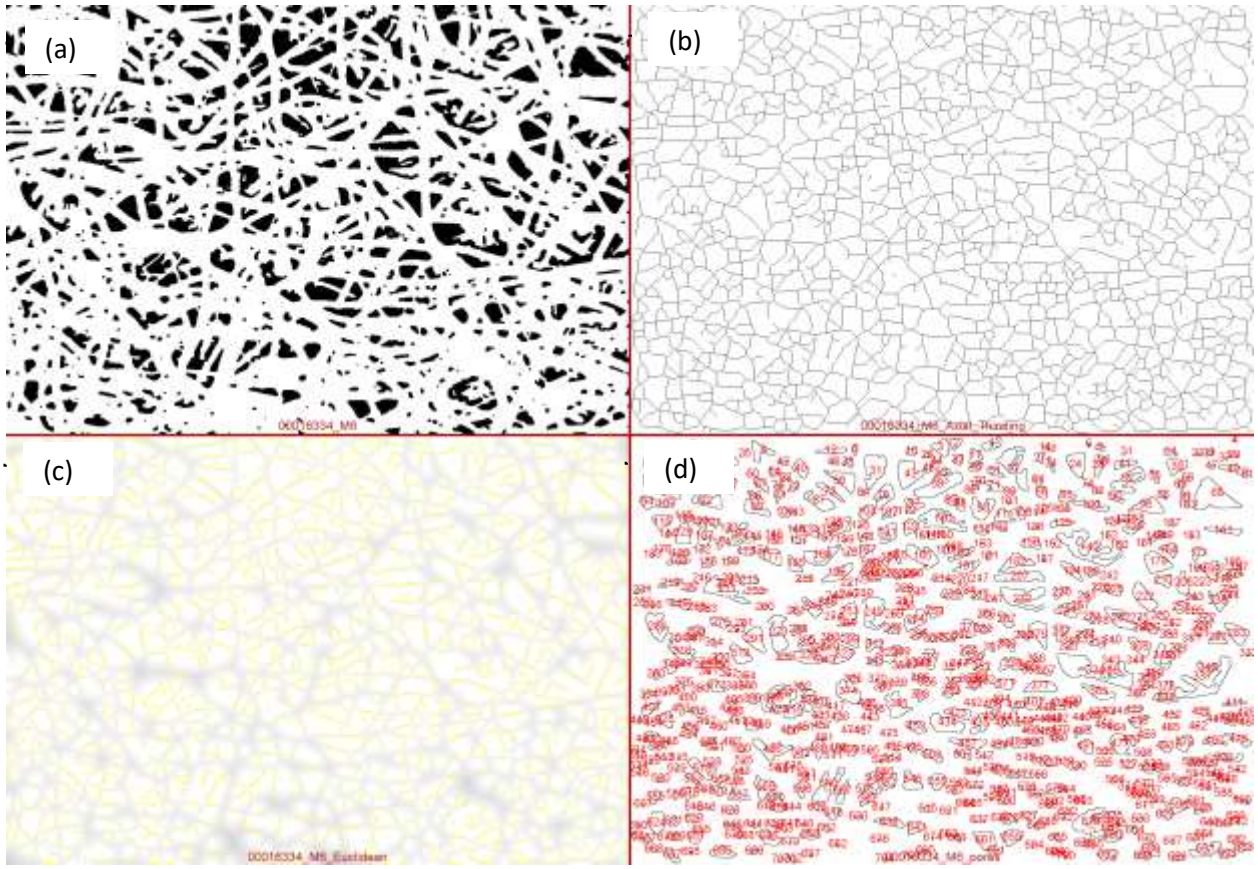

Figure 20: (a) Segmented image (b) Skeletonization/thinning (c) Euclidean distance transform (d) measurement of fiber diameter

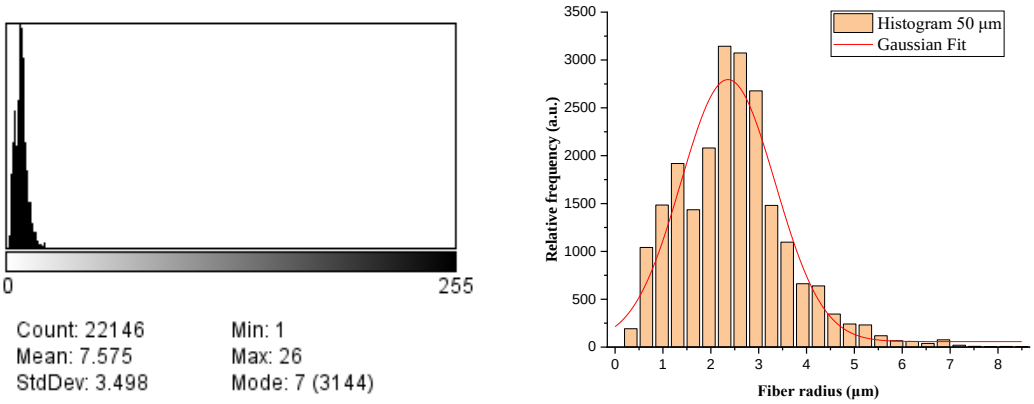

Figure 21: (a) Histogram of fiber diameter (b) Gaussian fit of histogram

Thirty Micrometer Magnification SEM image Automated measurement

The diagrams given below that the show the segmentation, skeletonization/thinning, distance transform and measurement of fiber diameter of the thirty micrometer magnification SEM images, resulted in a histogram that isn't quite a perfect fit to the Gaussian distribution function. This can be easily justified by a literature mentioned back in the manual measurement section. It is a literature published in 2017 on the characterization of fiber diameter that proved the fact that manual measurement is the routine and best method of fiber diameter measurement. Especially for the interlocked fiber SEM images like the one being dealt with on this research project, there is need of an automated measurement system to justify the output of the manual system; the manual measurement outputs still being the best and reliable output to verify the fiber diameter distribution.

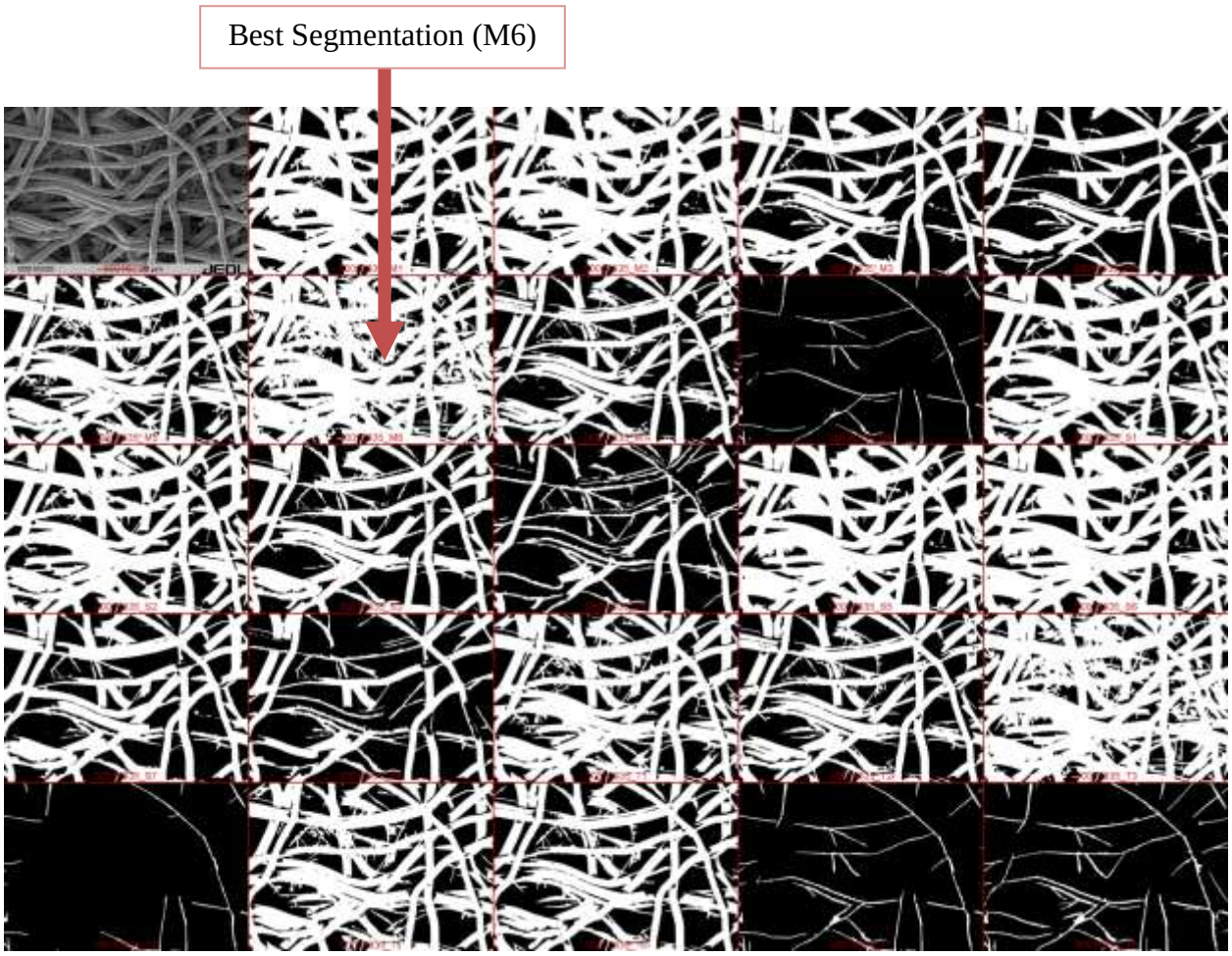

Figure 22: Montage of segmented images of 30 micrometer magnification SEM images

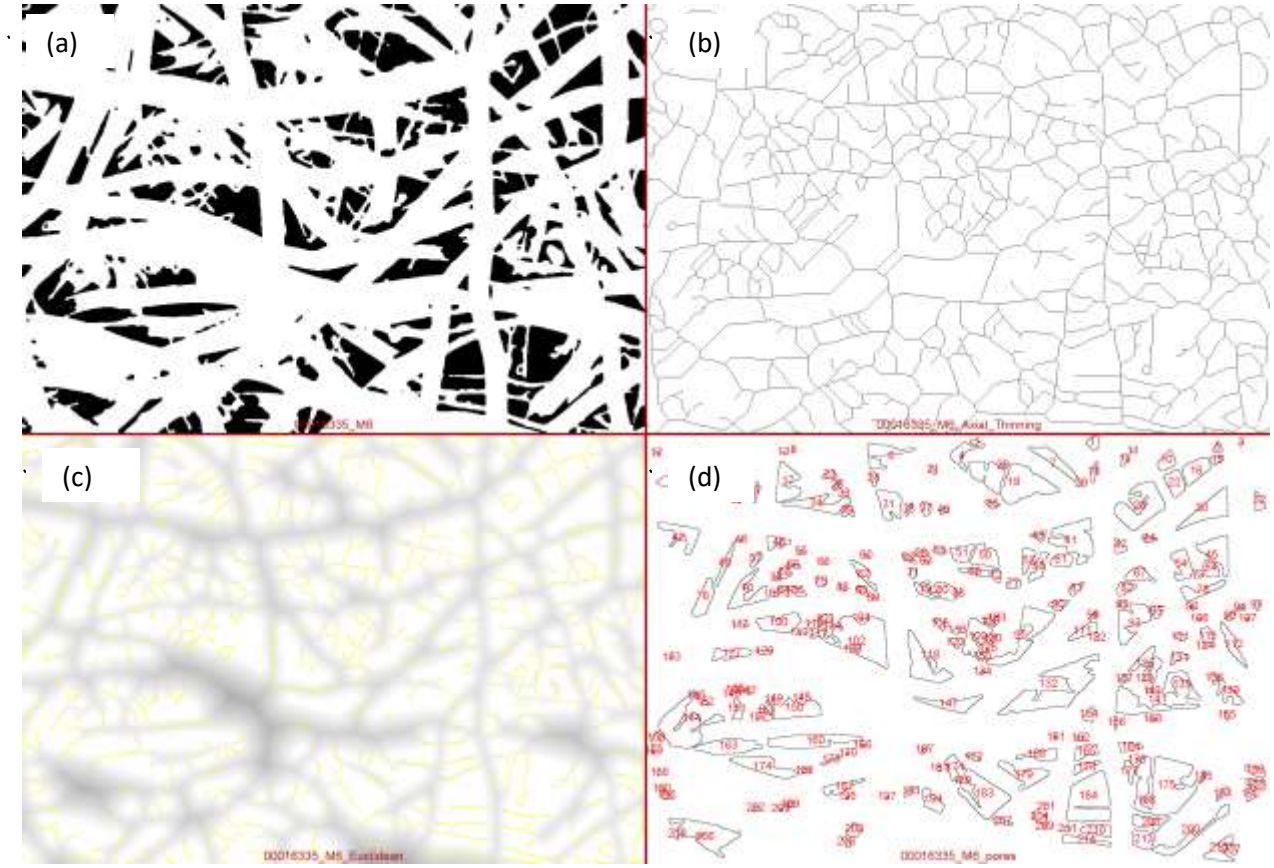

Figure 23: (a) Segmented image (b) Skeletonization/thinning (c) Euclidean distance transform (d) measurement of fiber diameter

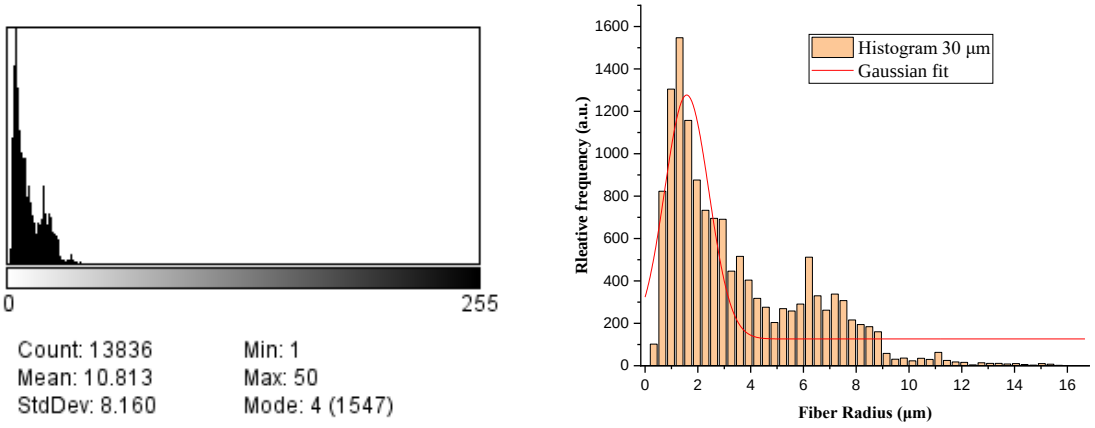

Figure 24: (a) Histogram of fiber diameter (b) Gaussian fit of histogram

SEM Data Analysis Discussion

The fiber diameter characterization done by making use of scanning electron microscopy was mainly by three magnification scales set to 30, 50 and 100 μm. These SEM data analyzed by manual and automated methods gave results showing plots resembling Gaussian distribution curve showing normal distribution of fiber diameters. The average value, standard deviation, the maximum and minimum value and mode of the fiber diameters of manual method and automated methods shown close resemblance with minor effect of the number of counts that are considered on the manual measurement and the default number of counts the automated method makes use of.

The normal (Gaussian) distribution achieved by the electro spun PLA/MWCNT nanocomposite is indicated on the result found by both manual and automated methods to identify the morphology of the nanocomposite. The normal distribution (Gaussian distribution) achieved is an indirect pointer of the great actuating tendency that the nanocomposite fiber is able to perform. By identifying the normal distribution of the diameter of the fibers of the nanocomposite; the specific area, the Rheology study and deformation characteristics of the nanocomposite can be elaborated. And these three factors, specific area, rheology and deformation characteristics highly affect the process of photo-induced actuation of the nanocomposite. The surface area of a material directly correlates with desired material properties such as Reactivity, Dissolution, and Catalysis & Separation. The surface area that is accessible to react with the applied stimulus on the material under investigation has a gigantic impact on the reactivity. On this case the stimulus applied is an IR light whose photons induce the actuation on the nanocomposite fiber is enhanced due to the normal distribution achieved.

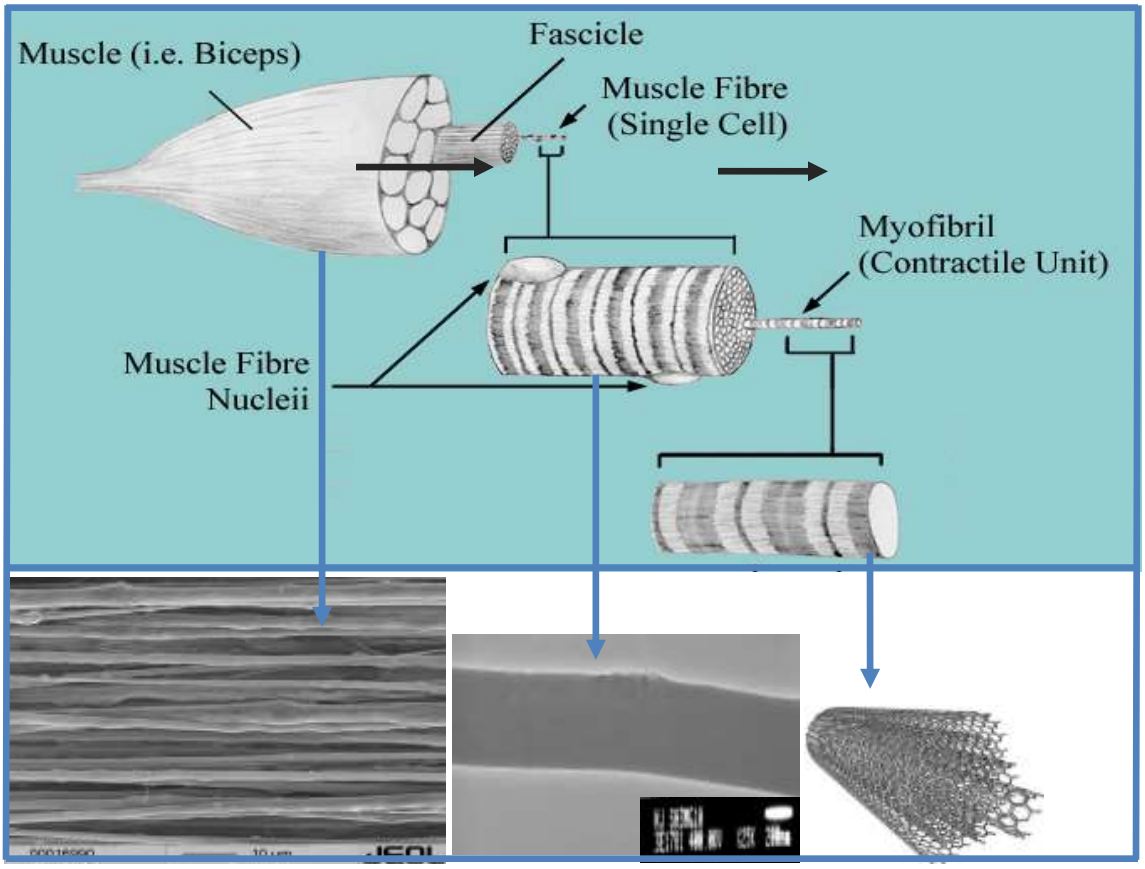

Figure 25: Analogy of nanocomposite structure with skeletal muscle micro-anatomy

(a) (b)

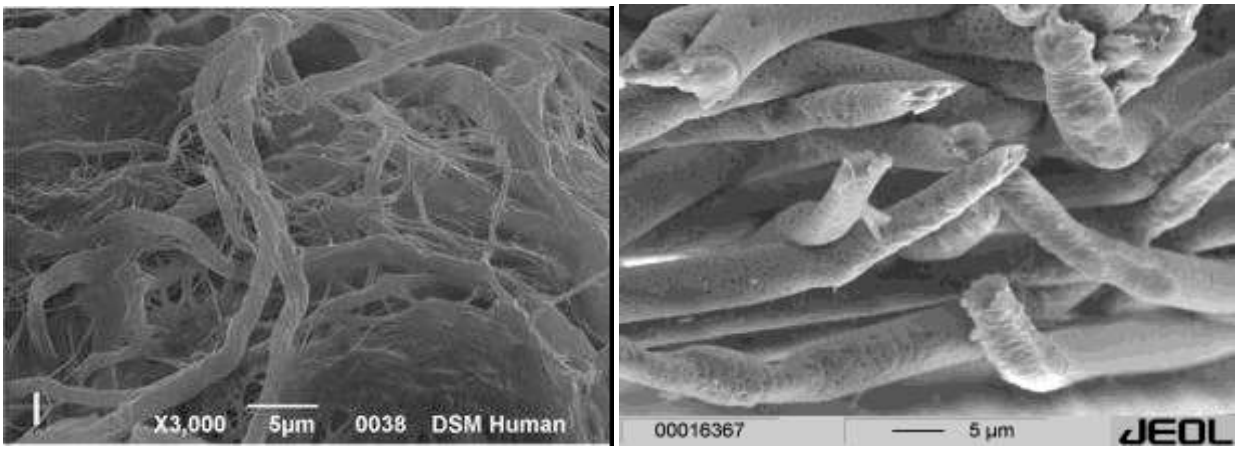

(c) (d)

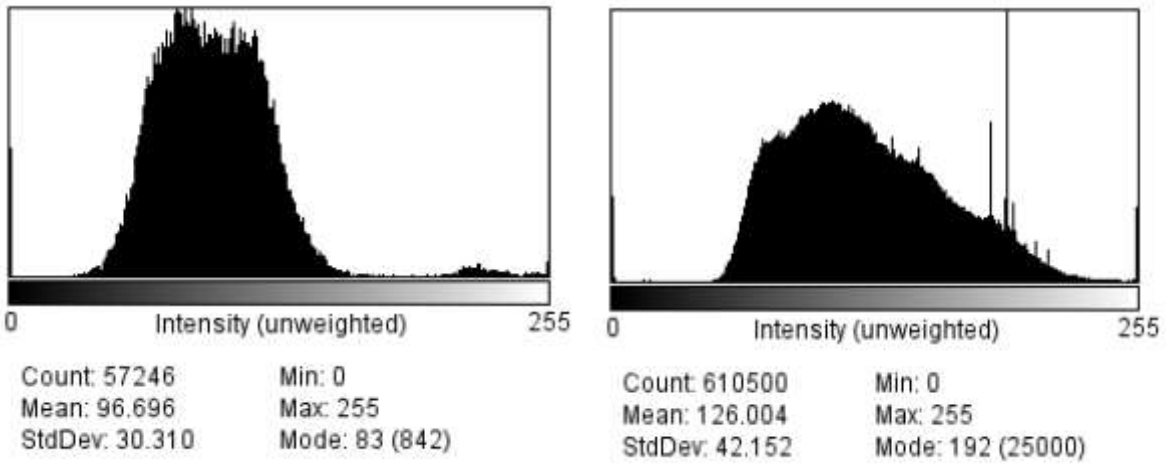

Figure 26: (a) Decellularized skeletal muscle of human (b) Electro-spun nanocomposite fiber SEM image under investigation (c) Histogram of Decellularized Skeletal muscle of Human (d) Histogram of Electro-spun PLA/MWCNT nanocomposite fiber

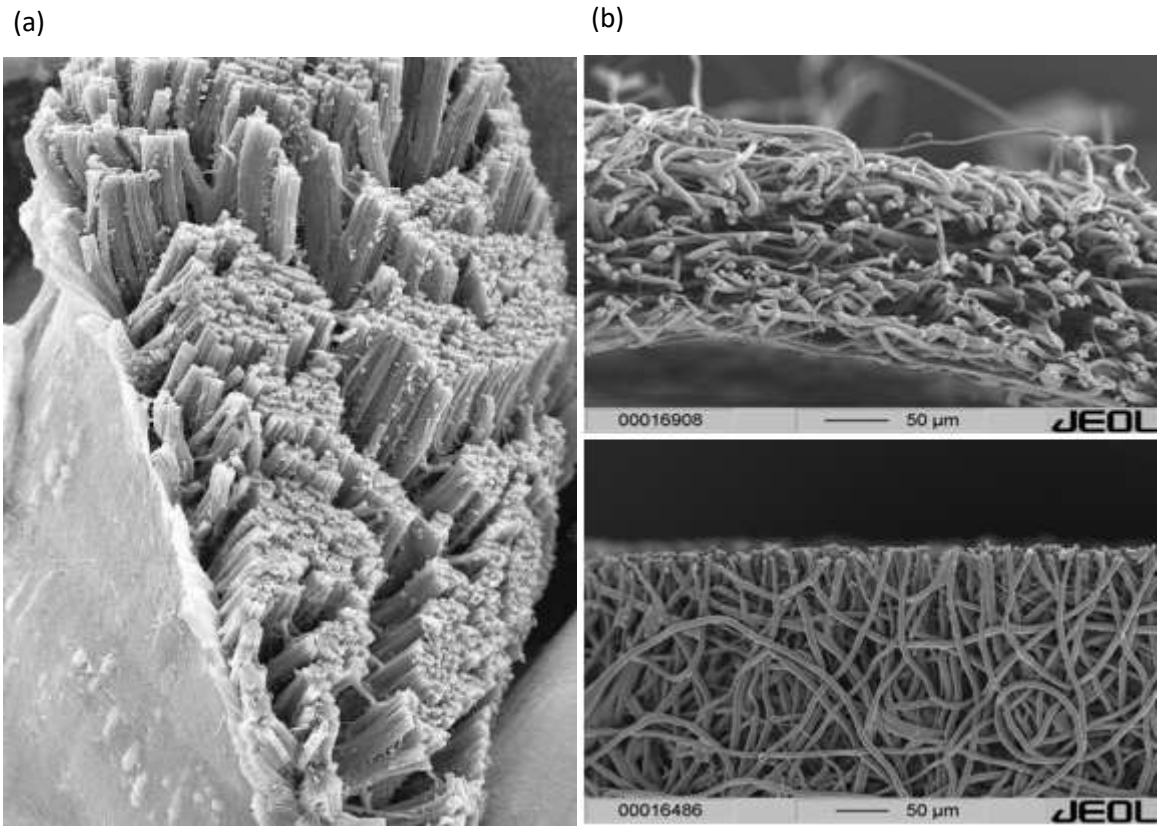

Figure 27: (a) SEM image of human skeletal muscle (b) SEM image of electrospun nanocomposite fiber under investigation

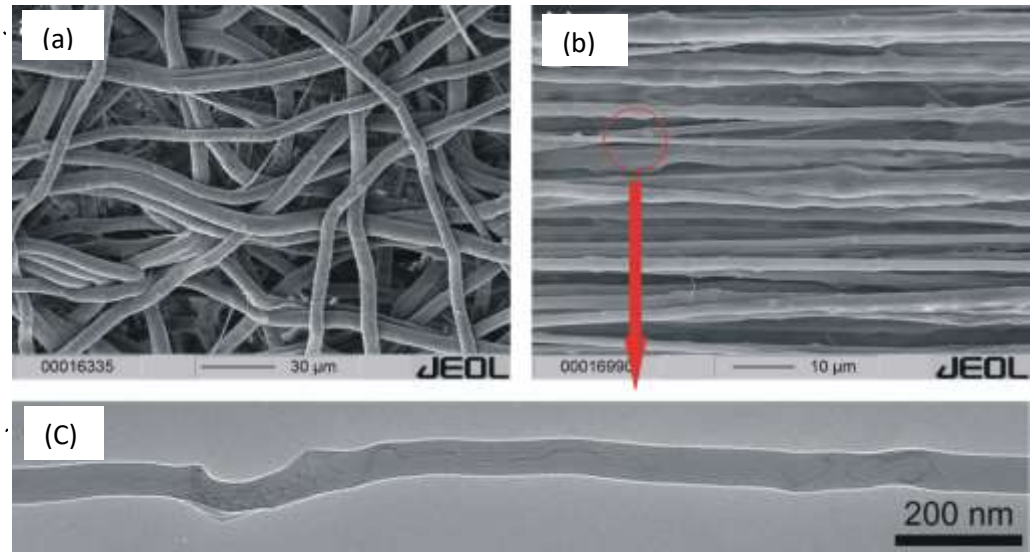

Figure 28: (a) SEM image of the as-electro spun PLA/MWCNT nanocomposite fibers for the bilayer. (b) SEM micrograph of the uniaxially stretched state for the bilayer which was at first uniaxially stretched with a strain of 250% at a temperature of 75ºC and then followed by a quenching at room temperature. (c) TEM image of a single uniaxially deformed fiber form.

7.2.DMA data analysis

7.2.1. Qualitative Analysis

Under this subtopic, the basic requirement for the mechanical behavior of artificially fabricated skeletal muscle fibers is presented with a justification from the DMA characterization output of pure polymer fibers and nanocomposite fibers. The DMA characterization is performed in the Martin Luther University, Halle-Wittenberg, Germany. The raw data from the characterization technique has been provided and the further qualitative and quantitative analysis has been done on this research project. Under the qualitative data analysis, the three data found; loss modulus, storage modulus and $tan\,\delta$ variations of pure PLA and PLA/MWCNTs composite will be thoroughly investigated in relation to the human skeletal muscle property and the required power criteria that need to be considered to use the nanocomposite fiber under investigation for the fabrication of artificial human skeletal muscles.

Contrasting conventional thermal bimorph actuators that consist of two layers with different thermal expansion coefficients and thermal conductivities, the fabricated actuator consists of two identical layers of uni-axially pre-strained electrospun PLA/MWCNT nanocomposite nanofibers. It should be emphasized here that neither the bi-layer composed of as electrospun fibers for the neat PLA nor its stretched version showed discernible responses under exposure to IR irradiation, indicating that they are essentially infrared transparent. Even more, the bi-layer consisted of as-electrospun fibers for PLA/MWCNT nanocomposites also did not exhibit any actuation

characteristics under IR-irradiation. Surprisingly, only uni-axially pre-deformed bi-layers for PLA/MWCNT nanocomposite fibers exhibited the unprecedented actuation behavior.

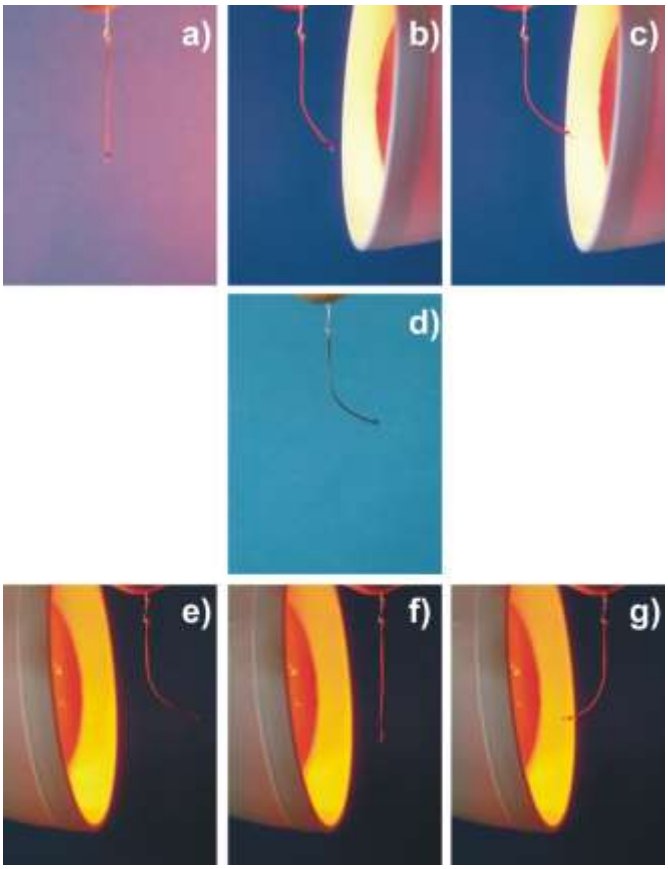

Figure 29: Photo-induced actuation as seen in an optically thick, pre-deformed fiber. Upper images: the fiber was irradiated from the right side: a) t=0 s; b) t= 5 s; c) t = 10 s. Middle image d): a bent state of fiber, at which the IR source was switched off. Lower images: the fiber was irradiated from the left side: e) t = 2 s; f) t = 5 s; g) t= 10 s.

An intriguing photo-induced actuation experiment on the uni-axially stretched bi-layer for PLA/MWCNT nanocomposite fibers is shown in Figure 29, which demonstrates the bending of the actuator at different stages of the IR-irradiation cycles. The first row in the figure shows the bending of the bi-layer, illuminated on the right side. Under IR exposure, after a certain illumination period for reaching an equilibrium temperature through the whole sample, the free-standing bi-layer underwent a distinct anisotropic bending movement towards the IR source. As clearly seen in Figure 29d, upon removal of IR illumination, the bending stopped and the bi-layer was preserved in its last state of shape. This indicates that our actuator is not elastic but just plastic, i.e., irreversible, unlike most conventional polymer actuators based on elastomers which recover their original form after the IR source is turned off. When the IR source was switched on again, the bending motion continued to progress towards the direction of IR-illumination. When the fixed

bent bi-layer was re-illuminated on its opposite side, as shown in Fig. 40e, f and g, the actuator began to bend directly opposite towards the IR-illumination; first being stretched to its original form, and then bent in the opposite direction.

Muscle proteins Vs CNT

In order to fabricate an artificial skeletal muscle fiber, the issue of functionality highly depends on finding a component that can imitate the function of skeletal muscle proteins. This research project suggests the application of MWCNTs to replace or mimic the function of skeletal muscle proteins in the fabricated nanocomposite fiber. In order to show the similar or resembling functionality of MWCNTs with skeletal muscle proteins, the DMA characterization output of pure PLA versus the DMA characterization output of PLA/MWCNT nanocomposite are thoroughly investigated to show the difference of viscoelasticity achieved under thermal stress. The viscoelasticity property gives information about the actuation achieved by the nanocomposite fiber under investigation.

The DMA characterization technique was held in a pure PLA fiber as well as electrospun PLA/MWCNTs nanocomposite fibers. As it was discussed on Chapter Four, the three main outputs that are acquired from a DMA characterization technique are the storage modulus, loss modulus and tan δ.

Table 6: DMA outputs of PLA and PLA/MWCNTs fibers

Parameters	ϵ' minimum (MPa)	ϵ' maximum (MPa)	ϵ'' minimum (MPa)	ϵ'' maximum (MPa)	Tg by $tan\ \delta$	Tg by ϵ''
Pure PLA	5.2	327	0.87	62.5	73.5	68.7
PLA/MWCNTs	1.9	371	0.44	76.1	75.4	67.2

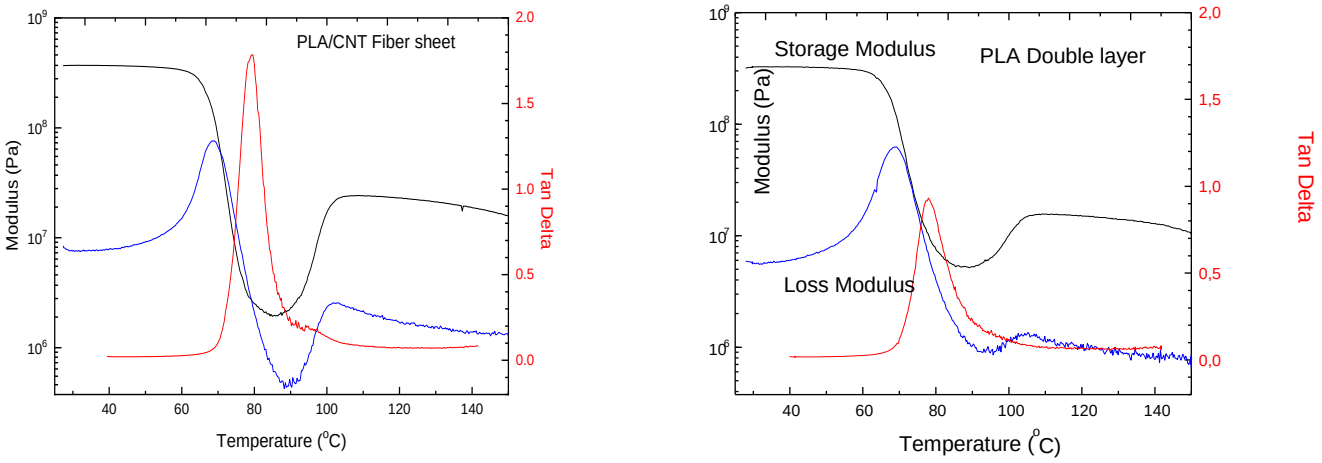

Figure 30: (a) pure PLA DMA outputs (b) PLA/MWCNTs DMA outputs

From the qualitative analysis of the DMA measurements for both pure and nano-composite fibres, the basic differences noticed are listed below:

- Due to the effect of the MWCNTs the storage modulus and the loss modulus increase,
- The increase in tanδ upon adding MWCNTs is almost double,
- The level of storage moduli at the starting temperature (25°C) retain quite constant until approaching the corresponding glass transition temperatures, then decrease rapidly until reaching their minima, and again increase to a certain level, then after decrease moderately with temperature,
- The loss moduli and tan δ undergo distinct maxima when both systems are heated through the grass transition temperatures. With further increasing temperature the loss moduli drop off on the minima, and then increase to a certain level, then after decrease moderately with temperature, whereas the tanδ decrease drastically after passing the glass transition temperature, approaching a certain level and stay at constant level of final value.

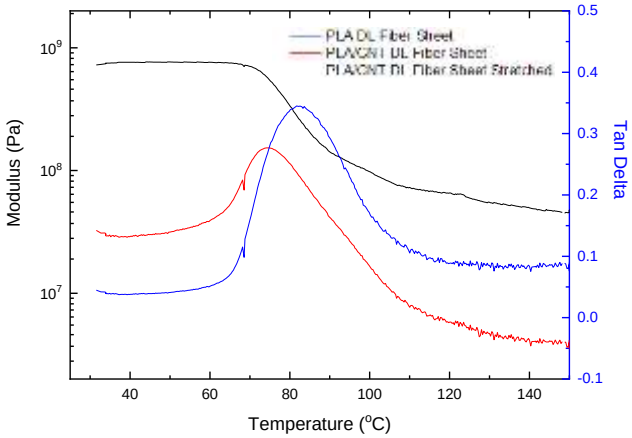

Figure 31: Damping factor variation of pure PLA, PLA/MWCNTs and stretched PLA/MWCNTs

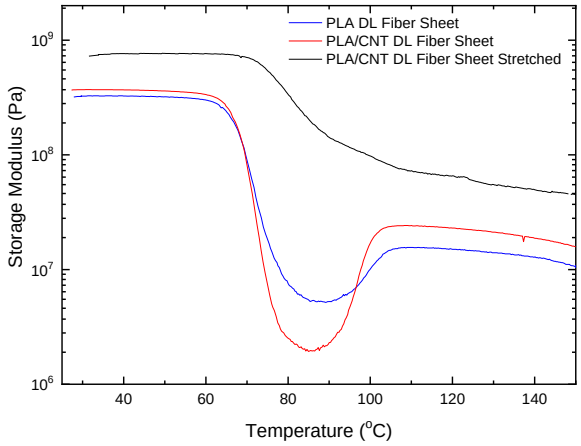

Figure 32: Storage modulus variation of pure PLA, PLA/MWCNTs and stretched PLA/MWCNTs

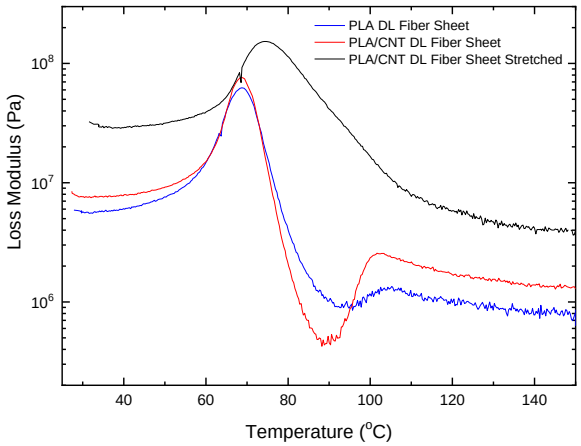

Figure 33: Loss modulus variation of pure PLA, PLA/MWCNTs and stretched PLA/MWCNTs

Interesting feature is the variation in the storage moduli with respect to temperature. After passing the glass transition temperature the moduli drop rapidly, as generally expected, but the minimum level reached in the bilayer composed of electrospun fibers (ESFs) for PLA/MWCNT nanocomposite (1.9 MPa) is considerably lower compared with that of the ESFs for pure PLA (5.2 MPa). In addition, with increasing temperature the slope of decreasing rate in storage modulus for the bilayer of PLA/MWCNT nanocomposite ESFs is much steeper than that of a bilayer for the pure PLA fibers. This may be understood by the fact that the PLA/MWCNT nanocomposite absorbs extensively more thermal energy upon heating during the DMA operation due to extremely high thermal conductivity of MWCNTs; as a consequence, the bilayer of PLA/MWCNT nanocomposite will be softer in this temperature range.

7.2.2. Quantitative Analysis

Under the quantitative analysis of the PLA/MWCNTs nanocomposite fibers, the stress relaxation and creep plots along with the stress versus strain relationship are presented and discussed. Since the stress applied is thermal stress, the three required to investigate the property of the nanocomposite fiber are not only dependent on time but also temperature. To make use of both independent variables at a time, another variable zeta (z) is introduced. Starting from the stress versus strain relationship of the nanocomposite fiber under investigation, the stress relaxation and creep are presented as followed.

Stress Vs Strain

Stress σ_T is the amount of load that is applied on the three-element model. The thermal stress is applied on a form of a photo-induced stimulus by making use of radiation. The range of this thermal stress is ranging from 27^0C to 165^0C. Up on the application of this dynamic thermal stress, the PLA/MWCNT nanocomposite fibers will react by a physical movement. This physical movement is what we have referred to as actuation on Chapter One. The deformation, also known as strain, that varies up on the application of variable dynamic thermal stress is what measures the actuating property of the nanocomposite fibers. Thus, the stress versus strain plot of the nanocomposite fibers is one of the essential results that are needed to draw conclusion about the viscoelastic property of the nanocomposite fibers modeled as a three-element model.

Since the applied stress is thermal stress, there is a need to change the parameter in to a normal stress form that can be scaled by a Pascal unit. In order to do so, we need to use the scientific formula of thermal stress analysis given below.

$$Thermal\ stress = \alpha \times dT \times \epsilon_{storage}$$

Where, α is linear coefficient of thermal expansion

dT is the change in temperature

And $\epsilon_{storage}$ is the storage modulus

Making use of thermal stress equation, the thermal stress applied in temperature ranging from 27.28℃ to 160℃ can be used to present and discuss the viscoelastic property of the PLA/MWCNTs nanocomposite fibers. From the calculated thermal stress and the experimentally provided elastic modulus the strain value can be calculated. Once the stress and strain are calculated, it is possible to model the stress and strain relationship on Matlab.

Stress relaxation

The oscillatory stress that is used to represent the reaction of the fiber up on the irradiation of the nano-composite fiber under IR with in the first 10 seconds. The temperature difference versus the thermal stress given below is the modeled stress relaxation making use of the SLS three element model of viscoelasticity. The matlab code used that generated the plot is provided on appendix 2.

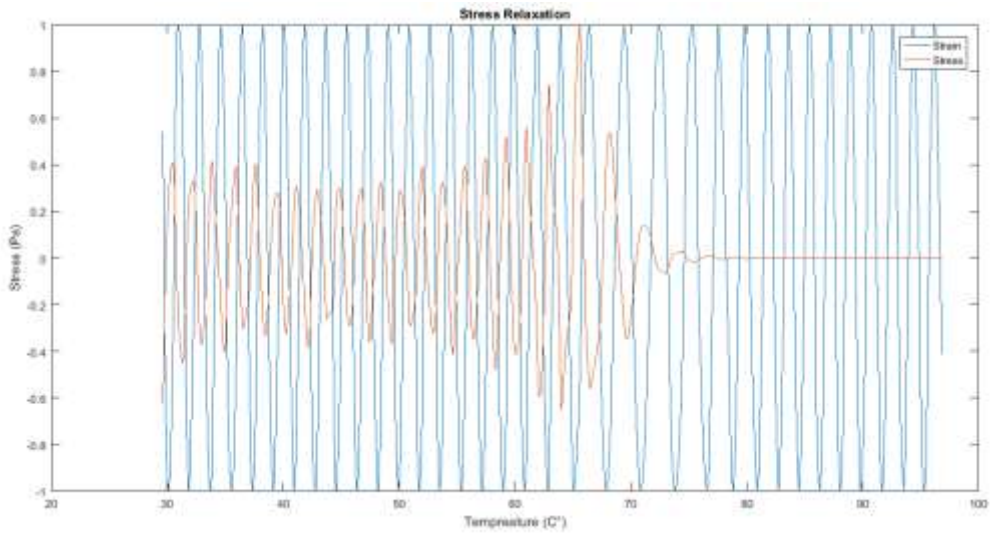

Figure 34: Stress Relaxation Plot of PLA/MWCNT nanocomposite fiber

As shown in the plot above, the thermal stress shows a relatively constant stress up to 60 degrees with minor increase and decrease of ±0.1 to ±0.2 Pa. The stress of the material reaches at its peak on the temperature ranging from 60 to 70 degrees. It then shows a rapid decrease after 70 degrees and reached a constant value after 75 degrees.

Creep

The creep plot of the PLA/MWCNT is as given below on Figure 35. The strain shown under a constant stress showed constant increase up to 60 degrees and gradual decrease starting from 60 degrees. It then undergoes rapid decrease in strain from 70 to 75 degrees. The material then exhibits constant strain after 80 degree centigrade.

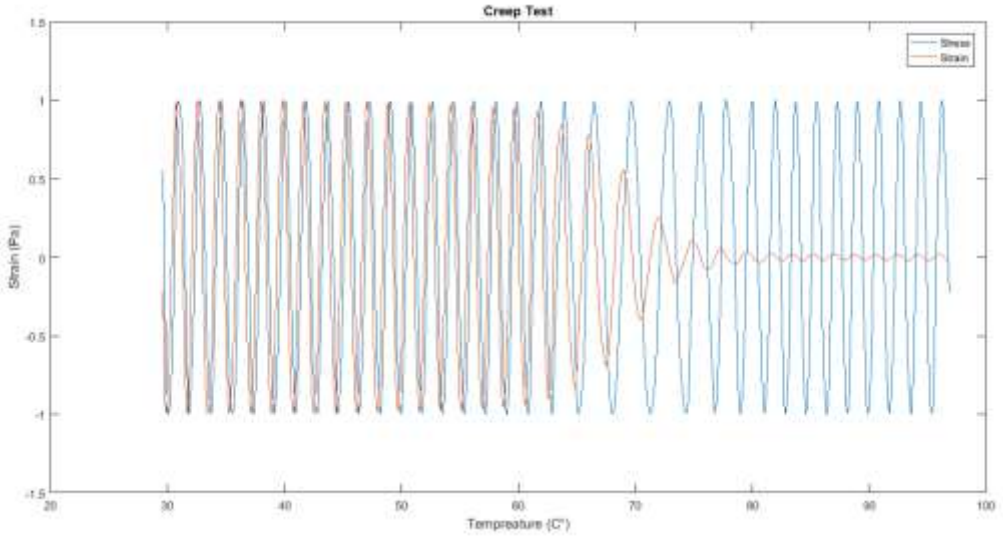

Figure 35: Creep plot of PLA/MWCNT nanocomposite fiber

DMA Data Analysis Discussion

As per the result presented on the previous section, only the uni-axially pre-deformed bi-layers of PLA/MWCNT nanocomposite fibers have shown the unprecedented actuation behavior towards the irradiated IR stimulus.

The qualitative and quantitative approaches resulted in positive effects on the actuation property of the nanocomposite fibers. On the qualitative approach clear deviation of parameter values such as Loss modulus, Storage modulus and tan delta are presented.

Based on the analysis of the data from DMA on Table 6, the storage modulus (371 MPa) of the ESF for PLA/MWCNT exhibits 14% increment compared with that for the ESF of pure PLA (327 MPa) within the glassy plateau, indicating the moderate improvement of mechanical properties upon loading 10wt.-% MWCNTs. Taking into account from the fact that in general, the peak temperature of the loss modulus (E´´) curve at a frequency of 1Hz is used as the glass transition temperature (Tg), we get the corresponding glass transition temperatures of 69^{o}C and 67^{o}C for the pure PLA ESFs and PLA/MWCNT ESFs, respectively. The glass transition temperatures by DMA are almost invariant to the incorporating chemically unmodified MWCNTs into ESFs, probably

indicating that the interaction between the MWCNTs and PLA molecules are poor, because fewer constraints from one-dimensional MWCNTs are imposed on the PLA macromolecules.

It is found to be a quite interesting feature in the progress of storage moduli as well as loss moduli with temperature. After passing the glass transition temperature the moduli drop rapidly, as generally expected, but the level reached a minimum value (1.9 MPa) in ESFs of PLA/MWCNT nanocomposite is considerably lower compared with that of the ESFs of pure PLA (5.2 MPa). In addition, the decreasing rate in ESFs of PLA/MWCNT nanocomposite is quite higher with increasing temperature than in ESFs of pure PLA. This might be understandable from the fact that the PLA/MWCNT nanocomposite extensively absorbs more thermal energy upon heating during the DMA operation due to extremely high thermal conductivity of MWCNTs; consequently, the ESFs of PLA/MWCNT nanocomposite will be softer at this temperature range. Pass over the minimum values the both moduli begin to increase gradually with temperature and reach the terminal levels, of which the modulus for the ESFs of PLA/MWCNT nanocomposite is again higher than that of ESFs of pure PLA. After reaching their minima, the moduli start to rise again with increasing temperature that is directly attributed to the cold crystallization of PLA matrix material in the ESFs, as confirmed by DSC. The terminal peak in the increase of moduli in DMA after passing glass transition is exactly coincident with the peak of cold crystallization in DSC. This means that in the temperature range of 90-100^{o}C both ESFs will be crystallized.

Generally speaking, E´ is the storage modulus which is representative of the elastic or solid-like behaviour and E´´ is the loss modulus indicative of the lost energy due to the resistance to flow of the polymer chains relating to the liquid-like or viscous behaviour of the material, the ratio between E´/E´´ is known as the tan δ which is indicative of the material's ability to dissipate energy in the form of heat.

As seen in Figure 30, the peak height of tanδ for the ESFs of PLA/MWCNT nanocomposite ($H_{tan\delta}$) is almost twice compared with that of the ESFs of PLA, and in addition, the full width half maximum of the ESFs of PLA/MWCNT nanocomposite ($\Delta T_{FWHM} = 9\ ^{o}C$) exhibits quite narrower than that of the ESFs of PLA/. The results allow us these materials with the steepness of the modulus change around Tg to show significant shape memory effects owing to the ability of storing the mechanical energy, when stretched them above Tg but below the completion of cold crystallization temperature and then cooled down to the room temperature, keeping the transient shape. The higher and the narrower tanδ occur in a material, the more mechanical energy will be absorbed and the more strain that is effective fixing will be.

Chapter Eight

Conclusion and Recommendation

As it was clearly discussed in depth on the result and discussion section of this research project, the investigated nanocomposite fibers were found to reflect the morphological and thermos-mechanical behavior of skeletal muscle fibers. This can drive us to the conclusion that PLA along with multi-walled carbon nanotube produces nanocomposite fibers that brings up suitable characteristics for the application skeletal muscle. Both the morphological and thermo-mechanical characteristics were deeply investigated by making use of manual and automated methods and the results were analyzed and presented qualitatively and quantitatively.

The output of the SEM characterization analysis clearly showed that there is Gaussian distribution of fiber diameter. Both manual and automated measurements were performed and both have presented a normal distribution function with equivalent measurements of 6.7 μm and 7.7 μm mean respectively. This Gaussian distribution shows that the fabricated nanocomposite fibers have increased reactivity with an external stimulus. As for the Dynamic mechanical analysis, both qualitative and quantitative analysis were done and both displayed the suitable viscoelastic behavior of the fabricated nanocomposite fiber for the application of artificial human skeletal muscle. From the results acquired from the morphological and thermo-mechanical analysis, the fabricated nanocomposite fibers showed properties that proved applicability for the fabrication of artificial human skeletal muscle.

The fabrication of the nanocomposite fibers can be further be used for the detailed study and analysis of several forms of muscular malfunctions. The study of the nature and cure of paralysis is one major area of application of an artificial skeletal muscle. Due to accidents or pressure sour of paralyzed and bed-ridden patients, a tissue can be damaged and removed from the area. The artificial skeletal muscle fiber proposed on this paper can be applied non-invasively to replace some of the functions missed by the removal of the natural skeletal muscle. Cerebral palsy is rather an important area of application of the fabricated nanocomposite fibers. Since cerebral palsy is a yet to be explored area of technical orthopedics. Finally yet importantly, robotic limb is an area of technical orthopedics that can make an ample amount of use of the fiber that was analyzed on this paper.

References

[1] World Health Organization. World Report on Disability [Internet]. WHO Press; 2011 December 30 [cited 2021 February]. Available from: https://www.who.int/teams/noncommunicable-diseases/disability-and-rehabilitation/world-report-on-disability.

[2] Ursula Miller. Country Strategy 2016-2020. Vienna: Light for the World International; 2017.

[3] Mishra, Anurag. Lower Limb Amputations; 2015; New Delhi, India:ResearchGate;1-2 p.

[4] Nature.com ISSN [Internet]. Nature Research; [cited 2021 Februray 11]. Available from: https://www.nature.com/subjects/orthopaedics.

[5] Dr.Grant McGimpsey, Terry C. Bradfored. Limb Prosthetics Services and Devices: Critical Unmet Need: Market Analysis. Worcester Polytechnic Institution:NIST; 2017 Apr 28.

[6] Dheeman Bhuyan, Kaushik Kumar. A Brief History of Prosthetics and Orthotics of the Lower Body and Their Types. Academia. 2019 May 26: 36-56.

[7] Vadalà, G., Di Pino, G., Ambrosio, L., Diaz, B. L., & Denaro, V. Targeted muscle reinnervation for improved control of myoelectric upper limb prostheses. Journal of biological regulators & homeostatic agent. 2017 Oct; 31(4):183-189.

[8] Istituto Italiano di Tecnologia [Internet]. Genova: IIT; 2016 May [Cited 2021 Feb 11]. Available from: https://iit.it/technology-transfer-docs/524-technology-teaser-actuators-for-robotic-applications-z-0/file.

[9] Victor Scheinman, J. Michael McCarthy. Springer Handbook of Robotics. ResearchGate; 2008 January. Mechanisms and Actuation; P.67-86.

[10] SolidsWiki contributors. Actuators [Internet]. SolidsWiki; 2012 December 3 [cited 2021 Feb 21] Available from:http://www.idconline.com/technical_references/pdfs/mechanical_engineering/Types_of_the_Actuators%20.pdf.

[11] Wang T, Farajollahi M, Choi YS et al. Electroactive polymers for sensing. ResearchGate. 2016 Aug 6: 1-4. http://dx.doi.org/10.1098/rsfs.2016.0026

[12] A.S.Bhattib, R.Afrina, N.A.Shaha, M.Abbasa, M.Amina. Design and analysis of functional multiwalled carbon nanotubes for infrared sensors. ScienceDirect. 2013 Dec 1 203:142-148. https://doi.org/10.1016/j.sna.2013.08.018.

[13] Abozar Akbari, Mainak Majumder, A. Tehrani. Polylactic Acid (PLA) Carbon Nanotube Nanocomposites. ResearchGate. 2015 January: 283-297. DOI: 10.1007/978-3-642-45229-1_45

[14] Shady Farah, Daniel G. Anderson, Robert Langer. Physical and mechanical properties of PLA, and their functions in widespread applications — A comprehensive review. ScienceDirect. 2016. http://dx.doi.org/10.1016/j.addr.2016.06.012.

[15] Donald Garlotta. Airex Rubber Products Company. A Literature Review of Poly (Lactic Acid). ResearchGate. 17 June 2019: 63-82

[16] Nanowerk.com. Birth and early history of carbon nanotubes [Internet]. 2016 June 03[cited 2021 February 22]. Available from: https://www.nanowerk.com/spotlight/spotid=43558_1.php.

[17] Zhang Y1, Bai Y, Yan B. Functionalized carbon nanotubes for potential medicinal applications. Europe PMC. 2016 Apr 13; 15(11-12):428-435 https://dx.doi.org/10.1016%2Fj.drudis.2010.04.005.

[18] Li, Yan. Light Driven Polymer Actuators with pre stored strain energy. Polymer science, Advanced science news. 2017 July 9:1.

[19] Medical News Today. A brief introduction to physiology [Internet]. 2017 October 13[cited 2021 March 21] Available from: file:///C:/Users/Abyssinia/Desktop/Chapter%20Two%20Litrature/Introduction%20to%20physiology_%20History,%20biological%20systems,%20and%20branches.html.

[20] Spencer, Herb. Organ-systems: an essay on a systematic approach to human. ResearchGat*e*. 2020 February: 1-20.

[21] Nursing Times.Skeletal system 1: the anatomy and physiology of bones [Internet]. 2020 January 27. [cited 2021 March 21] Available from: https://courses.lumenlearning.com/ap1/chapter/divisions-of-the-skeletal-system/.

[22] AndrewC.Murphy. Structure,function,and control of the human musculoskeletal system. PLOS Biology. 2018 January 18:1-19.

[23] The health site. The massive muscle anatomy and body building guide you always wanted![Internet]. 2014 Augest 28 [cited 2021 March 21] Available: https://www.thehealthsite.com/fitness/the-massive-muscle-anatomy-and-body-building-guide-you-always-wanted-100583/.

[24] Visone, Roberta. Cardiac Meets Skeletal: What's New in Microfluidic Models for Muscle Tissue Engineering. ResearchGate. 2016 August; 10(3390):1-16.

[25] Andrew J. Galpin, Ulrika Raue, Bozena Jemiolo et al. Human Skeletal Muscle Fiber Type Specific Protein Content. Anal Biochem. 2012 june 15; 425(2):175–182.

[26] Squire, John. Special Issue: The Actin-Myosin Interaction in Muscle: Background and Overview. Molecular science. 2019 November 14; 5715(20):1-39.

[27] Danny Christiansen, Martin J. MacInnis, Evelyn Zacharewicz, Hongyang Xu, Barnaby p. Frankish, Robyn M. Murphy. A fast, reliable and sample-sparing method to identify fibre types of single muscle fibres. Sceintific Reports. 2019 April 24 ; 1038(10) :1.

[28] Mansson, Alf. Hypothesis and theory: mechanical instabilities and non-uniformities in hereditary sarcomere myopathiesAl. Frontires in Physiology. 2014 September; 5(350): 1-7.

[29] Arend hintze. Understanding the Four Types of Artificial Intelligence[Internet]. Michigan State University; 2016 November 14 [cited 2021 March 22] Available from: https://www.govtech.com/computing/Understanding-the-Four-Types-of-Artificial-Intelligence.html.

[30] Princeton Brown. Sensors and Actuators: Technology and Application. New York, USA: Library Press; 2017.

[31] Mihálcz, István. Fundamental Characteristics and Design Method. Periodica polytechnica ser. Mech. Eng. 2001; 45(1):75–86.

[32] Rahimatpure Asim. Smart Memory Alloys. Proc. of Int. Conf. on Advances in Mechanical Engineering; Mumbai-72, India: 2012

[33] Langea, Gerrit. Shape Memory Alloys as Linear Drives in Robot Hand Actuation. ScienceDirect. 2015; 10(1016): 168 – 173.

[34] Roy, B. N. Future of Shape Memory Alloy and its Utilization. International Journal of Current Research. 2016 May; 8(05): 31646-31651.

[35] Andrianesis Konstantinos , Tzes Anthony , Kolyvas E. , Koveos Yannis. Development and Control of an Ultra-Lightweight Anthropomorphic Modular Finger Actuated by Shape Memory Alloy Wires. 2007 June.

[36] Simone Filomena. Design and Fabrication of a Three-Finger Prosthetic Hand using SMA muscle wires. Proceedings of SPIE - The International Society for Optical Engineering; Gebäude 9, 66121, Saarbrücken, Germany: 2015.

[37] Kretzer, Manuel. Electroactive Polymers [Internet]. Chair for CAAD, ETH Zürich; 2013[cited 24 March 2021] Available from: http://materiability.com/portfolio/electroactive-polymers/.

[38] Bhadra, Kiran Kumar Sappati, Sharmistha. Piezoelectric Polymer and Paper Substrates: A Review. Sensors. 2018 October 24; 18(3605): 1-4.

[39] Alaei, Zohreh. Power Enhancement in Piezoelectric Harvesting. Stockholm, Sweden: kth royal institute of technology; 2016.

[40] S. V. Ahir, A. M. Squires, A. R. Tajbakhsh, E. M. Terentjev. Infrared actuation in aligned polymer-nanotube composites. Phys.Rev.B. 2006 Feb;73(8): 085420. DOI: 10.1103/PhysRevB.73.085420

[41] Mahimwalla, Zahid S. Characterization of Photo-Induced Mechanical Responses in Azobenzene Polymers. Department of Chemistry, McGill University, Montreal Quebec, Canada. 2012 September: 13-52.

[42] Xiaobo Zhang, Zhibin Yu, Chuan Wang et al. Photoactuators and motorsbased on carbon nano tubeswith selective chilaritydistribution. Nature Communications. 2014 January 07; 5(2983):1-8. https://doi.org/10.1038/ncomms3983

[43] Li, by Yan. Light-Driven Polymer Actuators with Prestored Strain Energy. Advanced Science News. 2017 July 9.

[44] Bertrand Tondu. What Is an Artificial Muscle? A Systemic Approach. MDPI. 2015 December 11: 1-15.

[45] Simeon L. Smith, Eric J. Hunter. Aviscoelastic laryngeal muscle model with active components. The Journal of the Acoustical Society of America. 2014: 2041–2051.

[46] Wei Liang, Hao Liu, Kunyang Wang, zhihui Qian Luquan Ren, Lei Ren. Camaprative study of robotic artificial actuators & biological muscles. Advances in Mechanical Engineering. 2020 May 19; 12(6): 1-25.

[47] Hyegyo Son, ChangKyu Yoon. Advances in Stimuli-Responsive Soft Robots with Integrated Hybrid Materials. MDPI Actuators. 2020 November 14: 38-47.

[48] Yujie Chen, Chi Chen, Hafeez Ur Rehman et al. Shape-Memory Polymeric Artificial Muscles: Mechanisms, Applications and Challenges. MDPI Molecules. 2020 September 16; 25(18):1-27. https://doi.org/10.3390/molecules25184246

[49] Guo,Qipeng. Polymer Morphology. Hoboken,New Jersey: John Wiley & Sons, Inc.,; 2016.

[50] Escalante, Cristian Fabian. Fundamentals of transmission electron microscopy, the technique with the best resolution in the world. ResearchGate. 2019 February: 1-7.

[51] Olson, Veronica. Mr. Mak's Grade 8 Science Website [Internet]. 2017 October 26[cited 2021 April 26]. Available from: http://mrmakgrade8science.blogspot.com/2017/10/transmission-vs-scanning-electron.html.

[52] Dr Saurabh Bhargava. Scanning Electron Microscopy (SEM) lecture[Internet]. 2016 Augest 30[cited 2021 March 2]. Available from: https://www.slideshare.net/drbhargava5745/scanning-electron-microscopy-sem-lecture.

[53] Dr. M. Kannan. A Textbook on Fundamentals and Applications of Nanotechnology, New Delhi: Daya Publishing House® A Division of Astral International Pvt. Ltd.; 2018 March. Chapter 8, Scanning Electron Microscopy: Principle, Components and Applications; p. 81-92.

[54] Chaoying Ni. Scanning Electron Microscopy (SEM). Springer Link. 2013: 82-109. https://doi.org/10.1007/978-0-387-92897-5_1217

[55] Kevin P. Menard, Noah R. Menard. Dynamic Mechanical Analysis. ResearchGate. 2020 May: 21-36.

[56] Dynamic Mechanical Analysis Basic Theory & Applications Training [Internet]. Waters TA Instrument ; [cited 2021 May 16]. Available from: https://www.tainstruments.com/.

[57] Principles of Thermal Analysis (DSC, TG/DTA, TMA & DMA) [Intenet]. Hitachi-hightech; [cited 2021 May 16]. Available from: https://www.hitachi-hightech.com/global/products/science/tech/ana/thermal/descriptions/dma.html.

[58] Debra Dunson, Ph.D. Characterization of Polymer by Using Dynamic Mechanical Analysis (DMA). EAG Laboratories , Eurofins Material Science. 2017: 1-8.

[59] Kelly. Solid Mechanics Part I, University of Aukland; 2018 April 10. Chapter 10 Viscoelasticity; p.1-60

[60] Limited, Malvern Instruments. A Basic Introduction to Rheology. Technology Network. 2016.

Appendix One

SEM Images

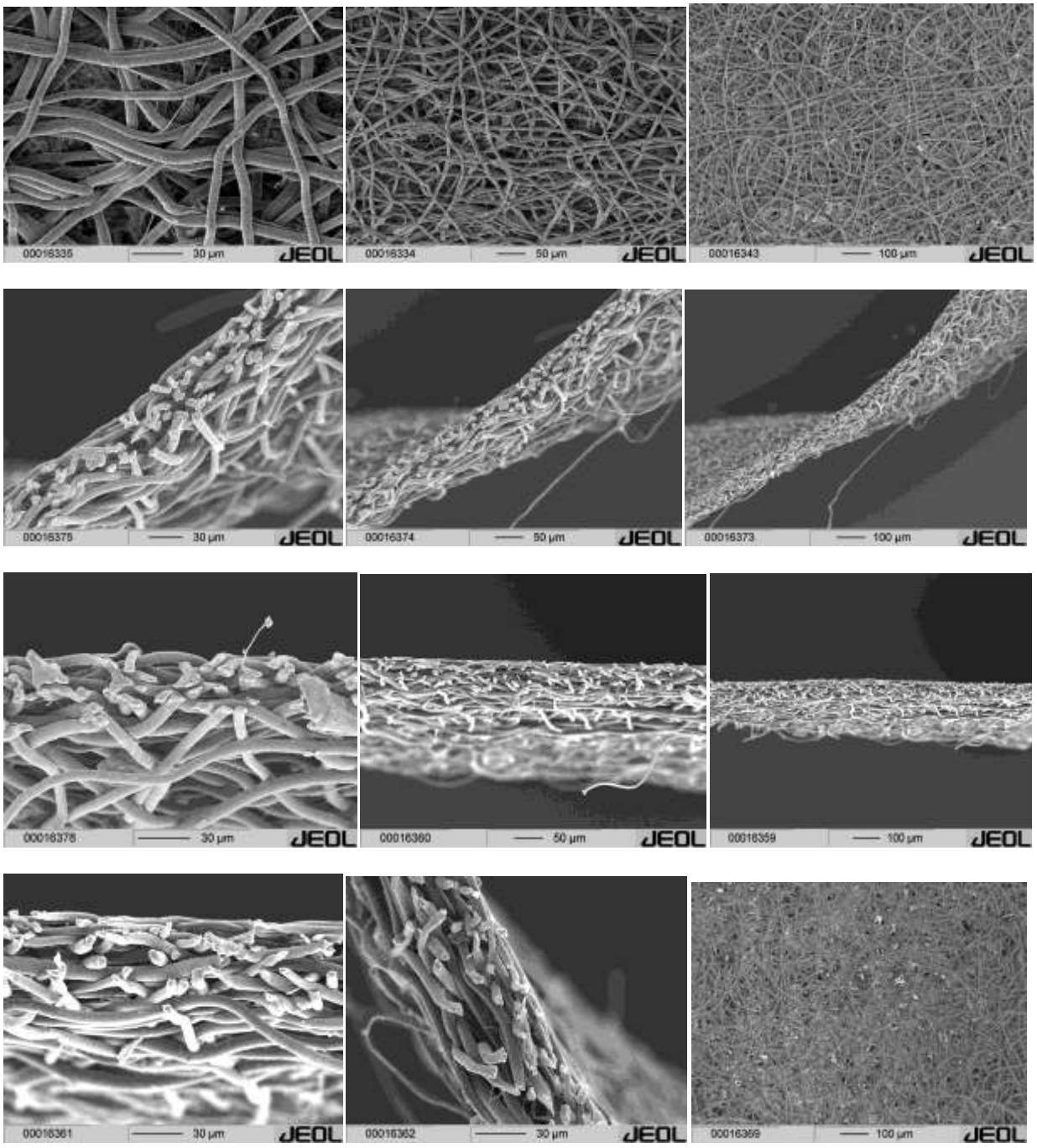

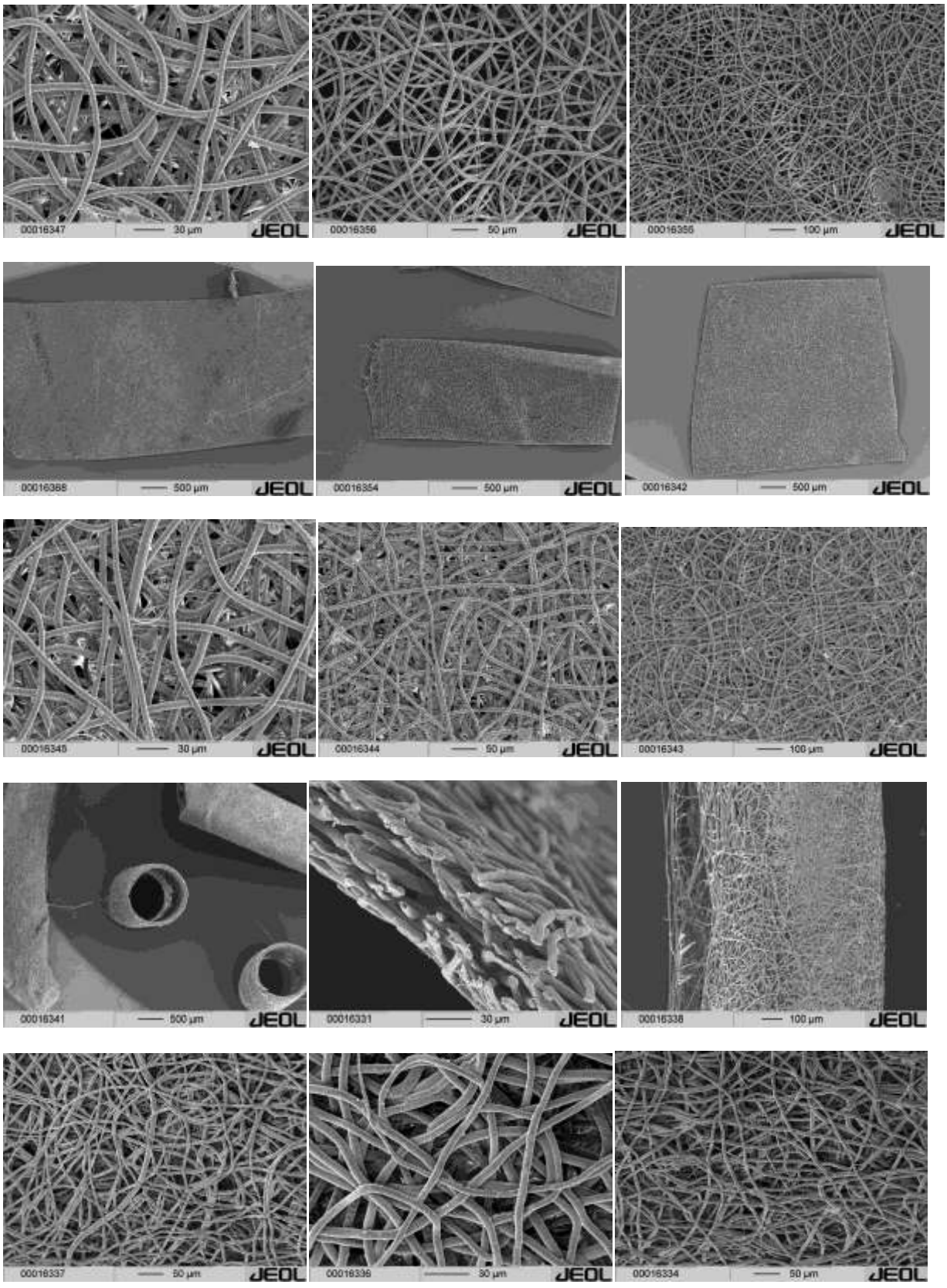
00016347 30 µm JEOL
00016356 50 µm JEOL
00016355 100 µm JEOL
00016388 500 µm JEOL
00016354 500 µm JEOL
00016342 500 µm JEOL
00016345 30 µm JEOL
00016344 50 µm JEOL
00016343 100 µm JEOL
00016341 500 µm JEOL
00016331 30 µm JEOL
00016338 100 µm JEOL
00016337 50 µm JEOL
00016336 30 µm JEOL
00016334 50 µm JEOL

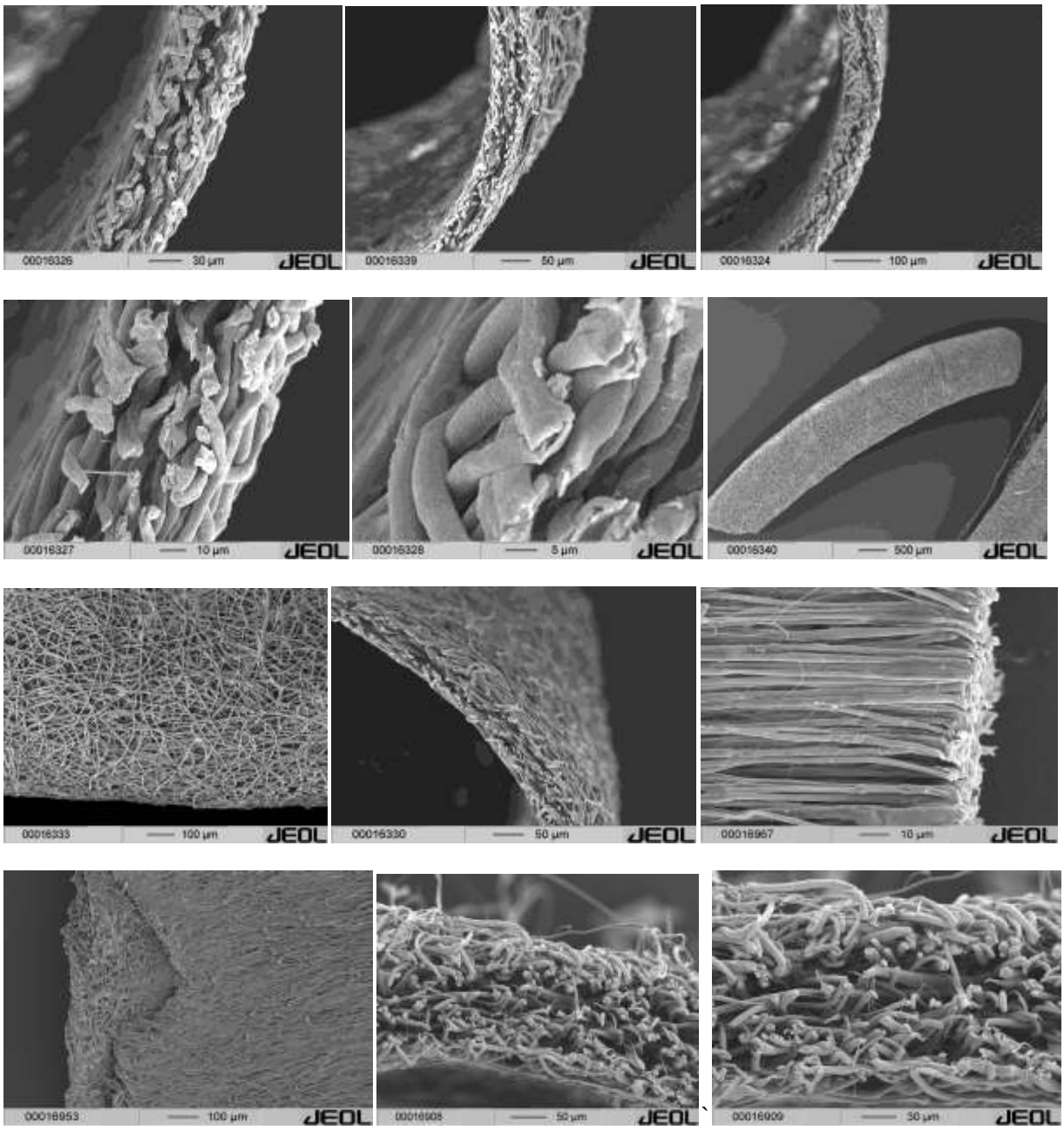
00016326 30 µm JEOL
00016339 50 µm JEOL
00016324 100 µm JEOL
00016327 10 µm JEOL
00016328 5 µm JEOL
00016340 500 µm JEOL
00016333 100 µm JEOL
00016330 50 µm JEOL
00018967 10 µm JEOL
00018953 100 µm JEOL
00018908 50 µm JEOL
00016909 30 µm JEOL

Appendix Two

MATLAB Codes

```
%% Load and plot the data
clear;  clc;  close all;
% [ temp temp_change  Young's_modulus Loss_modulus viscosity tan_delta]
% [tp dt ym lm v td]

load dma_data

% Initialize
s = 8;   % data start point @ temp = 29.65
tp = dma_data(s:end-1, 1);    % tempreature
% e = dma_data(s:end-1, 2);     % strain
E = dma_data(s:end-1, 3);
G = dma_data(s:end-1, 4);
U = dma_data(s:end-1, 5);
delta = dma_data(s:end-1, 6);
t = linspace(1, numel(tp)+1, numel(tp));
t = t';
E1 = E;
E2 = G;

% Plot data
figure, plot(tp), xlabel('Time (s)'), ylabel(['Tempreature (C' char(176)
')'])

figure,
yyaxis left
semilogy(tp, E), xlabel(['Tempreature (C' char(176)  ')']),
ylabel('Youngus Modules (Pa)')
yyaxis right
plot(tp, delta, 'linestyle','none'), ylabel('tan(\delta)'),

figure,
yyaxis left
semilogy(tp, G), xlabel(['Tempreature (C' char(176)  ')']), ylabel('Loss
Modules (Pa)')
yyaxis right
plot(tp, delta, 'linestyle','none'), ylabel('tan(\delta)')

figure,
plot(tp(1:end-1), U(1:end-1))
xlabel(['Tempreature (C' char(176)  ')']), ylabel('Viscosity (Pa s)'),

%% Creep Test.
ss_0 = 1;
w = 1;
ss = ss_0*cos(w*t - delta);
% figure, plot(ss, 'b-o'), xlabel('Time (s)'), ylabel('stress (Pa)')

Y1 = -ss_0*(E1+E2);
```

```
Y2 = (ss_0*E2)./(U.*(E1 + E2));

sn = ((Y1 + Y2)/2).*sin(w*t) - ((Y1 - Y2)/2).*cos(w*t);

sni = interp(sn, 4);
ssi = interp(ss, 4);
tpi = interp(tp, 4);
figure, plot(tpi, ssi);
% hold on, plot(tpi, normalize(stress,'range')),
hold on, plot(tpi, sni/max(sni)),
xlabel(['Tempreature (C' char(176)  ')'])
ylabel('Strain (Pa)')
title('Creep Test')
legend('Stress', 'Strain')


%% Stress Relaxation

sn_o = 1;
w = 1;
sn = sn_o*cos(w*t);
% figure, plot(sn,'b-o'), xlabel('Time (s)'), ylabel('Stress (Pa)')

E1 = E;
E2 = G;

ss_0 = sn_o*E1(1);

Z1 = -sn_o*(E1+E2);
Z2 = (sn_o*E1.*E2)./U;
W = E2./U;
C = ss_0 + 0.5*(Z2 - Z1);  % let c = 0;

ss = (0.5*(Z1 + Z2)).*sin(w*t) - (0.5*(Z1-Z2)).*cos(w*t);
% stress = ( ((-e_o*E2.*E1)./(w*U)) + ( (sig_o*E2.*cos(td))./(w*U))
).*sin(w*t') + ((sig_o*E2.*sin(td))./(w*U)).*cos(w*t');

ssi = interp(ss, 4);
tpi = interp(tp, 4);
sni = interp(sn, 4);
figure, plot(tpi, sni);
% hold on, plot(tpi, normalize(stress,'range')),
hold on, plot(tpi, ssi/max(ssi)),
xlabel(['Tempreature (C' char(176)  ')'])
ylabel('Stress (Pa)')
title('Stress Relaxation')
legend('Strain', 'Stress')
```

Appendix Three

PURE PLA DMA DATA

D(X)	A	B(Y)	C(Y)
Temp	E'	E''	tan_delta
ºC	Pa	Pa	
27.86	3.19E8	5.89E6	0.01847
28.79	3.23E8	5.84E6	0.01811
29.36	3.23E8	5.79E6	0.0179
29.62	3.24E8	5.72E6	0.01766
29.74	3.24E8	5.81E6	0.01792
29.75	3.25E8	5.65E6	0.01739
29.71	3.25E8	5.6E6	0.01725
29.65	3.25E8	5.58E6	0.01717
29.83	3.25E8	5.64E6	0.01735
30.08	3.25E8	5.69E6	0.01751
30.41	3.25E8	5.6E6	0.01725
30.69	3.25E8	5.61E6	0.01726
30.87	3.25E8	5.65E6	0.0174
31.31	3.27E8	5.66E6	0.01732
31.56	3.27E8	5.54E6	0.01694
31.8	3.27E8	5.55E6	0.017
32.04	3.27E8	5.58E6	0.01707
32.4	3.26E8	5.54E6	0.017
32.64	3.27E8	5.64E6	0.01723
32.94	3.27E8	5.73E6	0.01752
33.22	3.27E8	5.63E6	0.01724
33.53	3.27E8	5.69E6	0.01743
33.86	3.27E8	5.69E6	0.01742
34.09	3.26E8	5.79E6	0.01775
34.44	3.26E8	5.7E6	0.01747
34.69	3.26E8	5.81E6	0.01783
35.03	3.26E8	5.71E6	0.01751
35.26	3.26E8	5.74E6	0.01762
35.62	3.27E8	5.89E6	0.018
35.96	3.27E8	5.73E6	0.01751
36.2	3.27E8	5.75E6	0.01758
36.49	3.27E8	5.81E6	0.01777
36.74	3.27E8	5.76E6	0.01761
37.09	3.27E8	5.85E6	0.01791
37.33	3.26E8	5.79E6	0.01773
37.65	3.26E8	5.92E6	0.01815
37.89	3.26E8	5.84E6	0.01792
38.18	3.26E8	5.89E6	0.01809
38.46	3.25E8	5.87E6	0.01804
38.74	3.27E8	5.86E6	0.0179
39.06	3.27E8	6E6	0.01835
39.33	3.27E8	5.95E6	0.01821
39.69	3.27E8	5.98E6	0.0183
39.95	3.26E8	6.05E6	0.01853
40.23	3.26E8	5.99E6	0.01838
40.5	3.26E8	6.1E6	0.01873
40.83	3.25E8	6.09E6	0.01871
41.07	3.25E8	6.12E6	0.01884
41.36	3.25E8	6.17E6	0.019
41.67	3.26E8	6.06E6	0.01856
41.94	3.26E8	6.27E6	0.01925
42.25	3.26E8	6.23E6	0.01912
42.47	3.25E8	6.3E6	0.01936
42.83	3.25E8	6.26E6	0.01925
43.09	3.25E8	6.34E6	0.0195
43.42	3.24E8	6.37E6	0.01965
43.71	3.24E8	6.38E6	0.0197
43.97	3.23E8	6.45E6	0.01995
44.34	3.25E8	6.41E6	0.01973
44.52	3.25E8	6.55E6	0.02018
44.86	3.24E8	6.67E6	0.02057
45.16	3.24E8	6.62E6	0.02042
45.43	3.23E8	6.69E6	0.0207
45.71	3.23E8	6.72E6	0.0208
46.02	3.23E8	6.75E6	0.02094
46.29	3.22E8	6.79E6	0.02108
46.56	3.24E8	6.88E6	0.02127
46.9	3.23E8	6.92E6	0.02141
47.13	3.23E8	7E6	0.02169
47.45	3.22E8	7.12E6	0.0221
47.69	3.22E8	6.98E6	0.02171
48.02	3.21E8	7.06E6	0.02198
48.29	3.21E8	7.2E6	0.02244
48.58	3.22E8	7.26E6	0.02253
48.86	3.22E8	7.3E6	0.02268
49.15	3.21E8	7.31E6	0.02277
49.45	3.21E8	7.36E6	0.02296
49.68	3.2E8	7.51E6	0.02346
50	3.21E8	7.61E6	0.02369
50.27	3.21E8	7.57E6	0.02362
50.6	3.2E8	7.74E6	0.02418
50.87	3.19E8	7.85E6	0.02458
51.13	3.18E8	7.92E6	0.02487
51.47	3.2E8	8.02E6	0.02507
51.71	3.19E8	8.03E6	0.02515

52.01	3.19E8	8.1E6	0.02543
52.25	3.18E8	8.12E6	0.02555
52.59	3.17E8	8.39E6	0.02646
52.87	3.18E8	8.38E6	0.02634
53.18	3.17E8	8.48E6	0.02674
53.41	3.16E8	8.68E6	0.02742
53.71	3.16E8	8.8E6	0.0279
54.01	3.17E8	8.95E6	0.02827
54.3	3.16E8	9.09E6	0.0288
54.62	3.15E8	9.22E6	0.02928
54.85	3.14E8	9.31E6	0.02965
55.18	3.15E8	9.53E6	0.03027
55.47	3.14E8	9.73E6	0.03103
55.79	3.13E8	9.87E6	0.03156
56.03	3.12E8	9.96E6	0.03195
56.3	3.12E8	1.03E7	0.03293
56.59	3.11E8	1.05E7	0.0336
56.91	3.1E8	1.09E7	0.03503
57.2	3.1E8	1.1E7	0.03546
57.51	3.09E8	1.13E7	0.0365
57.77	3.08E8	1.15E7	0.03738
58.07	3.08E8	1.2E7	0.03892
58.37	3.07E8	1.22E7	0.03975
58.62	3.05E8	1.25E7	0.04098
58.93	3.05E8	1.32E7	0.04315
59.26	3.04E8	1.34E7	0.04403
59.51	3.02E8	1.38E7	0.0457
59.8	3.02E8	1.43E7	0.04756
60.07	3E8	1.49E7	0.04972
60.41	2.99E8	1.56E7	0.05215
60.71	2.96E8	1.64E7	0.05538
61.01	2.95E8	1.7E7	0.05767
61.28	2.93E8	1.78E7	0.06085
61.78	2.89E8	1.94E7	0.06699
62.04	2.86E8	2.03E7	0.071
62.34	2.83E8	2.16E7	0.0763
62.64	2.8E8	2.3E7	0.08226
62.95	2.76E8	2.43E7	0.08829
63.19	2.72E8	2.59E7	0.09507
63.71	2.57E8	2.46E7	0.09588
64	2.59E8	3.14E7	0.12135
64.31	2.54E8	3.38E7	0.13337
64.85	2.43E8	3.82E7	0.15708
65.09	2.36E8	4.06E7	0.17225
65.62	2.24E8	4.5E7	0.20101
65.9	2.15E8	4.78E7	0.22255
66.39	2.02E8	5.18E7	0.2568
66.76	1.94E8	5.39E7	0.27754
67.36	1.76E8	5.82E7	0.32958
67.8	1.64E8	5.98E7	0.36599
68.27	1.46E8	6.18E7	0.42418
68.74	1.3E8	6.25E7	0.48157
69.29	1.15E8	6.2E7	0.53781
69.72	9.89E7	6E7	0.60665
70.18	8.52E7	5.69E7	0.6672
70.65	7.3E7	5.31E7	0.72722
71.15	6.18E7	4.88E7	0.78998
71.71	5.2E7	4.38E7	0.84202
72.17	4.26E7	3.78E7	0.88765
72.68	3.56E7	3.26E7	0.91642
73.17	3.1E7	2.84E7	0.91624
73.49	2.82E7	2.63E7	0.93238
73.99	2.35E7	2.16E7	0.92005
74.53	2.04E7	1.84E7	0.89927
74.84	1.9E7	1.69E7	0.8881
75.41	1.67E7	1.45E7	0.86472
75.71	1.53E7	1.28E7	0.8396
76.09	1.42E7	1.15E7	0.81027
76.61	1.26E7	9.86E6	0.77958
76.92	1.2E7	8.87E6	0.73843
77.3	1.15E7	8.28E6	0.72038
77.52	1.08E7	7.45E6	0.69072
77.88	1.04E7	7.05E6	0.68039
78.42	9.18E6	5.79E6	0.63076
78.76	8.77E6	5.37E6	0.61252
79.07	8.37E6	4.92E6	0.58755
79.41	8.08E6	4.6E6	0.57001
79.73	7.98E6	4.39E6	0.55018
80.04	7.51E6	3.99E6	0.53083
80.31	7.26E6	3.73E6	0.51456
80.78	7.07E6	3.4E6	0.48031
81.08	6.87E6	3.15E6	0.4582
81.41	6.75E6	3.05E6	0.45153
81.67	6.49E6	2.81E6	0.43261
81.99	6.41E6	2.6E6	0.40558
82.29	6.1E6	2.56E6	0.42022
82.58	6.13E6	2.39E6	0.3907
82.82	5.98E6	2.23E6	0.37358
83.15	6.03E6	2.14E6	0.35483
83.4	5.86E6	2.09E6	0.35623
83.67	5.72E6	1.99E6	0.34754
83.96	5.67E6	1.9E6	0.33543
84.24	5.62E6	1.83E6	0.32489
84.54	5.54E6	1.73E6	0.31287
84.81	5.5E6	1.71E6	0.31077
85.15	5.37E6	1.61E6	0.29974

85.37	5.26E6	1.59E6	0.30301
85.74	5.33E6	1.55E6	0.29113
85.92	5.37E6	1.51E6	0.28054
86.23	5.38E6	1.35E6	0.25156
86.53	5.31E6	1.36E6	0.25562
86.83	5.24E6	1.25E6	0.23871
87.14	5.24E6	1.25E6	0.23909
87.4	5.31E6	1.21E6	0.22776
87.68	5.25E6	1.26E6	0.23976
87.93	5.3E6	1.24E6	0.23461
88.25	5.27E6	1.13E6	0.2145
88.47	5.23E6	1.15E6	0.2203
88.77	5.23E6	1.07E6	0.20433
89.06	5.17E6	1.1E6	0.2119
89.36	5.19E6	1.07E6	0.20548
89.64	5.25E6	1.01E6	0.19286
89.92	5.25E6	1.02E6	0.19411
90.25	5.27E6	1.07E6	0.20221
90.48	5.24E6	1.04E6	0.19786
90.84	5.35E6	979000	0.18293
91.09	5.39E6	988000	0.18321
91.4	5.44E6	911000	0.16732
91.7	5.4E6	919000	0.17028
91.99	5.52E6	909000	0.16462
92.32	5.57E6	917000	0.16463
92.58	5.66E6	896000	0.15815
92.89	5.72E6	896000	0.15652
93.12	5.81E6	961000	0.16537
93.49	6.06E6	896000	0.14778
93.72	5.91E6	927000	0.15682
94.02	6.07E6	970000	0.15989
94.28	5.98E6	1.01E6	0.16914
94.56	6.17E6	916000	0.14854
94.89	6.26E6	885000	0.14122
95.14	6.35E6	926000	0.14595
95.48	6.41E6	959000	0.14965
95.69	6.53E6	852000	0.13044
96.02	6.72E6	919000	0.1367
96.29	6.82E6	911000	0.13349
96.62	7.02E6	939000	0.13369
96.92	7.2E6	1.03E6	0.14249

PLA/MWCNT DMA DATA

D(X)	A	B(Y)	C(Y)
Temp	E'	E"	tan_delta
°C	Pa	Pa	
27.36	3.65E8	8.47E6	0.02321
27.43	3.68E8	8.15E6	0.02214
27.85	3.69E8	8.04E6	0.0218
28.14	3.69E8	7.88E6	0.02135
28.35	3.69E8	7.84E6	0.02123
28.76	3.7E8	7.73E6	0.02092
29.01	3.7E8	7.62E6	0.02062
29.31	3.7E8	7.6E6	0.02054
29.56	3.7E8	7.68E6	0.02077
29.85	3.7E8	7.61E6	0.02057
30.14	3.7E8	7.65E6	0.02068
30.43	3.7E8	7.52E6	0.02032
30.78	3.71E8	7.64E6	0.02061
31	3.71E8	7.58E6	0.02047
31.36	3.71E8	7.55E6	0.02037
31.61	3.71E8	7.65E6	0.02065
32.04	3.71E8	7.49E6	0.02022
32.3	3.7E8	7.58E6	0.02047
32.58	3.7E8	7.58E6	0.02047
33	3.7E8	7.75E6	0.02093
33.18	3.7E8	7.59E6	0.0205
33.31	3.7E8	7.64E6	0.02064
33.64	3.7E8	7.58E6	0.02048
33.99	3.7E8	7.61E6	0.02056
34.18	3.7E8	7.68E6	0.02076
34.73	3.7E8	7.68E6	0.02074
35.03	3.7E8	7.59E6	0.0205
35.16	3.7E8	7.62E6	0.02058
35.64	3.7E8	7.73E6	0.02087
35.9	3.7E8	7.65E6	0.02066
36.04	3.7E8	7.57E6	0.02045
36.34	3.7E8	7.73E6	0.02089
36.66	3.7E8	7.76E6	0.021
36.89	3.7E8	7.63E6	0.02065
37.28	3.7E8	7.66E6	0.02073
37.5	3.69E8	7.69E6	0.02082
37.78	3.69E8	7.72E6	0.0209
38.04	3.69E8	7.66E6	0.02075
38.33	3.69E8	7.78E6	0.02109
38.74	3.69E8	7.73E6	0.02095
38.93	3.69E8	7.79E6	0.02113
39.35	3.69E8	7.9E6	0.02141
39.55	3.69E8	7.78E6	0.02109

39.91	3.69E8	7.8E6	0.02117
40.09	3.68E8	7.94E6	0.02155
40.51	3.68E8	7.95E6	0.02158
40.75	3.68E8	7.85E6	0.02133
41.01	3.68E8	7.87E6	0.02137
41.45	3.68E8	7.97E6	0.02168
41.61	3.68E8	7.99E6	0.02173
41.89	3.67E8	7.95E6	0.02163
42.14	3.67E8	7.98E6	0.02173
42.52	3.67E8	7.92E6	0.02158
42.77	3.67E8	8.01E6	0.02183
43.11	3.67E8	7.97E6	0.02174
43.39	3.67E8	8.15E6	0.02222
43.62	3.67E8	8.19E6	0.02233
44	3.66E8	8.14E6	0.02222
44.24	3.66E8	8.28E6	0.02261
44.58	3.66E8	8.26E6	0.02258
44.84	3.66E8	8.36E6	0.02287
45.21	3.65E8	8.29E6	0.02269
45.44	3.65E8	8.29E6	0.02271
45.75	3.65E8	8.37E6	0.02294
45.99	3.65E8	8.44E6	0.02316
46.28	3.64E8	8.42E6	0.02313
46.59	3.64E8	8.55E6	0.02348
46.86	3.64E8	8.67E6	0.02382
47.19	3.64E8	8.63E6	0.02373
47.48	3.63E8	8.66E6	0.02383
47.86	3.63E8	8.69E6	0.02393
48.08	3.63E8	8.76E6	0.02416
48.39	3.62E8	8.83E6	0.02436
48.62	3.62E8	8.86E6	0.02449
48.96	3.62E8	8.9E6	0.02461
49.2	3.61E8	8.99E6	0.0249
49.43	3.61E8	9.06E6	0.02507
49.84	3.61E8	9.1E6	0.0252
50.04	3.61E8	9.2E6	0.02551
50.41	3.6E8	9.24E6	0.02565
50.67	3.6E8	9.3E6	0.02585
51.03	3.59E8	9.37E6	0.02607
51.23	3.59E8	9.41E6	0.02624
51.59	3.58E8	9.51E6	0.02655
51.82	3.58E8	9.58E6	0.02678
52.09	3.58E8	9.75E6	0.02725
52.52	3.57E8	9.81E6	0.02745
52.69	3.57E8	9.87E6	0.02765
53.05	3.56E8	9.97E6	0.02796
53.29	3.56E8	1.01E7	0.02828
53.61	3.55E8	1.02E7	0.02877
53.86	3.54E8	1.03E7	0.02907
54.16	3.54E8	1.05E7	0.02975
54.46	3.54E8	1.07E7	0.0303
54.72	3.53E8	1.07E7	0.03045
55.06	3.52E8	1.08E7	0.03076
55.3	3.52E8	1.1E7	0.03126
55.62	3.51E8	1.11E7	0.03169
55.89	3.51E8	1.14E7	0.0324
56.2	3.5E8	1.15E7	0.03279
56.47	3.49E8	1.17E7	0.03345
56.84	3.48E8	1.19E7	0.03415
57.08	3.47E8	1.2E7	0.03456
57.34	3.47E8	1.23E7	0.0354
57.65	3.46E8	1.25E7	0.03621
57.93	3.45E8	1.27E7	0.03696
58.3	3.43E8	1.3E7	0.03786
58.53	3.43E8	1.34E7	0.03902
58.89	3.41E8	1.37E7	0.04001
59.12	3.4E8	1.4E7	0.04116
59.43	3.38E8	1.44E7	0.04247
59.92	3.36E8	1.49E7	0.04438
60.23	3.34E8	1.53E7	0.04589
60.45	3.32E8	1.59E7	0.04777
60.78	3.31E8	1.65E7	0.04992
61.03	3.29E8	1.71E7	0.05194
61.39	3.26E8	1.78E7	0.05444
61.59	3.24E8	1.86E7	0.05743
61.94	3.21E8	1.95E7	0.0609
62.44	3.15E8	2.11E7	0.06682
62.75	3.12E8	2.23E7	0.0715
63.01	3.08E8	2.36E7	0.07672
63.32	3.03E8	2.52E7	0.08333
63.83	2.94E8	2.85E7	0.09677
64.09	2.88E8	3.07E7	0.10658
64.65	2.77E8	3.52E7	0.1272
64.88	2.67E8	3.86E7	0.14441
65.51	2.51E8	4.61E7	0.18389
66.05	2.34E8	5.33E7	0.22774
66.52	2.12E8	6.1E7	0.28765
67.17	1.93E8	6.76E7	0.35061
67.72	1.73E8	7.23E7	0.41836
68.27	1.51E8	7.57E7	0.49975
68.91	1.26E8	7.61E7	0.60468
69.42	1.06E8	7.44E7	0.70309
71.3	4.54E7	5.32E7	1.17034
71.79	3.5E7	4.58E7	1.30967
72.47	2.43E7	3.59E7	1.47822
72.99	1.89E7	3.02E7	1.59448

73.43	1.47E7	2.47E7	1.68199
73.91	1.17E7	2.04E7	1.73908
74.4	9.46E6	1.66E7	1.75241
74.96	7.53E6	1.34E7	1.78282
75.54	5.94E6	1.06E7	1.78428
76.02	5.02E6	8.68E6	1.72913
76.29	4.69E6	7.78E6	1.65901
76.66	4.39E6	7.01E6	1.59838
77.12	3.88E6	5.67E6	1.46065
77.51	3.43E6	4.91E6	1.43119
77.88	3.24E6	4.35E6	1.33976
78.11	3.04E6	3.85E6	1.26719
78.43	2.9E6	3.44E6	1.18687
78.95	2.8E6	2.9E6	1.03603
79.3	2.66E6	2.68E6	1.00689
79.51	2.62E6	2.41E6	0.92247
79.88	2.54E6	2.18E6	0.85969
80.14	2.5E6	1.99E6	0.79525
80.49	2.46E6	1.84E6	0.74655
80.76	2.36E6	1.67E6	0.70721
81.04	2.36E6	1.52E6	0.64346
81.36	2.28E6	1.45E6	0.63677
81.66	2.22E6	1.3E6	0.58505
81.98	2.24E6	1.21E6	0.54001
82.23	2.21E6	1.13E6	0.50854
82.58	2.11E6	1.06E6	0.50326
82.82	2.09E6	958000	0.45831
83.2	2.12E6	969000	0.45688
83.42	2.05E6	857000	0.4175
83.72	2.02E6	777000	0.38536
84.03	2.04E6	804000	0.39398
84.32	1.95E6	732000	0.37472
84.61	2.01E6	702000	0.3502
84.95	1.93E6	700000	0.36313
85.24	1.95E6	604000	0.3093
85.53	1.97E6	606000	0.30709
85.84	1.95E6	600000	0.30822
86.12	1.96E6	566000	0.28815
86.47	1.95E6	542000	0.27762
86.73	2E6	538000	0.26817
87.04	2.02E6	484000	0.24017
87.33	2.09E6	485000	0.2323
87.62	1.97E6	500000	0.25353
87.91	2.08E6	492000	0.23625
88.23	2.1E6	425000	0.20217
88.56	2.19E6	480000	0.21925
88.83	2.12E6	436000	0.20532
89.15	2.17E6	448000	0.20698
89.43	2.17E6	447000	0.20627
89.74	2.22E6	515000	0.23171
90.02	2.31E6	454000	0.1967
90.33	2.32E6	437000	0.18821
90.59	2.4E6	534000	0.22257
90.87	2.46E6	493000	0.20064
91.19	2.55E6	473000	0.18548
91.47	2.59E6	470000	0.18155
91.78	2.72E6	526000	0.19309
92.06	2.84E6	495000	0.17444
92.38	2.84E6	501000	0.17618
92.6	2.94E6	501000	0.1706
92.97	3.01E6	617000	0.20483
93.23	3.21E6	619000	0.19267
93.55	3.37E6	659000	0.19568
93.85	3.64E6	725000	0.19942
94.13	3.78E6	694000	0.18369
94.49	4.05E6	741000	0.18324
94.73	4.42E6	783000	0.17733
95.08	4.74E6	876000	0.18465
95.57	5.32E6	924000	0.17375
95.84	5.78E6	1.04E6	0.18019
96.15	6.22E6	1.05E6	0.16939
96.45	6.75E6	1.23E6	0.18229
96.98	8.05E6	1.4E6	0.1744
97.22	8.8E6	1.42E6	0.16107
97.73	1.01E7	1.67E6	0.16507
98.05	1.09E7	1.7E6	0.15545
98.32	1.19E7	1.81E6	0.15251
98.84	1.34E7	1.98E6	0.14821
99.1	1.43E7	2.11E6	0.14739
99.63	1.6E7	2.22E6	0.1389
99.95	1.69E7	2.34E6	0.13886
100.23	1.77E7	2.38E6	0.13446
100.72	1.89E7	2.46E6	0.1299
101.01	1.96E7	2.47E6	0.12586
101.4	2.02E7	2.51E6	0.12425
101.64	2.07E7	2.56E6	0.12332
101.98	2.12E7	2.54E6	0.11994
102.43	2.2E7	2.53E6	0.11472
102.75	2.24E7	2.55E6	0.11426
103.03	2.27E7	2.55E6	0.11273
103.35	2.3E7	2.55E6	0.11106
103.64	2.31E7	2.49E6	0.10757
103.94	2.33E7	2.48E6	0.10613
104.19	2.35E7	2.44E6	0.10361
104.55	2.37E7	2.42E6	0.10234
104.79	2.37E7	2.44E6	0.10269

105.13	2.38E7	2.36E6	0.09935
105.38	2.39E7	2.35E6	0.09837
105.7	2.39E7	2.36E6	0.09874
106.03	2.4E7	2.34E6	0.09732
106.23	2.4E7	2.33E6	0.09683
106.56	2.41E7	2.28E6	0.0945
106.82	2.41E7	2.3E6	0.09546
107.21	2.41E7	2.31E6	0.09552
107.37	2.41E7	2.21E6	0.09159
107.72	2.41E7	2.24E6	0.09287
108.03	2.41E7	2.25E6	0.09327
108.25	2.42E7	2.18E6	0.09023
108.58	2.42E7	2.18E6	0.09031
108.88	2.42E7	2.18E6	0.08996
109.16	2.42E7	2.15E6	0.08901
109.42	2.41E7	2.14E6	0.08868
109.78	2.41E7	2.13E6	0.08843
110.02	2.42E7	2.17E6	0.08964
110.35	2.4E7	2.09E6	0.08689
110.59	2.4E7	2.06E6	0.08574
110.91	2.4E7	2.04E6	0.08469
111.23	2.41E7	2.02E6	0.08366
111.5	2.41E7	2.02E6	0.0838
111.79	2.4E7	2.03E6	0.08474
112.08	2.39E7	2E6	0.0837
112.42	2.4E7	1.99E6	0.08312
112.68	2.39E7	1.91E6	0.0799
112.93	2.38E7	1.97E6	0.08261
113.22	2.4E7	1.99E6	0.08291
113.55	2.38E7	1.92E6	0.08077
113.82	2.37E7	1.95E6	0.08218
114.07	2.37E7	1.95E6	0.082
114.44	2.38E7	1.92E6	0.08094
114.69	2.37E7	1.89E6	0.07996
115.02	2.37E7	1.93E6	0.08176
115.26	2.37E7	1.96E6	0.08245
115.6	2.36E7	1.81E6	0.0768
115.86	2.35E7	1.88E6	0.07992
116.14	2.36E7	1.83E6	0.07768
116.44	2.35E7	1.81E6	0.07723
116.7	2.34E7	1.8E6	0.07696
117.05	2.34E7	1.81E6	0.0772
117.3	2.34E7	1.81E6	0.07739
117.61	2.33E7	1.79E6	0.07689
117.85	2.33E7	1.79E6	0.07677
118.19	2.33E7	1.78E6	0.07637
118.46	2.32E7	1.77E6	0.07657
118.75	2.32E7	1.77E6	0.076

119.06	2.31E7	1.79E6	0.07762
119.26	2.3E7	1.75E6	0.07625
119.65	2.31E7	1.73E6	0.07472
119.92	2.3E7	1.7E6	0.07364
120.22	2.3E7	1.67E6	0.07285
120.44	2.3E7	1.7E6	0.07419
120.83	2.29E7	1.71E6	0.07456
121.02	2.28E7	1.66E6	0.07289
121.32	2.27E7	1.64E6	0.07214
121.68	2.28E7	1.63E6	0.07144
121.93	2.27E7	1.69E6	0.07452
122.28	2.26E7	1.67E6	0.07356
122.49	2.26E7	1.67E6	0.07367
122.88	2.25E7	1.62E6	0.07202
123.07	2.25E7	1.67E6	0.07416
123.39	2.24E7	1.68E6	0.07482
123.66	2.24E7	1.67E6	0.07452
123.99	2.23E7	1.69E6	0.07572
124.28	2.23E7	1.64E6	0.07343
124.52	2.23E7	1.58E6	0.07096
124.81	2.22E7	1.6E6	0.07213
125.11	2.21E7	1.56E6	0.07061
125.39	2.21E7	1.6E6	0.0723
125.72	2.2E7	1.61E6	0.07323
126.07	2.19E7	1.59E6	0.07236
126.31	2.2E7	1.59E6	0.0725
126.58	2.19E7	1.61E6	0.07344
126.84	2.19E7	1.55E6	0.07103
127.13	2.18E7	1.57E6	0.07232
127.47	2.17E7	1.61E6	0.07428
127.74	2.17E7	1.56E6	0.07219
128.06	2.17E7	1.53E6	0.07084
128.32	2.16E7	1.54E6	0.07149
128.66	2.15E7	1.51E6	0.07022
128.92	2.14E7	1.57E6	0.0731
129.21	2.14E7	1.55E6	0.07229
129.49	2.13E7	1.49E6	0.07004
129.76	2.12E7	1.55E6	0.07288
130.15	2.12E7	1.55E6	0.07302
130.35	2.12E7	1.55E6	0.07315
130.66	2.11E7	1.5E6	0.07115
130.94	2.1E7	1.49E6	0.07086
131.3	2.09E7	1.58E6	0.07533
131.54	2.09E7	1.53E6	0.07311
131.81	2.08E7	1.49E6	0.0715
132.12	2.09E7	1.49E6	0.07129
132.36	2.07E7	1.49E6	0.07185
132.71	2.06E7	1.52E6	0.07366

132.94	2.05E7	1.47E6	0.07176
133.32	2.05E7	1.5E6	0.07304
133.55	2.04E7	1.45E6	0.07101
133.87	2.04E7	1.49E6	0.07321
134.12	2.03E7	1.43E6	0.0707
134.39	2.02E7	1.4E6	0.0695
134.7	2.02E7	1.48E6	0.07346
134.96	2E7	1.42E6	0.07098
135.34	2E7	1.42E6	0.07098
135.55	1.99E7	1.44E6	0.07213
135.9	1.99E7	1.44E6	0.07234
136.12	1.98E7	1.41E6	0.07117
136.48	1.97E7	1.4E6	0.07115
136.74	1.96E7	1.44E6	0.07312
137.02	1.96E7	1.41E6	0.07208
137.3	1.75E7	1.41E6	0.07203
137.57	1.94E7	1.38E6	0.07103
137.91	1.94E7	1.36E6	0.07016
138.16	1.93E7	1.35E6	0.06994
138.5	1.93E7	1.42E6	0.07394
138.72	1.91E7	1.42E6	0.07419
139.07	1.91E7	1.34E6	0.07015
139.32	1.9E7	1.38E6	0.07274
139.63	1.9E7	1.39E6	0.07307
139.91	1.88E7	1.39E6	0.07407
140.21	1.87E7	1.38E6	0.07334
140.51	1.87E7	1.41E6	0.07507
140.75	1.86E7	1.39E6	0.07509
141.12	1.85E7	1.42E6	0.07675
141.35	1.85E7	1.34E6	0.07253
141.68	1.84E7	1.33E6	0.07236
142.11	1.82E7	1.38E6	0.0759
142.45	1.82E7	1.34E6	0.07365
142.7	1.81E7	1.34E6	0.07396
143.03	1.8E7	1.36E6	0.07567
143.26	1.8E7	1.33E6	0.07419
143.61	1.79E7	1.35E6	0.07564
143.89	1.77E7	1.36E6	0.07686
144.2	1.77E7	1.35E6	0.07626
144.45	1.76E7	1.35E6	0.07669
144.74	1.74E7	1.36E6	0.07772
145.07	1.74E7	1.28E6	0.0737
145.33	1.73E7	1.33E6	0.07676
145.65	1.73E7	1.37E6	0.07912
145.89	1.71E7	1.34E6	0.07801
146.24	1.71E7	1.41E6	0.08288
146.5	1.69E7	1.31E6	0.07756
146.81	1.69E7	1.32E6	0.07801
147.04	1.67E7	1.34E6	0.07986
147.37	1.66E7	1.38E6	0.08322
147.67	1.66E7	1.36E6	0.08206
147.94	1.66E7	1.34E6	0.08102
148.29	1.64E7	1.33E6	0.08088
148.52	1.63E7	1.32E6	0.081
148.85	1.62E7	1.31E6	0.08094
149.13	1.6E7	1.33E6	0.08283
149.47	1.6E7	1.34E6	0.0842
149.69	1.59E7	1.34E6	0.0842
150	1.58E7	1.29E6	0.08167
	--	--	--
	--	--	--
	--	--	--
	--	--	--
	--	--	--
	--	--	--
	--	--	--
	--	--	--
	--	--	--
	--	--	--